



Safety in Mines Research Advisory Committee

Final Project Report

**Performance of various types of
containment support under quasi-static
and dynamic loading conditions**

Part I

J.S. Kuijpers, A.M. Milev, A.J. Jager & E. Acheampong

Research agency: CSIR: Division of Mining Technology

Project number: GAP 810

Date: May 2002

Executive Summary

Seismicity causes the most severe loading conditions for tunnel support systems in deep-level South African gold mines. The design of such support systems should therefore incorporate the potential effect of seismicity on support requirements. Unfortunately, this is presently not possible, as such effects have not been adequately quantified. Within the current project, an attempt has been made to address this shortcoming.

The main objective of this project is to determine the support performance of various tunnel support systems and components under dynamic loading conditions. Deficiencies in the performance of wire mesh were highlighted in the investigations conducted for this project. Investigations were limited to support systems consisting of yielding tendons, wire mesh and steel ropes (lacing). Part I of this project represents the contribution of CSIR: Miningtek while the contribution of SRK is represented in Part II.

A special testing rig, which was designed to incorporate full size tunnel support systems in a realistic rock mass environment, was used for dynamic as well as quasi-static loading tests. While impact loading was used to represent the effects of seismicity as realistically as possible, quasi-static loading tests were conducted in order to obtain accurate load-deformation characteristics of the system and its components. These (calibrated) characteristics could subsequently be used to interpret more complex systems under both dynamic and quasi-static loading conditions.

A conceptual model, describing the fundamental and essential characteristics of cable systems, such as mesh and lacing, is presented in this report. This model enables a direct assessment of the effect of relevant parameters and is therefore of great practical use. The model can also be used to obtain a better understanding of the mechanisms involved in the support function of mesh and lacing.

One of the most revealing findings from this project was the general incompatibility between wire mesh and lacing and the yielding tendons in terms of stiffness and strength. The effective strength of the wired mesh was found to be severely reduced by stress concentrations associated with the tendons and, to a lesser extent, the lacing. As the effective stiffness of mesh and lacing increases with increasing deformation, the incompatibility is especially evident at the initial stages of deformation. Suggestions to improve the compatibility are made, even though the practical feasibility of these suggestions was not investigated in any detail. A potential problem with providing too much stiffness to fabric support has also been identified.

Other relevant observations were the erratic performance of some cone bolts and a relatively high peak resistance compared to the yielding resistance in Durabar tendons. The characteristics of the yielding tendons control to a large extent the performance of the support systems that have been tested and it is therefore important that these characteristics match specifications under all loading conditions.

Contrary to previous findings, welded mesh was *not* found to be stiffer than diamond mesh. A possible explanation for this finding is the full-scale size of the current tests, compared to the small-scale tests previously conducted.

Acknowledgements

The work presented here results from funding provided by SIMRAC. The co-operation, support and constructive criticism of members of the SIMGAP committee were appreciated and are hereby acknowledged.

Table of Contents

- [EXECUTIVE SUMMARY](#) 2
- [ACKNOWLEDGEMENTS](#) 3
- [TABLE OF CONTENTS](#) 4
- [LIST OF FIGURES](#) 5
- [LIST OF TABLES](#) 6
- [1 INTRODUCTION](#)** 7
 - [1.1 GENERAL](#) 7
 - [1.2 AIMS AND OBJECTIVES](#) 10
- [2 LITERATURE SURVEY](#)** 10
 - [2.1 TUNNEL SUPPORT DESIGN CONSIDERATIONS](#) 10
- [3 MESH AND LACING CHARACTERISTICS](#)** 11
 - [3.1 CONCEPTUAL MODEL](#) 12
- [4 QUASI-STATIC TESTING](#)** 22
 - [4.1 RESULTS](#) 23
 - [4.1.1 Calibration of Load Cells and High Pressure Pump](#) 24
 - [4.1.2 Summary and Discussion](#) 24
 - [4.1.3 Conclusions](#) 29
- [5 DYNAMIC TESTING](#)** 30
 - [5.1 RESULTS](#) 31
 - [5.1.1 Summary and Discussion](#) 32
- [6 DISCUSSION AND RECOMMENDATIONS](#)** 34
- [7 REFERENCES](#)** 37
- [APPENDICES](#)** 38

List of Figures

FIGURE 1-1	LOAD TRANSFER IN A TYPICAL SUPPORT SYSTEM	8
FIGURE 1-2	ENERGY ABSORPTION THROUGH BULGING (TOP) AND INTO TENDONS (BOTTOM)	9
FIGURE 3-1	TYPICAL LOAD DISTRIBUTION IN MESH AND LACING SUBJECTED TO A POINT LOAD	12
FIGURE 3-2	RATIO BETWEEN VERTICAL LOAD AND MESH/CABLE FORCE AS A FUNCTION OF DEFORMATION	14
FIGURE 3-3	LOAD DEFORMATION CHARACTERISTICS FOR MESH AND LACING WITH AN IN-PLANE STIFFNESS OF 100 TON/M	15
FIGURE 3-4	LOAD-DEFORMATION CHARACTERISTICS FOR MESH AND LACING WITH AN IN-PLANE STIFFNESS OF 1000 TON/M	15
FIGURE 3-5	LOAD CARRYING CAPACITY FOR VARYING IN-PLANE STRENGTH AND STIFFNESS	16
FIGURE 3-6	ACTUAL STIFFNESS AS A FUNCTION OF DEFORMATION AND IN-PLANE STIFFNESS	17
FIGURE 3-7	LOAD BEARING CAPACITY AND REQUIRED STIFFNESS FOR A CONSTANT MESH/CABLE FORCE OF 10 TONS	18
FIGURE 3-8	ACTUAL STIFFNESS AS A FUNCTION OF (CONSTANT) IN-PLANE FORCE AND DEFORMATIONS	19
FIGURE 3-9	EFFECT OF VARYING IN-PLANE STIFFNESS ON ENERGY ABSORPTION CAPACITY FOR A MESH/CABLE STRENGTH OF 10 TON	20
FIGURE 3-10	EFFECT OF VARYING IN-PLANE STIFFNESS ON ENERGY ABSORPTION CAPACITY FOR A MESH/CABLE STRENGTH OF 20 TON 21	21
FIGURE 4-1	TESTS IN WHICH TENDONS WERE USED TO SUPPORT THE MESH/LACING	25
FIGURE 4-2	TESTS IN WHICH BRICK COLUMNS WERE USED TO SUPPORT THE MESH	26
FIGURE 4-3	TESTS IN WHICH BRICK WALLS WERE USED TO SUPPORT THE MESH/LACING (SPACED AT 1.0 M)	27
FIGURE 4-4	TESTS IN WHICH BRICK WALLS WERE USED TO SUPPORT THE MESH/LACING (SPACED AT 1.5 M)	27

List of Tables

[TABLE 3-1](#) [SUPPORT EFFECTIVENESS OF VARIOUS MESH/LACING SYSTEMS](#) 21
[TABLE 4-1](#) [CALIBRATED PARAMETERS FOR THE LOAD CELLS \(NUMBERS IN RECORDED UNITS\)](#)..... 24
[TABLE 5-1](#) [SUMMARY OF DYNAMIC PARAMETERS](#) 32

1 Introduction

1.1 General

Tunnel support systems, comprising tendons, fabric and the self-supporting characteristics of the rock mass, are typically designed to contain a potentially unstable fractured zone of rock mass around excavations in deep-level mining environments. Under quasi static loading conditions, the fractured rock mass zone may be subjected to large deformations that need to be accommodated by the support system. Dynamic loading conditions, which are induced either by external seismic activity, or by local strain bursts, can result in the ejection of unstable rock into the excavation. Tunnel support systems have to be designed for both quasi-static and dynamic loading conditions, but the latter imposes the most severe requirements, including absorption of the imparted kinetic energy and associated deformations. In this project, the effects of dynamic loading are therefore specifically addressed.

In order to monitor the effects of extreme dynamic loading conditions on various tunnel support systems, a real scale physical model has been used. This model consists of a simulated rock mass, contained by different support systems comprising both tendons and fabric elements in various tests. Impact loading from a drop weight induces the dynamic loading and impact energy and the monitored response allows an analysis of the support performance.

In addition to these impact tests, quasi-static tests have also been conducted. The purpose of these tests is to obtain the load deformation characteristics of support components and systems. The data obtained from the quasi-static tests have been used to interpret the results of the impact tests.

The test results are strictly applicable to situations in which similar boundary conditions, loading conditions and rock mass conditions prevail. Although an attempt has been made to reproduce such conditions as closely as possible, it is not claimed that the tests are a perfect representation of reality. Nevertheless, these tests do enable an assessment of the performance and capacity of realistic support systems and allow the identification of shortcomings and potential improvements. A conceptual, analytical model representing the load deformation behaviour of strings (lacing and mesh) has been developed. This model does allow for a quantification of stiffness, strength and energy absorption capacity and is applicable to static and dynamic loading conditions. Results of the quasi-static tests allowed for calibration of this analytical model. The analytical model can for instance be used to determine optimum boundary conditions for various support components and systems and is generally useful for a clear and concise description of system behaviour.

Containment of the rock can be achieved by ensuring anchorage beyond the limit of fractured rock mass in stable rock, with sufficient capacity within the support system to accommodate the full rock mass loading and deformation. In fragmented rock masses, a relatively large proportion of the loading may be transmitted via the fabric support according to this design concept. In such cases it is necessary to design the fabric support elements in terms of strength, stiffness and yielding capacity. It is equally important to avoid high stress concentrations, which may lead to premature failure of one or other of the support components. Alternatively, the support system may act to reinforce the skin of the unstable rock mass in such a way as to create a stable zone in the form of a strong shell, capable of withstanding envisaged loading conditions. In such designs, the requirements for fabric support are reduced as the interaction between

tendons and rock mass provides the necessary strength and stiffness. In reality, in highly stressed tunnels with severely fractured excavation walls and subjected to dynamic loading, some combination of these support mechanisms can be expected to act upon the rock mass within most support systems. To further complicate the design problem, the proportionate influence that each support component plays is affected by the “integrity” of the rock mass. With increasing deformations, unravelling and loss of integrity can have a pronounced effect on the load distribution between the rock mass and the various support components. Haile (1999) identified many of these issues and investigated their influence on support design by means of numerical modelling. This project builds on these foundations and attempts to quantify the support performance of various support combinations in order to provide a better basis for support design.

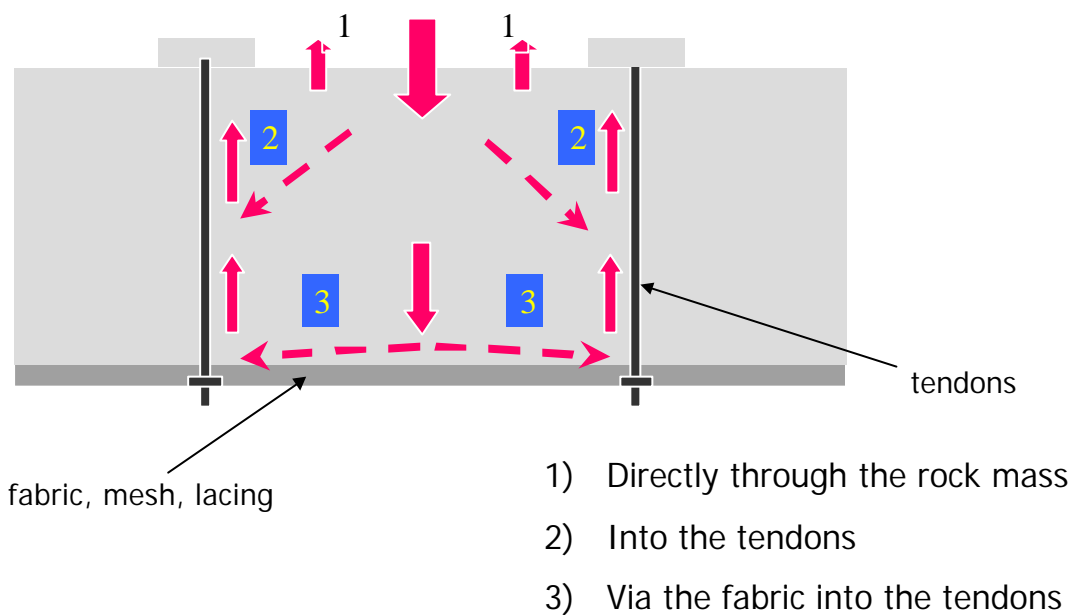


Figure 1-1 Load transfer in a typical support system

Energy can be absorbed in various ways. In the context of tunnel (and stope) support systems, energy absorption is often associated with yielding tendons (and props). However, this mode of energy absorption is only relevant in a relatively competent rock mass. As soon as relatively large rock mass deformations between the support units can take place, energy is absorbed locally by the fabric support and within the unraveling rock mass. In such cases, a stiff fabric support attracts large impact forces and small deformations, while a softer fabric will be subject to large deformations and smaller forces. The stiff fabric is therefore more prone to failure, but is able to prevent rock mass unravelling, as long as it does not fail. The softer fabrics have a much smaller capacity to prevent rock mass unravelling, but they do have a relatively large (elastic) energy absorption capacity. It is therefore important and relevant for any support system design to decide what the prevailing rock mass conditions are and how potential energy impulses are to be absorbed in the various components of such a system. Figure 1-1 demonstrates the concept of load transfer and Figure 1-2 illustrates the two extremes in terms of energy absorption.

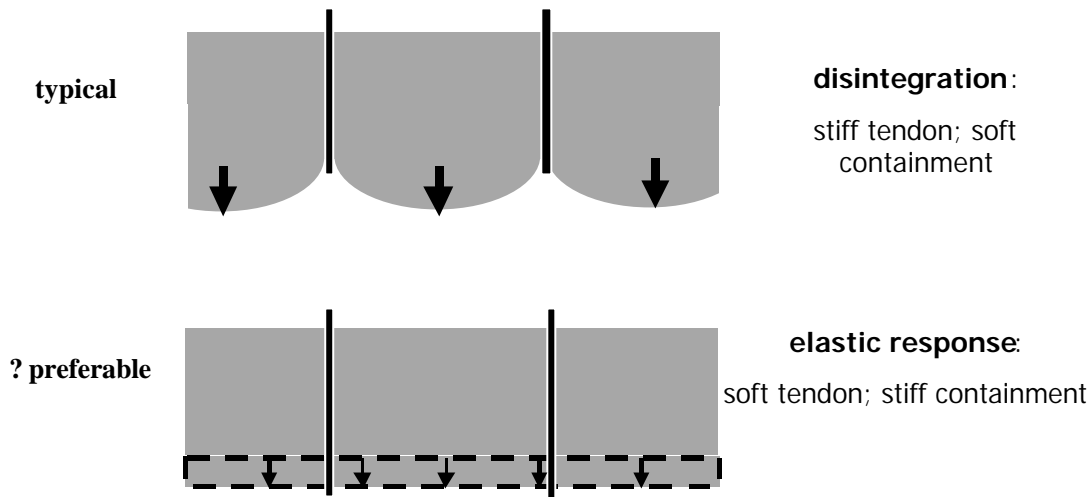


Figure 1-2 *Energy absorption through bulging (top) and into tendons (bottom)*

In this project, relatively soft fabric components, in combination with yielding tendons, have been evaluated in an artificial rock mass that could be described as “incompetent”. The results indicate the limitations of this type of support system in that the yielding of the tendons is often not invoked. A situation as shown in the top of Figure 1-2 is typical for most of the tests conducted: relatively soft fabric combined with stiff tendons leading to bulging of the rock mass and ultimate failure of the, relatively weak, fabric. Most of the impact energy is absorbed by the fabric and the dilating rock mass; the tendons hardly contribute in this scenario.

A response as sketched in the bottom of Figure 1-2 may be obtained with a relatively stiff fabric support. However, depending on the shape of the excavation, the associated deformations may be restricted. If that is the case, energy cannot be absorbed through large deformations and the system may thus attract large forces and be prone to violent failure. This issue requires further research, as it is extremely important to have a realistic understanding of energy absorption potential.

The original aim of this project was to investigate a large variety of fabric support components, including shotcrete and membranes. However, due to financial constraints, the SIMRAC committee has agreed upon limiting this project to the evaluation of mesh and lacing. This decision was made during one of the initial progress meetings.

1.2 Aims and Objectives

The main objective of the project is to determine the effectiveness of various support systems in rockburst conditions. By quantifying the impact absorption of a range of tunnel support systems and by quantifying the load distribution between the various components in a typical tunnel support system, this objective is addressed. Practical design considerations have been investigated as well.

In order to achieve these goals, various existing tunnel support components have been evaluated under conditions representing an underground tunnel rockburst as closely as possible. The relevant conditions can be summarised as follows:

- Application of a dynamic load that induces ground velocities of several metres per second
- Discontinuous, fragmented rock-like material
- Full scale components, assembled in a realistic support system

In order to obtain detailed and complete load-deformation characteristics of the various support components, quasi-static loading tests have been conducted. A conceptual model, capturing the essential characteristics of typical cable and mesh components, has also been developed.

2 Literature Survey

2.1 Tunnel Support Design Considerations

In order to provide stability around an underground excavation, two principal support mechanisms are available. The first is based on the containment of the unstable rock mass skin, while the second is based on creation of a stable shell. Containment is achieved by ensuring anchorage into stable rock, beyond the limit of unstable rock. Effectively, the unstable, fractured and fragmented rock mass is pinned to a substrate of solid rock. This is the most common support philosophy in a hard rock mining environment and the underlying assumption is that, beyond a relatively limited skin of unstable rock, stable elastic conditions prevail.

The creation of a stable shell can be achieved in various ways. Such a shell can be an artificial structure, which might be required when the rock mass itself is so incompetent that it cannot be effectively reinforced. Such conditions are mainly encountered in weak rock and soils. More competent rock can be reinforced by, for instance, tendons, and a stable shell may be generated within the skin of the excavation. These shells are capable of providing an effective support pressure and are in principle suitable to control unstable closures in an otherwise unstable excavation.

In most support systems, some combination of these two principal support mechanisms may be encountered (Haile, 1999). The concept of the creation of a structurally competent reinforced rock mass arch is the basis of most of the empirical rockbolt design methods (Stillborg, 1986) and thus generally applies in the South African gold mines as well.

The containment mechanisms allows for a straightforward and relatively simple support design methodology. In its simplest form, it is assumed that the tributary area theory can directly be applied to the tendons, which are supposedly anchored in stable rock beyond the limits of the fractured and fragmented skin (Wojno and Jager, 1987, Stilborg, 1986). Since rockbursts results in the most severe loading condition, the tendons are designed to absorb the energy associated with the arresting of a certain volume of unstable rock that has been accelerated to a certain velocity. The same principle is applied in stope support design (Wagner, 1983, Wojno, Jager and Roberts, 1987). While this method allows the selection of appropriate tendons with the required characteristics, case studies (Haile, 1999, Güler *et al.* 2001) suggest that the typical support failure is not associated with failure of tendons, but rather with the unravelling and ejection of rock in between such tendons. The tendons are not subjected to the assumed tributary area loading and hence even non-yielding tendons do survive rockbursts. Although the presence of mesh and lacing provides a local support function in the areas between tendons, it is obvious that this support function is relatively limited when compared to that of the tendons themselves. The support components within a typical tunnel support system are not compatible, which often results in premature failure of the mesh, being the weakest link in the system. (Haile, 1999, Güler *et al.* , 2001).

Previous studies on the performance of mesh and lacing (Güler *et al.*, 2001, Kaiser *et al.*, 1996, Ortlepp, 1983, Stacey and Ortlepp, 1997) have provided relevant data. It is important, however, to consider the boundary and loading conditions which were applied in these studies. Mesh and lacing are relatively simple components whose performance is controlled entirely by their tensile strength and *in-plane* stiffness. Shear forces are not transmitted directly as bending moments cannot be accommodated. The bending stiffness and bending resistance of these support components is negligible in comparison.

In the Canadian Rockburst Support Handbook (Kaiser *et al.*, 1996), recommendations are made with respect to the requirements for tunnel support under rockburst conditions. The function of the holding elements (i.e. the tendons) includes the absorption of energy under severe conditions according to this handbook. It is also mentioned that individual holding or retaining elements are ineffective in preventing rockfalls between directly supported areas. The requirements for the retaining elements are not quantified, but the ability to absorb kinetic energy and withstand impact loads is mentioned. Pull tests have been conducted to measure the load-deformation characteristics of mesh and shotcrete. Mesh-reinforced shotcrete was found to be more efficient in absorbing energy than mesh alone and, due to its initial high stiffness, has a better load bearing capacity compared to regular mesh *at small deformations*. (Kaiser *et al.*, 1996). As high stiffness and energy absorption capacity are mutually exclusive, it is unclear which property, under which conditions, is recommended to be desirable. From interpretation it appears that an initial stiffness and strength is useful to cater for less severe conditions, while large energy absorption capacity, associated with large bulking of the rock mass, is recommended for the more severe cases.

3 Mesh and Lacing Characteristics

In order to obtain a realistic insight in the performance and behaviour of typical mesh and lacing, the following conceptual model is presented. This model can be used to investigate

relevant properties such as stiffness, strength and energy absorption capacity and is applicable to both static and dynamic loading conditions.

Although the model is a two-dimensional representation, it is possible to expand it into a more realistic 3-D geometry. However, for the purpose of calibrating the tests conducted in this project, the two-dimensional model is of sufficient practical relevance. The non-linear stiffness characteristics (in the loading direction) and their effects on strength and energy absorption capacity can easily be assessed and investigated with the aid of the model.

The loading and boundary conditions have been simplified to a point load in the centre and either a constant *in-plane* stiffness (C), or a constant in-plane force (F). These conditions can also be changed into more realistic and complex ones, but this was not deemed to be necessary for the purpose of this project. The results of all tests can, in principle, be explained on the basis of this (simple) conceptual model.

3.1 Conceptual Model

The essence of the behaviour of mesh and lacing is the fact that these components can, for all practical purposes, not transmit any shear forces, but rely on their tensile strength and deformation capacity. In order to illustrate this concept, reference is made to Figure 3-1, where simple load distribution scenarios are analysed.

Figure 3-1 is a two dimensional representation and the load should be considered a line load in the case of mesh. Nevertheless, this representation illustrates the parameters that are relevant with respect to load deformation characteristics of mesh and lacing.

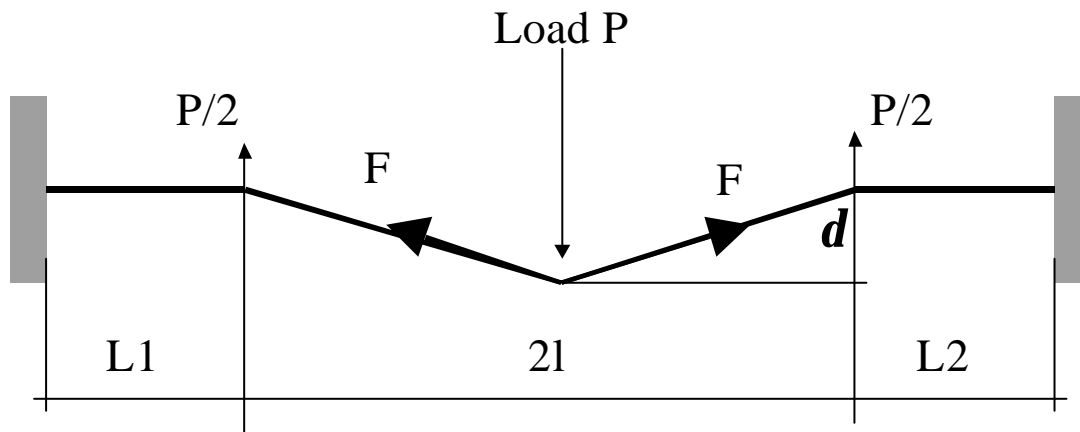


Figure 3-1 Typical load distribution in mesh and lacing subjected to a point load

The relationship between the force F and the load P is strongly dependent on the deformation d and this deformation in turn is directly related to the stiffness in the system. This stiffness is not only characterised by the tensile stiffness of the mesh or lacing, but also by the boundary conditions and the initial slack and shape. If it is assumed that the initial shape of the mesh or lacing is planar or straight and no initial slack is allowed for, then only the boundary conditions still need to be accounted for. The boundary conditions in Figure 3-2 are two fixed points where the vertical load is absorbed (tendons). The extensions $L1$ and $L2$ represent the potential for mesh or lacing to deform in a horizontal direction across the two fixed points. This potential can be quantified by a stiffness parameter which is a function of the in plane stiffness

and the length of the free extensions. The length of these extensions is related to local conditions and is inversely related to the system stiffness.

As

$$\frac{P}{F} = \frac{2}{\sqrt{1 + \left(\frac{l}{d}\right)^2}} \quad (3.2.1)$$

It follows that large deformations are leading to equivalent values for the vertical load (P) and the force (F) in mesh or lacing. Small deformations are associated with a small vertical load (P) in relation to the force (F). Large deformations can therefore not be avoided in mesh and lacing systems, as the capacity (F_{\max}) of such systems is obviously limited. In fact, any attempt to restrict the deformations by stiffening the system, may result in premature failure at relatively low loading and deformation.

Relationship (3.2.1) expresses the “efficiency” of the mesh and/or lacing and it is obvious that small deformations are associated with limited efficiency (Figure 3-2). The stiffness of the system does not affect this relationship, although it does affect the absolute values of force and load.

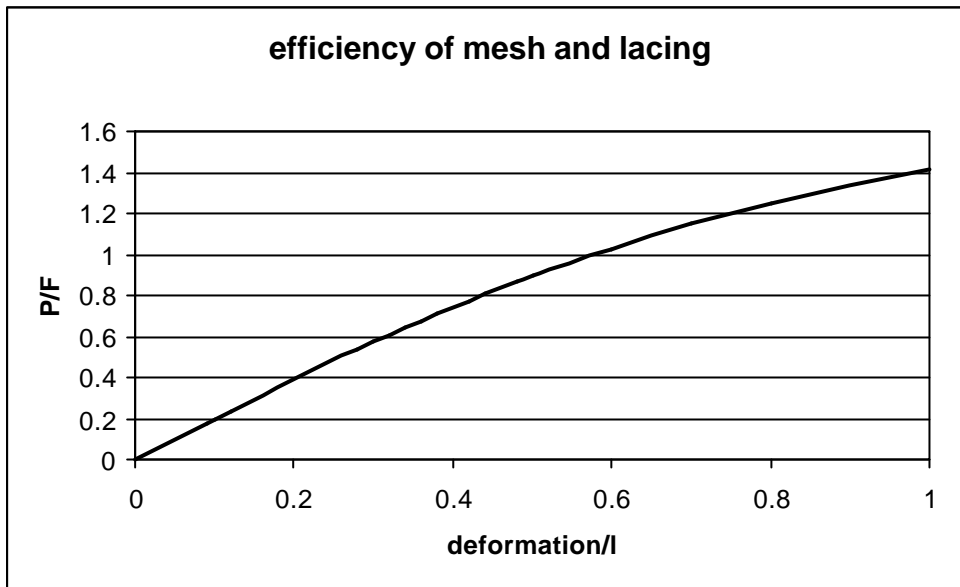


Figure 3-2 Ratio between vertical load and mesh/cable force as a function of deformation

The *in-plane* stiffness and strength of the lacing or mesh will determine the response to vertical loading. For this reason it is important to determine load deformation characteristics of the mesh and lacing in direct tension. If the in plane stiffness of the lacing or mesh, including “boundary stiffness” is expressed by $C = \frac{F}{\Delta l}$, it follows that:

$$P = \frac{2C\Delta d}{l + \Delta l} \quad (3.2.2)$$

This expression can also be expressed as:

$$P = \frac{2C\mathbf{d}(\sqrt{l^2 + \mathbf{d}^2} - l)}{\sqrt{l^2 + \mathbf{d}^2}} = 2C\mathbf{d} \left(1 - \frac{1}{\sqrt{1 + \left(\frac{\mathbf{d}}{l}\right)^2}} \right) \quad (3.2.3)$$

By combining (3.2.1) and (3.2.3), the in-plane force can be expressed as:

$$F = C(\sqrt{l^2 + \mathbf{d}^2} - l) \quad (3.2.4)$$

Expressions (3.2.3) and (3.2.4) are graphically displayed in Figure 3-3 for a particular stiffness $C = 100\text{ton}/m$ and $C = 1000\text{ton}/m$. Note that both the vertical load and the in-plane force are linearly related to the *in-plane* stiffness. An increase in stiffness will therefore lead to an increase in both the cable and/or mesh force as well as in the vertical load. Note how the system stiffness ($dP/d\mathbf{d}$) increases with increasing vertical deformation. This non-linear system stiffness is essential to the behaviour of mesh and lacing.

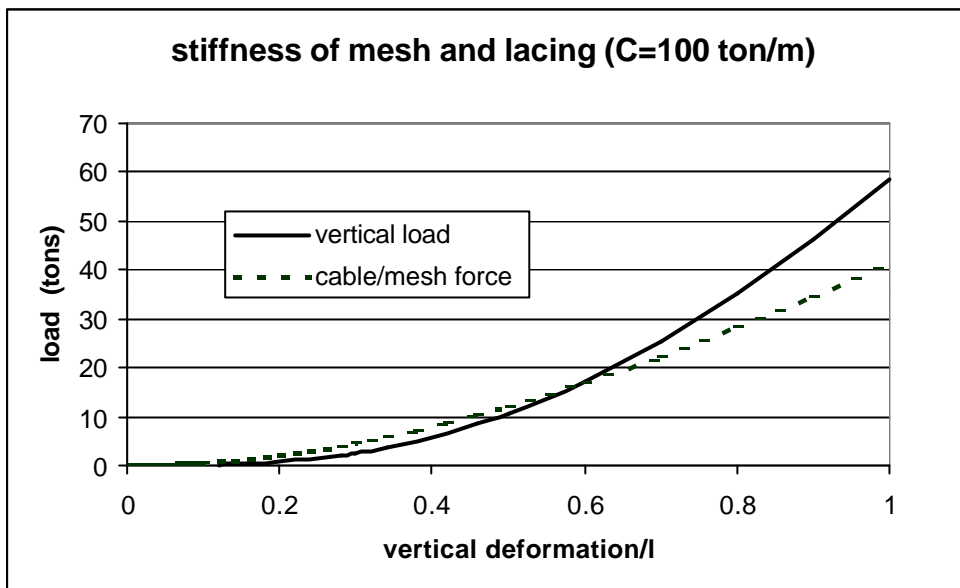


Figure 3-3 Load deformation characteristics for mesh and lacing with an in-plane stiffness of 100 ton/m

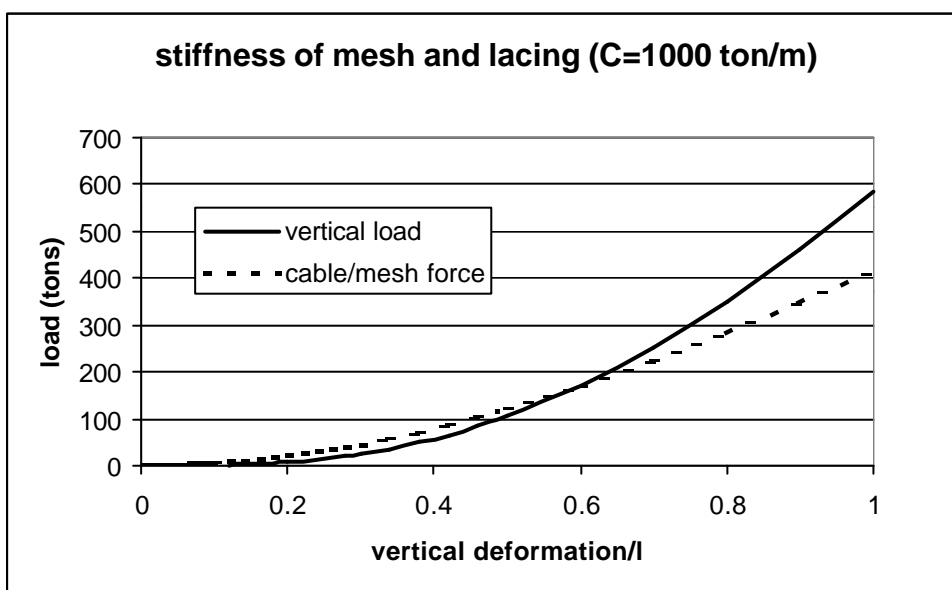


Figure 3-4 Load-deformation characteristics for mesh and lacing with an in-plane stiffness of 1000 ton/m

While limiting deformations may be a requirement for any support system, it is important to realise that such a requirement negatively affects the load bearing capacity of mesh and lacing. If it is important to limit deformations to relatively small levels, the strength and stiffness of the mesh/lacing has to be increased substantially in order to maintain the required load bearing capacity which would otherwise be associated with larger deformations.

As may be appreciated from Equations (3.2.3) and (3.2.4), both the cable or mesh forces and the vertical load are linearly related to the stiffness constant C . However, this does not imply that the load carrying capacity is linearly related to this stiffness constant. The mesh/cable will fail once the maximum strength has been reached and the relationship between load bearing capacity and stiffness can be established with the use of Equations (3.2.3) and (3.2.4) and the

assumption of a certain maximum *in-plane* force F_{\max} . The maximum allowable vertical load is then expressed as:

$$P_{\max} = 2\sqrt{\frac{2F_{\max}}{Cl} + \frac{F_{\max}^2}{(Cl)^2} \left(\frac{F_{\max}}{1 + F_{\max}/Cl} \right)} \quad (3.2.5)$$

Figure 3-5 demonstrates how the *in-plane* stiffness C and the *in-plane* strength F_{\max} affect the load carrying capacity.

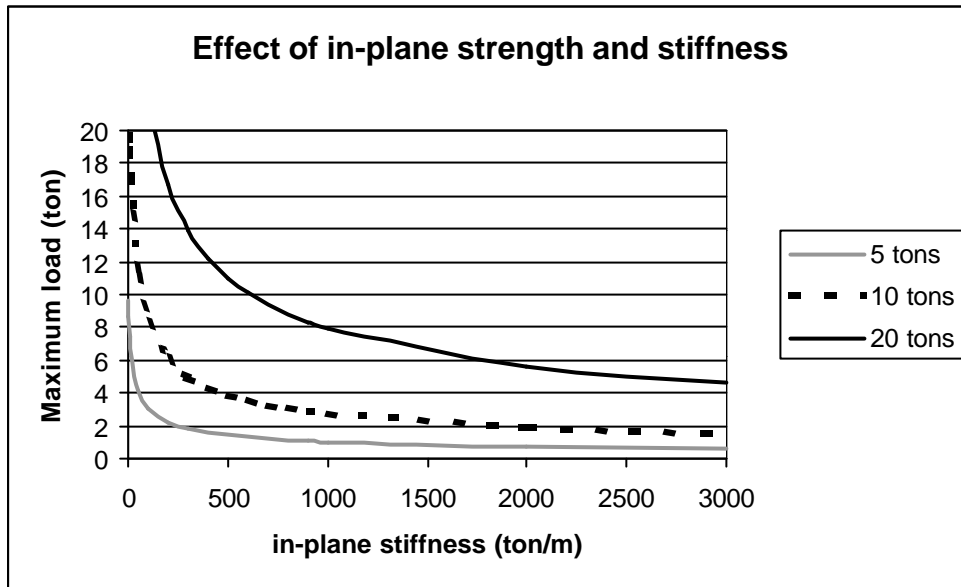


Figure 3-5 Load carrying capacity for varying in-plane strength and stiffness

Figure 3-5 shows how increasing *in-plane* stiffness leads to decreasing load carrying capacity. It also shows how increasing *in-plane* strength increases the load carrying capacity. What may not be immediately obvious is that an increase in strength becomes more effective with increasing *in-plane* stiffness. The reason for this is the fact that the increased strength allows for increased deformations and hence more efficient load distribution. The previous two figures, 3-3 and 3-4, enable an estimation of deformations associated with the maximum load carrying capacity as shown in Figure 3-5.

The actual stiffness can be derived from Equation (3.2.1) and (3.2.4) and is expressed by:

$$\frac{dP}{d\mathbf{d}} = 2C \left(1 - \frac{1}{\left(1 + \left(\frac{\mathbf{d}}{l} \right)^2 \right)^{3/2}} \right) \quad (3.2.6)$$

Figure 3-6 is a graphical representation of Equation (3.2.6) and shows how the actual stiffness develops with increasing deformation.

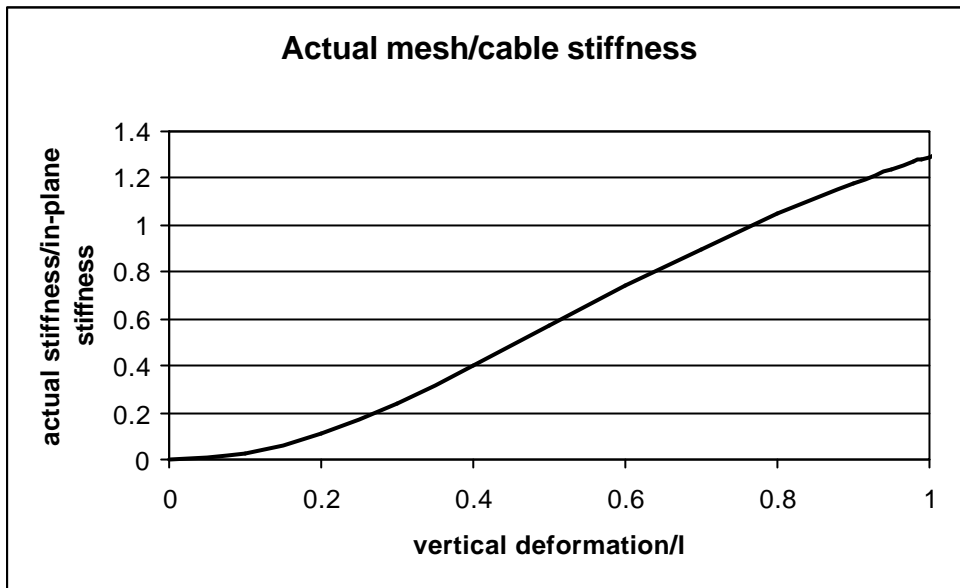


Figure 3-6 Actual stiffness as a function of deformation and in-plane stiffness

The non-linear stiffness of the mesh/cable can be obtained from Figure 3-6. With increasing deformations, the stiffness asymptotes to a maximum value of twice the *in-plane* stiffness, but this only applies to unrealistically large deformations. The stiffness values can directly be used to calculate the response of mesh and/or lacing to impacts, as the impact *force* and impact *duration* are directly related to this stiffness.

The vertical load shown in Figure 3-7 is derived from Equation 3.2.1 by assuming a constant mesh/cable force F . Such a condition could be achieved by pre-stressing the mesh/cable and by implementing some kind of yielding device. In such a case, optimum use is made of the potential of the mesh/cable. It is clear from this graph that, compared with the conventional situation as shown in Figure 3-3 and Figure 3-4, the mesh/cable is far more efficient at lower deformations.

In Figure 3-7 the *in-plane* stiffness, which would be required to induce the constant mesh/cable force, is also shown. In the absence of any pre-stressing and/or yielding devices, a variable *in-plane* stiffness could provide the same results. However, this appears to be an impractical solution.

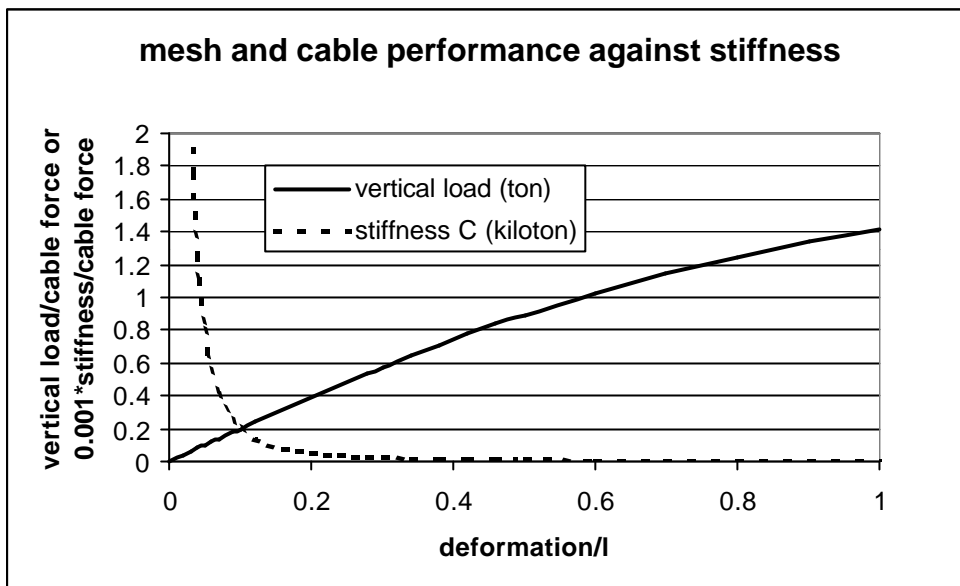


Figure 3-7 Load bearing capacity and required stiffness for a constant mesh/cable force of 10 tons

The actual non-linear stiffness can also be expressed for this case:

$$\frac{dP}{d\mathbf{d}} = \frac{2F}{\left(1 + \left(\frac{\mathbf{d}}{l}\right)^2\right)^{3/2}} \quad (3.2.7)$$

This expression is graphically depicted in Figure 3-8 where it is shown that the actual stiffness decreases with increasing deformation and that the actual stiffness is linearly related to the mesh/cable force. A direct comparison between Figure 3-8 and Figure 3-6 is not straightforward, as the actual stiffness is linearly related to the *in-plane* stiffness in the conventional case as shown in Figure 3-6. With increasing deformation, the mesh/cable force also increases in the conventional case and the strength of the mesh/cable will limit the allowable deformations and associated actual stiffness.

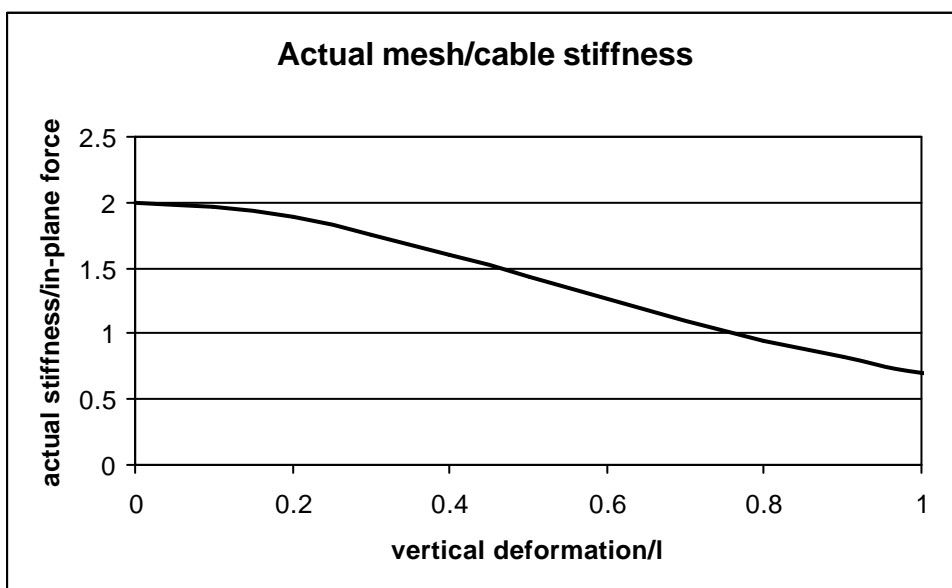


Figure 3-8 Actual stiffness as a function of (constant) in-plane force and deformations

From Figures 3-7 and Figure 3-8, it is clear that pre-stressing and maintaining a constant *in-plane* mesh/cable force can dramatically improve actual stiffness and resistance. However, some form of yielding device is required in order to prevent increasing *in-plane* forces and associated failure.

The limiting factor in most practical applications will be the strength of the mesh and lacing and this, in combination with the system stiffness C , will determine load bearing capacity, as well as energy absorption capacity. Two extreme cases can be considered again, namely the situation with a constant *in-plane* stiffness C and the situation with a constant (yield) force F . The energy absorption capacity, which is effectively a product of deformation and load bearing capacity, can be evaluated for both cases.

Energy absorption capacity in case of a constant *in-plane* stiffness C :

$$2C \int_0^{d_{\max}} \left(d - \frac{d}{\sqrt{1 + \left(\frac{d}{l}\right)^2}} \right) dd = 2C \left[\frac{d^2}{2} - l\sqrt{l^2 + d^2} \right]_0^{d_{\max}} = 2C \left(\frac{d_{\max}^2}{2} + l^2 - l\sqrt{l^2 + d_{\max}^2} \right) \quad (3.2.8)$$

whereby d_{\max} is the critical deformation at which the maximum *in-plane* force F_{\max} is reached. The critical deformation can be derived from equation 3.2.4 and can be expressed by:

$$d_{\max} = \frac{1}{C} \sqrt{F_{\max}^2 + 2F_{\max} Cl} \quad (3.2.9)$$

At this point the system fails and the maximum energy absorption capacity has been obtained.

In the case of a constant *in-plane* force F , the energy absorption capacity becomes:

$$2F \int_0^{d_{\max}} \frac{d}{\sqrt{l^2 + d^2}} dd = 2F \left[\sqrt{l^2 + d^2} \right]_0^{d_{\max}} = 2F \left(\sqrt{l^2 + d_{\max}^2} - l \right) \quad (3.2.10)$$

Equations 3.2.8 and 3.2.10 are graphically expressed in Figures 3-9 and 3-10 where the effect of stiffness on energy absorption capacity of the mesh/lacing can be observed for two *in-plane* strength values. The span l has been taken as 1 in both cases. Increasing stiffness leads to a decreased deformation capacity and thus energy absorption capacity. The constant force situation leads in all cases to the most efficient system allowing (theoretically) unlimited deformation. An increase in strength results in a similar increase of energy absorption capacity in the case of a constant *in-plane* force F . However, in the more common case of a constant *in-plane* stiffness C , an increase in strength leads to a disproportional increase in energy absorption capacity. Doubling the strength in the example cases resulted approximately in a six-fold increase of energy absorption capacity. (Termination of the graphs indicate the relevant failure point).

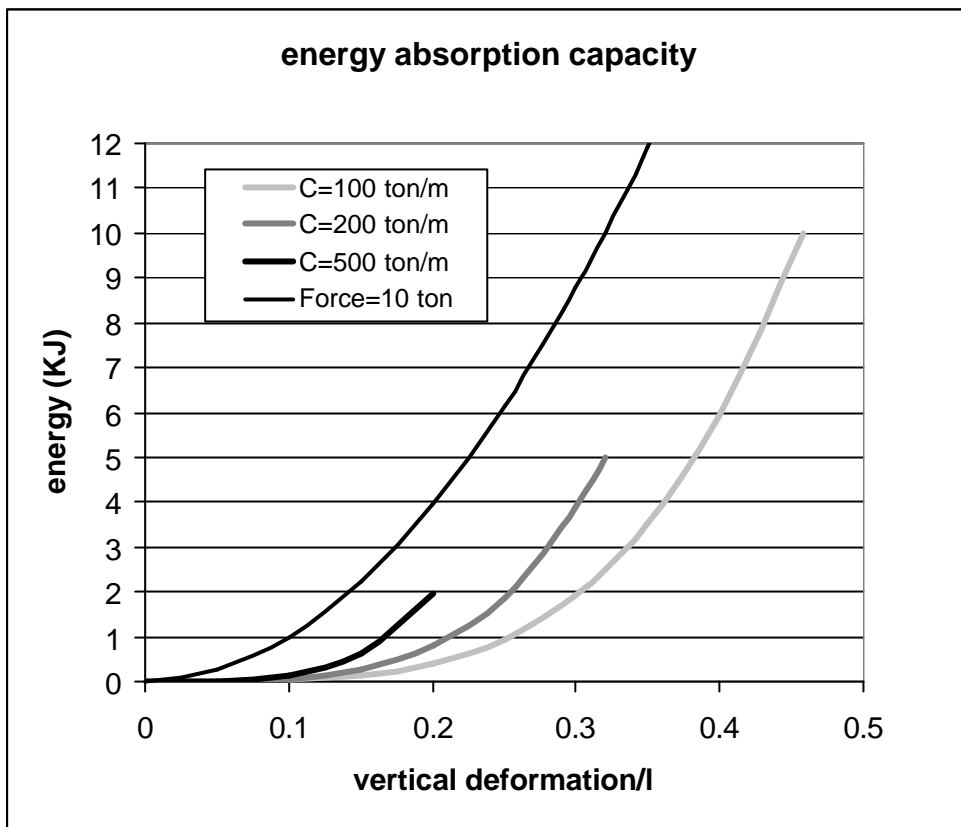


Figure 3-9 Effect of varying in-plane stiffness on energy absorption capacity for a mesh/cable strength of 10 ton

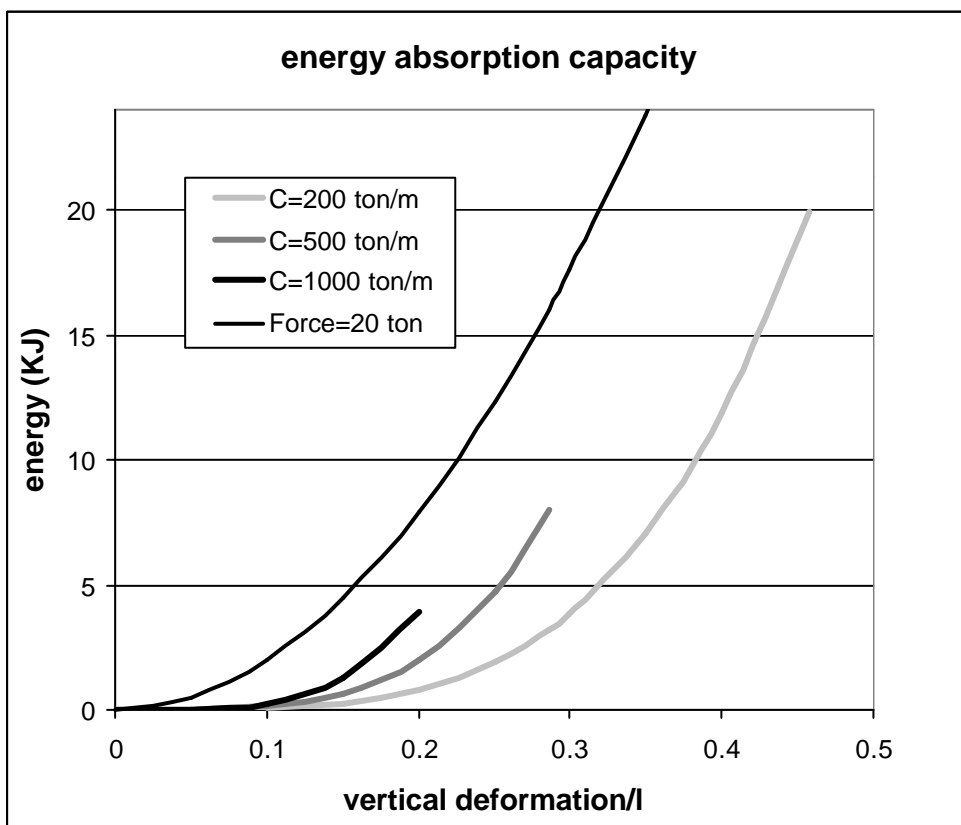


Figure 3-10 Effect of varying in-plane stiffness on energy absorption capacity for a mesh/cable strength of 20 ton

Figures 3-9 and Figure 3-10 illustrate the effects of *in-plane* stiffness and strength on energy absorption capacity in the same way as Figure 3-5 illustrates the effects on load carrying capacity.

The *in-plane* stiffness has a similar effect on load bearing capacity as on energy absorption capacity. A reduction in stiffness results in larger deformations that benefit both properties. The *in-plane* strength of the support system has a larger effect on energy absorption capacity than on load bearing capacity. This is related to the applicable influence of deformations, as can be appreciated from Equations 3.2.8 and 3.2.3, respectively. Limiting deformations will affect the load bearing capacity as well as the energy absorption capacity. In a mesh/cable system, it is impossible to obtain adequate support performance without accepting substantial deformations. These deformations are normally induced by the dilating rock mass.

An optimum balance may be found between maximizing load bearing capacity and limiting the deformations. Quantifying the ratio between load bearing capacity and deformation may appear a reasonable way of doing this, but this merely results in an exponential relationship with increasing deformations. A more realistic approach might be to assign weighting factors to these parameters. The maximum deformation considered is assigned a zero weighting factor, while zero deformation is associated with a maximum value. Any intermediate values can be determined according to a linear interpolation. The same can be done with the load bearing capacity, which may be given a different weighting according to its relative importance in a particular application.

As an example, the same weighting factor for deformations as for load bearing capacity has been used. Considering an absolute maximum deformation equal to half the span and an absolute maximum load bearing capacity of twice (Equation 3.2.1) the in plane strength, an optimum stiffness can be determined. With an *in-plane* stiffness of 1000 ton/m and an *in-plane* strength of 10 ton, the maximum deformation (Equation 3.2.9) is 0.14 m, while the load bearing capacity (Equation 3.2.3) is 2.7 ton in that case. The deformation therefore scores 72 % and the load bearing capacity a meager 13 %.

Similar calculations have been performed for a variety of strength and stiffness values and the results are shown in Table 3-1.

Table 3-1 Support effectiveness of various mesh/lacing systems

<i>In-plane</i> Stiffness (ton/m)	<i>In-plane</i> Strength	Actual load bearing Capacity/potential load bearing capacity	Actual deformation/ allowable deformation
100	10	0.42	0.08
200	10	0.30	0.36
500	10	0.19	0.60
1000	10	0.13	0.72
100	20	0.53	0

200	20	0.42	0.08
500	20	0.28	0.43
1000	20	0.19	0.60

Different ratio between weighting factors would obviously affect the judgment, but Table 3-1 can be used to assess the effectiveness of the support system. If deformation and load carrying capacity is given the same weighting factor, an optimum *in-plane* stiffness in excess of 1000 ton/m should be selected when the *in-plane* strength is 10 ton. However, if the load bearing capacity is considered to be four times as important as the deformations, a stiffness of less than 100 ton/m provides the most effective system. Increasing the *in-plane* strength to 20 ton merely results in a similar increase of optimum *in-plane* stiffness.

The same exercise may be done to account for energy absorption capacity.

The use of (yielding) tendons can provide additional energy absorption capacity. It is however essential that the load bearing capacity of the mesh and lacing is adequate, i.e. no failure should occur before the yield strength of the tendons is reached in a particular application. The load bearing capacity can be assessed with the aid of the formulae and graphs presented in this section.

The results presented in this section can be used to design and assess the capacity of mesh and lacing. It is however important that practical considerations such as stress concentrations, load distribution and the initial slack/deformation are taken into account. It is possible to expand the approach adopted here, and account for a large variety of practical possibilities.

4 Quasi-Static Testing

The main purpose of the quasi static testing programme was the evaluation of the load-deformation characteristics of various containment support systems. For practical purposes it has been decided to limit the investigations to support systems based on tendons, mesh and lacing, similar to those used in the impact testing programme.

Initially, the plan was to have an exact replica of the impact tests in order to be able to obtain applicable load deformation characteristics, which could be used to interpret the results from those impact tests. However, after a while it appeared that such an exercise does not provide the required information. The main cause of problems is the interaction of the support system with the artificial rock mass (the concrete bricks in this case). It was inherently assumed that this interaction would result in a certain load distribution, so that a constant percentage of the imposed load would be directly transferred into the tendons and the remainder via the mesh and the lacing. However, it became increasingly clear that the load distribution is subject to changes during each test and is very sensitive to the deformation of the system.

If the percentage of load which is being transferred via the mesh and/or lacing cannot be quantified, it is impossible to determine what the actual capacity and function of the mesh and/or lacing is. For this reason, it was decided to test the mesh and lacing directly, without the artificial rock mass, in order to obtain reliable and consistent load-deformation characteristics. The deformation profiles thus calibrated can be used to determine the actual resistance offered

by the mesh and/or lacing in more complex arrangements; both under static as well as dynamic loading conditions. These calibration tests are essential for any analysis of support systems that include mesh and/or lacing.

Another important practical consideration also became increasingly clear; while the basic behaviour of mesh may be considered as relatively easy to describe, many practical complications do affect its performance. Boundary conditions affect the mesh performance to a large extent and this immediately has implications for the load deformation characteristics, as well as to the load bearing capacity and the energy absorption capacity. Of special interest is the effect of stress concentrations, which are typically encountered at those locations where the mesh is attached to the tendons. Other locations of stress concentration in the mesh may be found around the lacing and, depending on the rock surface configuration, around certain key blocks or protrusions. As failure of the mesh is always initiated at these areas of stress concentrations, it is important to identify potential sources of stress concentration. This is especially relevant as the load bearing capacity of the mesh may be severely reduced due to a non-uniform load distribution associated with such stress concentrations.

Finally, it was considered that if the mesh and lacing have to be designed for a worse case scenario, such a scenario would involve a highly fragmented rock mass, which would be incapable of directing any forces directly to the tendons. In such a case, the tendons and the mesh can be considered as operating in series, as any load would have to be transmitted via the mesh (and lacing) into the tendons. For this reason, the mesh and lacing could be assessed separately and further tests were designed accordingly.

4.1 Results

Various combinations of mesh and lacing were tested in the same rig that was used for the drop tests. The rig was modified to accommodate a hydraulic prop capable of exerting a force of around 220 kN. A high-pressure pump was especially designed so that the prop forces could be varied between zero and the maximum. Initial tests were conducted on support systems that were equivalent to those used in the impact tests and consisted of tendons, an artificial rock mass made up of concrete blocks and mesh and/or lacing. The forces in the tendons were monitored with the aid of specially designed load cells that were also used to record the impact forces. However, in these quasi-static tests, it became clear that the load distribution characteristics changed with increasing deformations, so that the interpretation of the test results became increasingly complicated. With hindsight, this effect might have been expected, as the load distribution is related to the integrity of the artificial rock mass, which in turn is directly associated with imposed deformations. Further tests were therefore conducted on systems consisting of mesh and lacing only, without the additional complication of the artificial rock mass. These tests allowed for a direct assessment of the performance and characteristics of the mesh and lacing and the results could therefore be used to interpret support resistance in the impact tests.

Calibration of the strain gauged load cells was conducted before the actual testing programme. Each load cell was placed in a press and the applied load was related to the output of that load cell. Three sets of strain gauges are placed around the circumference of each load cell and the average monitored strain can be recorded continuously by analogue logging. In practice a data recorder was used which samples at a certain rate. The maximum rate is 3012 records per second and this maximum rate was used to monitor the load history during impacts. During the quasi-static tests, a sampling rate of 1 record per minute was automatically imposed, while manual triggering could also be used to enforce additional recording.

The mesh was firmly attached to and suspended in a frame constructed from tubular steel bars that provided a certain *in-plane* stiffness. The lacing was anchored at special anchor points embedded in the concrete floor of the test rig and this arrangement is also associated with a certain *in-plane* stiffness. The prop force was introduced into the system through a load spreader consisting of steel plates and concrete blocks.

All quasi-static tests and test results are presented in Appendix A, while an overview is given in Section 4.1.2. As has been mentioned before, initial tests were conducted on support systems consisting of tendons, an artificial rock mass and mesh and/or lacing. In the next series of tests, the artificial rock mass was replaced by simple load spreaders, while the tendons were replaced by (stiff) concrete columns. In the last series of tests, the concrete columns were replaced by concrete walls; in order to avoid local stress concentrations as much as possible. From the last two series of tests, calibrated load-deformation characteristics for the mesh and/or lacing can be obtained. These characteristics are essential for any support system analysis.

4.1.1 Calibration of Load Cells and High Pressure Pump

All four strain gauged load cells were calibrated by means of a compression test. Strain changes are monitored in an electric circuit and induce a change in voltage. Actual voltages are recorded and ultimately displayed in numbers. The calibration procedure established the relationship between those numbers and the applied load. This relationship is linear and the parameters are calibrated as shown in Table 4-1.

Table 4-1 **Calibrated parameters for the load cells (numbers in recorded units)**

	Channel 5	Channel 6	Channel 7	Channel 8
No loading	-1929	-1848	-1842	-1759
Change per ton	+37.5	+37.8	+39.6	+37.7

Channel 5 was incorrectly tuned and only started to record loads in excess of a few tons. This channel was therefore ignored in the earlier tests, before the setting was changed. The parameters shown in Table 4-1 were used to quantify tendon forces during the tests.

A high-pressure pump, with a maximum output pressure of 80 MPa, was developed in order to obtain the maximum capacity from the hydraulic prop used to load the system. With the aid of a pressure gauge, the output pressure from the pump could be adjusted manually to any required value. By recording the prop force for certain pump pressures, a relationship between pump pressure and prop force could be obtained. This relationship is linear and it was found through calibration that any 10 MPa pump pressure induces a force of around 55 kN into the hydraulic prop (5.5 ton). The maximum prop force at a pump pressure of 80 MPa is therefore approximately 440 kN.

4.1.2 Summary and Discussion

Details of each quasi-static test are presented in Appendix A. A summary and interpretation of those results are given here. In Appendix A, the energy absorption capacity and the theoretical *in-plane* stiffness of each system have been identified. The last parameter should be treated with some caution, as the boundary conditions for the various tests differ from the simple model

discussed in Chapter 3. In addition, the initial sag, due to dead weight, has not been taken into account. Nevertheless, the presented values are useful for comparative purposes.

The results from the static tests can in principle be explained from mechanisms as described in Section 3.2. In order to facilitate a comparison between the various results, the following graphs have been generated. The graphs in Figure 4-1 show all the results of tests in which tendons and an artificial rock mass were incorporated. The monitored deformations are displayed along the vertical axis, while the induced prop force is displayed along the horizontal axis. Conventionally, deformations are displayed along the horizontal axis and this is therefore emphasized here. In the tests conducted for this programme, the imposed load was transmitted to four or six tendons. In the four-tendon arrangement, the tendons carried on average a quarter of the load, while one panel of fabric was subjected to the full load. In reality, a more uniform load distribution may be imposed, whereby each tendon carries the load imposed on one fabric panel. In the latter case, the strength requirements for the fabric can be severely reduced.

Typical mesh used was either a diamond mesh with an aperture of 100 mm and a wire thickness of 4.2 mm or a welded mesh with the same aperture but with a wire thickness of 3.15 mm.

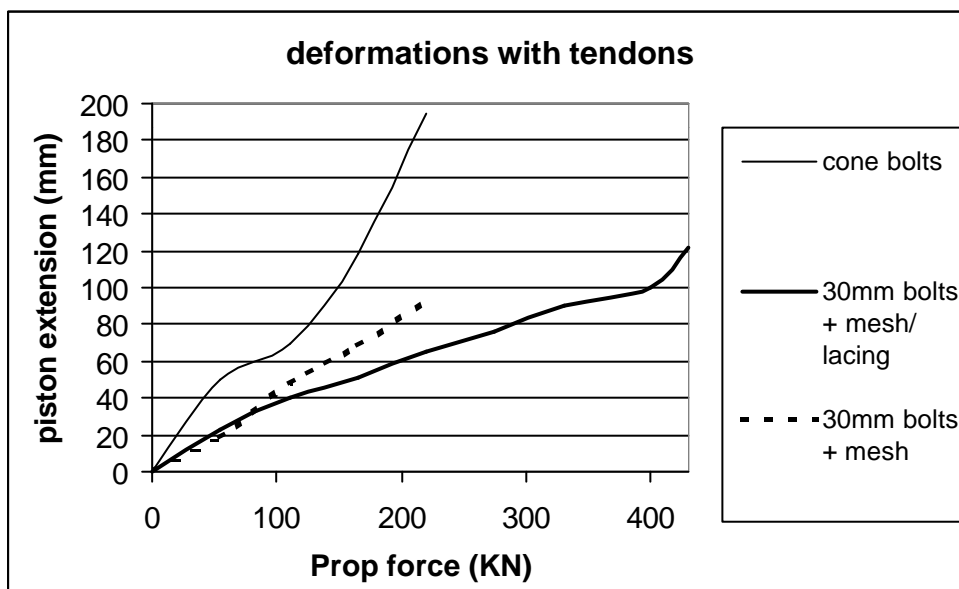


Figure 4-1 Tests in which tendons were used to support the mesh/lacing

The cone bolts were grouted in thin walled piping (3.5 mm) in order to provide relatively low yield resistance. The fabric containment was thus protected from high forces and associated failure. Low resistance, combined with large deformations, resulted from the impact test with cone bolts and no damage occurred to the mesh and lacing. As the cone bolts started yielding at forces that were lower than expected, the resistance of the total support system was too low. The 30 mm non-yielding bolts with mesh, but without lacing, resulted in mesh failure at prop forces in excess of 220 kN and deformations of around 100 mm. The presence of lacing caused an increase in stiffness, as well as strength. At a maximum prop force of 430 kN, only localised mesh damage near the tendons could be observed. The piston extension at that stage was approximately 120 mm. From these observations, the contribution of the various support components is evident. The difference in tendons is most clearly manifested in terms of stiffness. Even before any yielding is observed in the cone bolts, i.e. up to a prop force of 110 kN, the deformations in the system with cone bolts exceeds the deformations in the systems with the 30 mm bolts by more than 50 per cent. This difference can only be explained from the difference in bending and shear resistance between the two bolt types. As the vertical deformations are associated with differential movements in the various brick layers, any

resistance against these differential movements will reduce such movements, as well as the associated vertical deformations.

Besides the fact that the load transfer is not constant in these support systems made up of tendons, artificial rock mass and mesh and/or lacing, another complication is present. The potential for the tendons to move orthogonal to their axis does not appear to be realistic and introduces relatively “soft” boundary conditions.

The lacing appears to contribute to both stiffness as well as strength. With the 30 mm bolts a difference in stiffness can only be observed at prop forces in excess of 110 kN. The combined effect of lacing and mesh results in a 100 per cent increase in strength and a 50 per cent increase in stiffness.

Figure 4-2 shows results in which brick columns have been used instead of tendons. In all of these tests, the diamond mesh has been used without any lacing. In two of the tests the bar frame, used to suspend the mesh, was directly supported by columns, effectively creating a 2 m span. This resulted in bar failure in one of the tests, so that in the other test tie cables were used to reinforce the frame. In that test, the mesh was ripped from the frame, so that premature failure was initiated as well. The final test was done with a reinforced frame and a column spacing of 1.0 m. The columns directly engaged with the mesh in that case and the local stress concentrations led to a decrease in stiffness relative to the 2.0 m span. A shorter span should in theory lead to an increase in stiffness and this result is therefore indicative of the influence of stress concentrators. As a consequence, (premature) mesh failure was localised around the columns and took place at a prop force in excess of 110 kN.

Reducing the column spacing from 1.0 m to 0.7 m led to a dramatic increase in stiffness. It is believed that in this case only a limited amount of load was transmitted through the mesh while the bulk is directed straight into the columns. However, localised mesh failure still took place around the columns at a prop force in excess of 110 kN. Even the reduced mesh load resulted in premature failure due to a combination of increased mesh stiffness and stress concentrations.

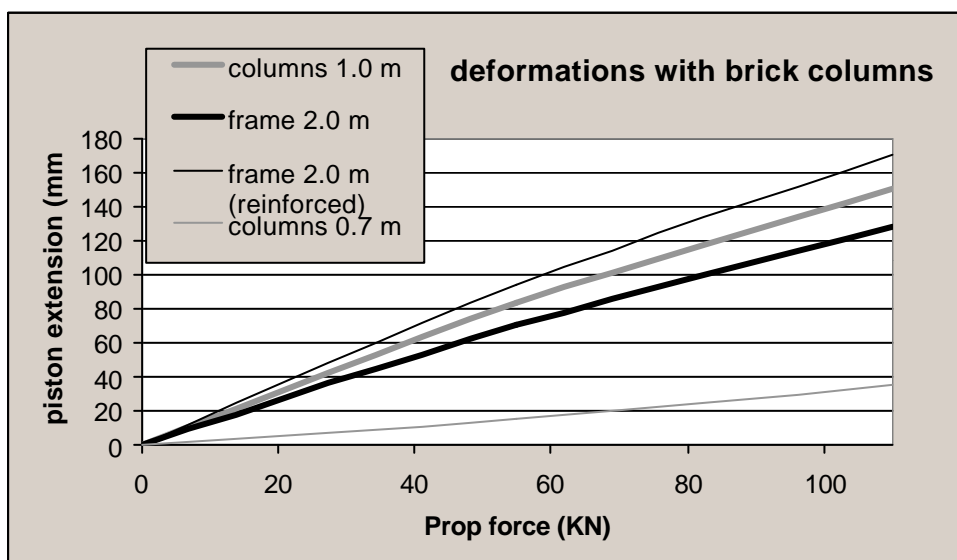


Figure 4-2 Tests in which brick columns were used to support the mesh

In order to avoid stress concentrations and to ensure a maximum load transmission through the mesh and/or lacing, the remainder of the tests was done with the use of brick walls. The results

are depicted in Figures 4-3 and 4-4 where the variations in stiffness and strength can be observed.

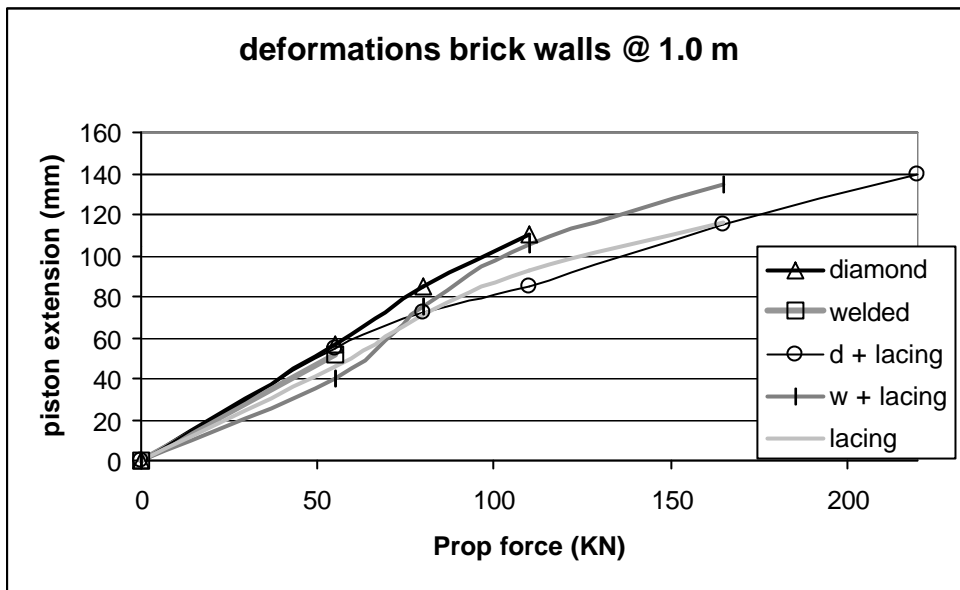


Figure 4-3 Tests in which brick walls were used to support the mesh/lacing (spaced at 1.0 m)

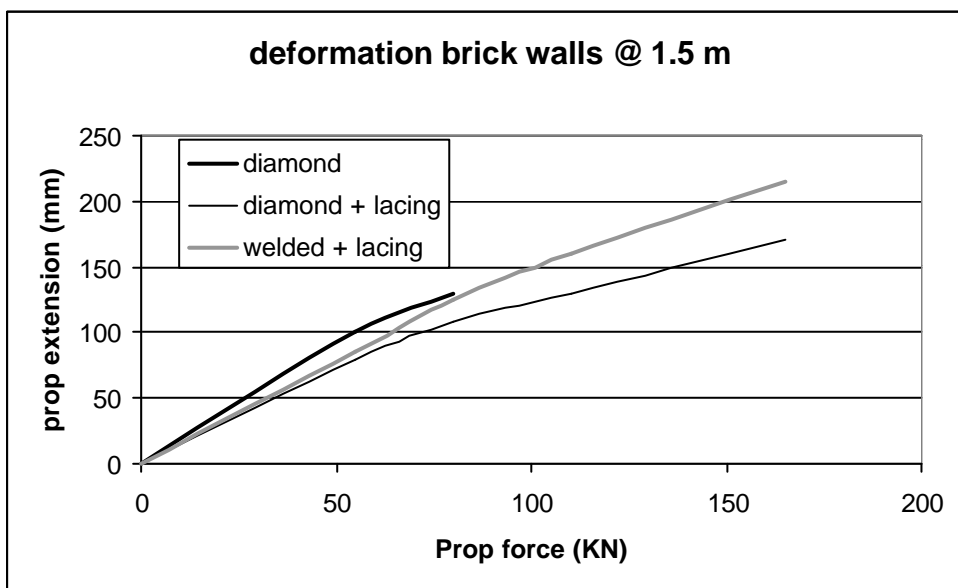


Figure 4-4 Tests in which brick walls were used to support the mesh/lacing (spaced at 1.5 m)

Five tests were done with a wall-to-wall spacing of 1.0 m (Figure 4-3), while another three tests were done with an increased spacing of 1.5 m (Figure 4-4). The influence of spacing on stiffness is quite clear from these graphs. Initially, a stiffness increase of approximately 100 per cent is obtained by reducing the span from 1.5 m to 1.0 m. This difference gradually decreases with increasing deformations and the associated increase in stiffness, but it is nevertheless quite relevant. No obvious difference in stiffness between welded mesh and diamond mesh could be found. If anything, the diamond mesh appeared to provide a stiffer response. This

finding is in stark contrast to previous findings (Haile, 1999 and Güler *et al.*, 2001) where it was found that welded mesh has a much larger initial stiffness than diamond mesh, while the strength of welded mesh was found to be consistently lower. The latter finding is consistent with the results of the current tests, as the strength of welded mesh was always lower than that of diamond mesh. Failure consistently occurred around the loading plate, as the wire at its periphery were subjected to the largest forces. Although the brick walls served their purpose, stress concentrations were still generated around the 75 x 75 cm steel plates where the load was introduced into the mesh.

An explanation for the fact that the welded mesh did not demonstrate a higher stiffness than the diamond mesh is not obvious. Although the smaller wire thickness accounts for a theoretical reduction of around 40 per cent in both stiffness and strength, this is not sufficient to explain the difference in the previous observations. It might be that geometrical effects do play a role and that the ratio of loaded area to span has a strong influence. It is also possible that with a relatively larger mesh density (wires/span), the increase in stiffness of the diamond mesh is disproportional. Previous tests on mesh were done on smaller scale samples with a relative small mesh density (Haile, 1999 and Güler *et al.*, 2001). If the results of the current tests are considered more realistically, then this is an important finding, because it indicates that, in practical applications, the stiffness of diamond mesh may not be substantially less than that of welded mesh.

The stiffness of the lacing by itself appears to be relatively high; no obvious explanation is available for this behaviour. The system strength is quite variable, but it clear that the absence of lacing reduces the strength substantially. The combination of diamond mesh and lacing appeared to be the most successful, both in terms of stiffness, as well as in terms of strength. The graphs in Figures 4-2 to Figure 4-4 portray the performance of the different systems and they can be used to quantify the contribution of the support in various applications.

The results shown in Figure 4-1 can now be interpreted with more confidence. The deformations associated with the 30 mm bolts and mesh can best be compared with the direct results on mesh supported by the 1.0 m spaced brick columns. In the latter case, a deformation of around 140 mm was associated with a maximum prop force of 110 kN. The results with the 30 mm bolts indicate a maximum deformation of 93 mm at a prop force of 220 kN. From the results of the tests in which the prop force was directly applied to the mesh and/or lacing, a deformation of 93 mm would be associated with a prop force of around 66 kN. This suggests that 155 kN of prop force, or 70 per cent of the load, is directly transferred into the tendons. The premature failure at 66 kN can be attributed to the large stress concentrations, generated by the washers around the tendons.

In hindsight, it can be argued that the systems in which tendons have been used could be made much stiffer by restraining the tendons from movements in the horizontal direction. The lacing did not contribute much to such a restraining function, as it was allowed to move freely along the washers. The mesh was clamped at the washers and therefore the mesh must have reduced the horizontal movement of the tendons to a certain extent. However, due to the large stress concentrations generated near the washers, the effect may be limited. By clamping the lacing at the washers a stiffer system would have been generated that would have caused a larger percentage of the load to be transmitted to the tendons.

Another obvious improvement to a system consisting of mesh and lacing is the avoidance of stress concentrations. The use of larger bearing plates, combined with a more efficient use of mesh is suggested. In principle, the mesh density should be matched with the force density (stress) in order to obtain the most effective system. This implies that at locations of stress concentrations such as the washers around the tendons, a larger mesh density is required than at mid-span between tendons. This condition is partially obtained with the "Brunswick" system that was used in some of the dynamic tests.

An increase in strength will be beneficial to the support performance as has been quantified in Section 3. Such an increase can obviously be obtained by using heavier mesh and/or lacing, with an associated increase in costs. However, by making effective use of the existing materials, a similar increase in load bearing capacity can also be achieved without resorting to larger volumes of support material.

The results of these static tests are directly applicable to the impact tests, as they allow for an estimation of the support forces generated by the mesh and lacing, in relation to monitored deformations.

4.1.3 Conclusions

Based on the results of the quasi-static tests, the following major conclusions can be drawn:

- Mesh and lacing provide an initially soft response.
 - Stiffness and strength only develop with increasing deformations and associated rock mass degradation.
 - The load carrying capacity of the rock mass decreases with increasing deformation.
 - Stress concentrations associated with tendons and lacing cause a reduction in strength.
 - Stiffer systems attract larger impact forces and are therefore more prone to failure, unless adequate yielding capacity is available.
 - If yielding tendons are used, it is essential that the fabric support does not fail before the yield strength of these tendons is reached.
 - Reducing the yield strength of tendons may lead to more uniform deformation of the rock surface (Figure 1-2) and an associated reduction in “unraveling”.
-
- Preventing rock mass unraveling reduces the demand on mesh and/or lacing.
 - Immediate improvements could be obtained by designing systems to cope with stress concentrations and by stiffening the systems while simultaneously providing sufficient yielding capacity.

5 Dynamic Testing

In this report, the impact tests, conducted by SRK and monitored by CSIR: Miningtek are presented and discussed. In the accompanying report from SRK (Part II), the impact tests are also presented and discussed.

Any impact can be viewed as a (pulse) force, acting over a limited period. A model for such a dynamic force is presented in Güler *et al.* (2001). With the use of that, or similar models, a relationship between system stiffness and (dynamic) force can be obtained. In principle, systems with higher stiffness are associated with smaller deformations and thus attract relatively large forces compared to systems with a lower stiffness. Large forces, combined with a low energy absorption capacity, do not create ideal conditions for an effective support system. For this reason, softer systems are more effective in accommodating dynamic impacts. Mesh and lacing lead to a relatively soft support system and therefore the following tests show responses typical of a system with a low stiffness, namely relatively low (impact) forces combined with relatively large deformations. The system response in the impact tests is similar to the system response in a static test, as far as the load-deformation characteristics are concerned.

The purpose of yielding tendons is to generate energy absorption capacity and to accommodate the associated deformations. If the system stiffness of the rock mass and fabric support is too soft, or the system strength of the rock mass and fabric support is too low, yielding tendons will not serve this purpose. Low system stiffness will cause deformations to be accommodated by the rock mass and the fabric, resulting in typical bulging. The associated forces are generally too low to induce yielding in the tendons at that stage. As can be appreciated from the model discussed in Chapter 3, increasing deformations are associated with increasing stiffness. An increased stiffness leads to an increase in (dynamic) forces from subsequent impacts and may result in ultimate failure if the system strength is less than the yield strength of the tendons. A relatively high initial system stiffness, which may for instance be obtained by the use of thick shotcrete, from a competent rock mass, by pre-deforming the mesh and lacing or by any other means, would prevent bulging of the rock mass and would immediately attract relatively large impact forces. If these forces exceed the system strength, system failure will occur. However, if again the system strength exceeds the yield strength of the tendons, deformation and energy will be absorbed by these tendons according to the original design philosophy. These considerations will assist in interpreting the results of the dynamic tests conducted by SRK for this project.

5.1 Results

Various combinations of mesh and lacing were tested in a specially designed test rig. An assembly of concrete bricks and steel blocks and plates was arranged in such a way as to create an artificial, fragmented rock mass. This assembly was suspended from four or six yielding tendons, which acted as retaining support. The mesh, with or without lacing, was attached to the bottom of the assembly and effectively acted as a containment support. A mass of approximately 3 tons was dropped from various heights in order to induce an impact onto the system consisting of an artificial rock mass, yielding tendons and mesh and lacing. A more detailed description can be found in the accompanying report by SRK (Part II).

The impact forces, which ultimately would be transmitted through the tendons, were monitored with the aid of specially designed load cells. Strain gauges attached to the surface of these load cells allowed for continuous recording by analogue logging using the CSIR: Miningtek ground motion monitor which digitised the data. A sampling rate of 3012 records per second was used to monitor the output from the strain gauges.

In addition to impact forces, the monitors also recorded accelerations. An accelerometer was attached to the bottom surface of the brick assembly and the data was used to calculate maximum induced velocities at that location.

Permanent deformations induced by the impact were also monitored, and they are tabled in the accompanying report. Unfortunately, the maximum (elastic) deformations during the impact were not monitored directly. These elastic deformations may account for a certain percentage of the energy absorption and they could make a considerable contribution. These deformations therefore had to be estimated.

All impact tests monitored by CSIR: Miningtek are presented in Appendix A.

5.1.1 Summary and Discussion

Table 5-1 summarises the results of the accelerometers

Table 5-1 Summary of dynamic parameters

Day dd mm yyyy	Time hh:mm:ss	Impact Velocity (m/s)	Drop Height (m)	A _{max} (m/s ²)	V _{max} (m/s)
4 December 2001	16:41:16	4.9	1.20	1100	0.99
4 December 2001	17:20:50	6.0	1.80	738	0.25
23 January 2002	16:51:03	5.0	1.25	2639	2.59
29 January 2002	15:06:43	5.0	1.25	1923	2.29
2 February 2002	14:48:17	5.0	1.25	1555	1.86
7 February 2002	09:50:42	1.1	0.60	799	1.43
19 February 2002	12:53:22	5.0	1.25	1893	2.02
25 February 2002	14:35:00	5.0	1.25	1045	1.21
11 March 2002	15:07:35	5.0	1.25	2700	3.20
19 March 2002	14:53:21	5.0	1.25	2575	2.48
22 March 2002	15:18:14	5.0	1.25	2113	2.00
12 April 2002	15:09:47	0.8	0.30	513	0.39
12 April 2002	16:02:09	4.9	1.20	1959	2.75
15 April 2002	17:11:02	5.0	1.80	2740	3.29
15 April 2002	12:59:47	6.3	2.00	2730	3.88

The results are discussed individually in Appendix B and the recorded impact forces are also presented there. In this summary, attention is drawn to some general observations and some potential misinterpretations.

The tests on the “Brunswick” type of support systems were conducted with the use of six tendons instead of four corner tendons as in the other tests. The reason for this arrangement is related to the fact that in the Brunswick system use is made of straps that span uni-directionally from one tendon to the other, instead of diagonally across the tendons in a similar manner to how the lacing was applied in the other tests. In the Brunswick system tests, the drop weight was impacted in the centre of the system, which is located between the two centre tendons. Of importance in this respect is that the span between these two centre columns is about 70 per

cent of the span measured diagonally across four corner bolts. A shorter span leads to an increase in system stiffness and, as has been argued before, an increase in stiffness leads to smaller deformations and larger impact forces. In addition, the impact load is mainly carried by the two centre bolts and not by four corner bolts as in the four-bolt arrangements. For this reason, the strength requirements of the mesh are drastically reduced. A direct comparison between the support systems in a six bolt arrangements and systems in the typical four bolts arrangements is therefore not possible.

An important observation is related to the performance of the yielding tendons. While the cone bolts may have demonstrated some erratic behaviour in relation to poor grouting and/or curing, the Durabar tendons showed a relative low yield resistance that was preceded by a relatively high initial peak resistance. It is not clear if this behaviour is associated with high velocities and how such velocities may affect the load deformation characteristics, but it is obvious that these characteristics influence the total system response.

General observations are related to the system strength and stiffness and the effect of boundary conditions and stress concentrations. These effects would be similar in a static loading case and are therefore not only related to dynamic loading. In the impact tests, the tendons are not firmly confined from swinging outward in a horizontal direction. This condition is associated with a relative “soft” boundary and the system response is affected accordingly. While the mesh offers some restraint to this form of displacement, the lacing does not, as it is free to slide through the chain links attached to the bearing plates. The connection of mesh and lacing at the tendons introduces stress concentrations and (premature) failure. Failure is typically initiated in the mesh around the bearing plates and subsequently expands around the lacing, which itself acts as a stress concentrator. (The lacing indirectly supports the mesh).

In most tests, except for the stiffer (and stronger!) six bolt arrangements, the tendons did not yield, while the mesh did fail. This indicates a lack of balance between the yield strength of the tendons and the effective strength of the mesh under the test conditions. Varieties of options are available to improve this balance. The most obvious one is increasing the *effective* strength of the mesh and/or decreasing the *maximum* resistance of the tendons. This will be discussed in more detail in the next chapter.

The following parameters have been found to play a role in the support performance:

- Strength of mesh/lacing
- Stiffness/compliance of mesh/lacing (yielding device, boundary conditions,
- Maximum force in tendons (initial peak in Durabar)
- Stress concentrations in mesh (washers, lacing)
- Lack of restraint to horizontal deformation of the tendons

6 Discussion and Recommendations

The results of the impact tests and the quasi-static tests, in combination with the theoretical model, clearly indicate the mechanisms and associated parameters which control load bearing capacity, energy absorption capacity and strength/failure.

From a practical point of view, it is important to realise that mesh and lacing systems are in principle relatively soft support systems attracting low forces and large deformations. The typical rock mass bulging between tendons is indicative of this behaviour. The stiffness of the mesh and lacing systems does however increase with increasing deformation and it is normally only at an advanced stage of deformation that the maximum strength is reached. At that stage the rock mass is typically unravelled and cannot be expected to contribute much to the support system. Failure is therefore directly associated with the strength of the mesh, which is relatively low when compared to the yield strength of tendons. Lacing contributes to the strength and stiffness, but failure is typically initiated in the mesh due to the existence of stress concentrations around washers and the lacing itself. Failure of the mesh could be sufficient to cause rock mass failure in the case of sufficiently fragmented and unravelled rock.

Limiting the occurrence of stress concentrations can increase the *effective* strength of mesh. This can be achieved by matching the mesh density to the expected force concentrations (i.e. stress). By providing a relatively high density around the tendons and a reduced density at mid span between the tendons, more effective use is made of the available material. If this proves to be too cumbersome, larger washer plates can reduce the effect of stress concentrations as well, while increasing the strength by the use more material is always an option.

Increasing the *effective* stiffness of the mesh and lacing is a possibility, but may not necessarily lead to a desired result. Increasing this stiffness would limit deformations and the associated unraveling of the rock mass. However, an increased stiffness would also lead to the induction of larger forces, especially during dynamic excitation. As a principle, the strength of the mesh should not be exceeded before yielding in the tendons is initiated. By maintaining the integrity of a rock mass, the percentage of load/impact transferred directly to the tendons can be increased, thus reducing the demand on the fabric support. The most efficient way to increase the *effective* stiffness of mesh and lacing is by applying it in a curved (pre-deformed) shape. While this appears to be difficult to achieve in practice, it might be an option worth considering.

Pre-stressing the mesh and/or lacing causes increased support efficiency, provided some yielding device is included to prevent premature failure. This has been demonstrated in Chapter 3. However, this increased support efficiency is still associated with a low *effective* stiffness at small deformations.

If mesh and lacing is compared with shotcrete, it is clear that the typical lack of initial stiffness is absent in shotcrete applications. In essence, the same mechanisms are applicable to both systems. The relatively high initial stiffness of shotcrete limits bulging of the rock mass, attracts relatively large forces and is not suitable for energy absorption. However, in combination with suitable (matching) yielding tendons, a support system is available which maintains rock mass integrity and is capable of energy absorption, provided rock wall deformations can take place. Again, the crucial requirement is that the shotcrete should not fail before yielding in the tendons is initiated. The shotcrete should not have to be designed to absorb energy. The initially relatively soft mesh and lacing system are in fact not very suitable for maintaining rock mass integrity and does allow relatively large deformations before being “activated”. However, the softness of the system provides mesh and lacing with considerable energy absorption capacity. If this capacity is sufficient, and the unravelling of the rock mass is acceptable, mesh and lacing

is capable of providing an adequate support function until deformations become excessive. Tendons are only required to provide an anchoring point in that scenario. However, once the rock mass bulging and associated deformations have exceeded a certain threshold, the system stiffness has increased and the energy absorption capacity of the system may be severely reduced. The presence of yielding tendons can be a solution in that scenario, provided again that the strength of the mesh is not exceeded before yield is initiated in the tendons and provided that rock wall deformations can be accommodated. Another, and perhaps more practical solution in this scenario is the inclusion of some yielding device in the mesh itself. Allowing yielding at the anchoring points (soft bearing plates at the tendons) for instance could prevent mesh failure while enabling further rock mass bulging between the anchoring points.

The above discussion is intended to provide practical suggestions towards more effective use of support components and systems. One of the main non-quantified parameters in this discussion is the fragmentation and the associated integrity of the rock mass. Relatively large fragments and an associated competent rock mass require less support action from containment support than in the case of a highly fragmented rock mass. It is the latter case that requires maximum support capacity and it is the latter case that has been addressed in this project. All conclusions and suggestions are therefore related to highly fragmented rock masses and should not necessarily be expanded to less extreme scenarios for which other solutions might be more applicable.

From the insights gained during this project, the following requirements for stabilisation of fragmented tunnel walls under rockburst conditions are considered most relevant:

- Keep fragmented rock in place and prevent further fracture development
- Minimise support requirements by maximising load carrying capacity of the rock mass
- Allow for energy absorption at limited (impact) forces and with limited deformation

Satisfying these requirements can be achieved in various ways and in principle four options are available:

- 1) Pin the rock locally by non-yielding tendons and allow all subsequent deformations to occur in between these units.
- 2) Pin the rock locally by yielding tendons and concentrate all subsequent deformations in these units.
- 3) Create a strong and stiff reinforced rock mass shell around the excavation; deformations will be inhibited (especially in curved shaped openings) and ultimate failure may be violent.
- 4) Create an artificial shell inside the excavation; yielding of this shell may still accommodate deformations.

Typically, option 1 is the one that is representative of the current situation. Deformations are taking place between support units and system failure is associated with fabric failure and deformation. By increasing the effective strength of the fabric and/or by incorporating a yielding system in the fabric or at the anchor points, fabric failure can be avoided and a support system capable of accommodating relatively small rock bursts is available.

A potentially more competent support system may be obtained by making use of yielding tendons. It is essential that in this case the fabric strength be not exceeded before the yield

strength of the tendons is reached. By maintaining (or even increasing) the load carrying capacity of the fragmented rock mass, the required fabric strength can be reduced. This can only be achieved with the use of a relatively stiff fabric however, which effectively is option 2) and, in the extreme, option 3).

Although the first two requirements may have been satisfied at this stage, a problem could still exist regarding the last requirement with respect to energy absorption. Once a relatively stiff and strong rock mass shell has been created, deformations into the excavation may be severely restricted, depending on the shape of the opening. While rectangular openings do not appear to impose severe restraints on rock wall deformation, oval shaped openings may cause problems in this respect. Although, and perhaps because, it is creating a more stable excavation, the oval reinforced shell may be more prone to violent failure than a square shell. Due to its inherent stiffness, dynamic impacts may induce extremely large forces and associated strain bursts. It is not clear to what extent a stiff reinforced rock mass shell would accommodate a rock burst. The actual shape of such a reinforced shell may play an important role in this respect.

An obvious way around this problem is to create a shell that can accommodate deformations through some yielding mechanism (option 4). Although the concept of shells is beyond the scope of this project, it is mentioned here in order to provide a wider perspective to the traditional tunnel support systems as tested in this project.

The creation of a shell that is too stiff may be associated with strain bursts, induced by incoming stress waves. This is a potential problem that has not been quantified but that appears to be very relevant to the performance of (tunnel) support under rock burst conditions. It is strongly recommended that this issue be further investigated. For the moment, caution is advised in this respect. Although fabric support requirements can be reduced by effectively stiffening the rock mass shell, it is possible that a rock mass shell that is too stiff and competent may ultimately fail in a violent fashion as deformation into the excavation are inhibited.

By allowing a certain amount of rock mass deformation between individual tendons (bulging), a reasonable balance may be found between rock mass carrying capacity, fabric strength and energy absorption potential. The strength of the fabric support has to be matched to the yield strength of the tendons. In the absence of any rock mass carrying capacity this implies that the fabric strength needs to exceed the yield strength of the tendons. Practical suggestions to improve the yield strength of the fabric have been made before and they essentially entail the avoidance of stress concentrations. Fabric should be placed where it is required; more near the bearing plates and less at mid-span between tendons. Reducing the yield strength of tendons immediately reduces fabric requirements as well and the use of tendons that have an excess strength is therefore counterproductive.

From the quasi-static test results it can be observed that the fabric strength ranges between 100 kN and 220 kN per square metre. This implies that in principle a tendon yield strength of 10 tons (100 kN) should prevent the test fabric to fail under uniform loading conditions with tendons spaced at 1.0 m. Unfortunately the test results do not represent uniform loading conditions, as the applied load was spread over four (and even six) tendons, while only one panel of fabric support had to accommodate the same load. To prevent fabric failure under the test conditions, tendon yield strength ranging between 25 kN and 55 kN would have been required. It is thus also important to determine the actual loading geometry. A uniformly distributed load is less demanding on the fabric support than a concentrated load.

7 References

Güler, G., Kuijpers, J.S., Wojno, L., Milev, A. and Haile, A. (2001), Determine the effect of repeated dynamic loading on the performance of tunnel support systems, Final Project Report, GAP 616, SIMRAC, Johannesburg, South Africa.

Haile, A.T. (1999), A mechanistic evaluation and design of tunnel support systems for deep level South African gold mines, PhD thesis, university of Natal, South Africa.

Kaiser, P.K., McCreath, D.R. and Tannant, D.D. (1996), Canadian Rockburst Support Handbook, Geomechanics Research Center, Laurentian University, Sudbury, Ontario, Canada.

Ortlepp, W.D. (1983), The design of support for rockburst prone tunnels, Rock Mechanics in the design of tunnels, SANGORM symposium, Johannesburg, South Africa.

Stacey, T.R. and Ortlepp, W.D. (1997), Testing of tunnel support: Dynamic load testing of rock support containment systems (e.g. wire mesh), Final Project Report, GAP 221, SIMRAC, Johannesburg, South Africa

Stillborg, B. (1986), Professional users handbook for rock bolting, Series on Rock and Soil Mechanics, Vol. 15, Trans Tech Publications.

Wagner, H. (1983), Some considerations concerning the support of tunnels in deep mines, Rock Mechanics in the design of tunnels, SANGORM symposium, Johannesburg, South Africa, pp. 51-59.

Wojno, L. and Jager, A.J. (1987), Rock reinforcement in tunnels under high stress conditions in South African gold mines, 6th Int. Conf. On ground control in mining, Morgantown, Virginia, USA.

Wojno, L. Jager, A.J. and Roberts, M.K.C. (1987), Recommended performance requirements for yielding rock tendons, Design of rock reinforcing, Components and Systems, SANGORM symposium, Johannesburg, South Africa.

APPENDICES

Results of quasi-static tests

A1 Test on 30/10/01

For this test, a diamond mesh with an aperture of 100 mm and a wire thickness of 4.2 mm was used. Lacing was done with a cable as shown in Figure A-1. Four cone bolts, grouted in thin walled pipes and spaced at 1 m, were used to suspend the assembly of concrete bricks that is shown in Figure A-1.



Figure A-1 *Lacing and diamond mesh used in the test on 30/10/01*



Figure A-2 Yielding of cone bolts at the end of the test on 30/10/01 (indicated by white tape relative to the bottom of the tube)

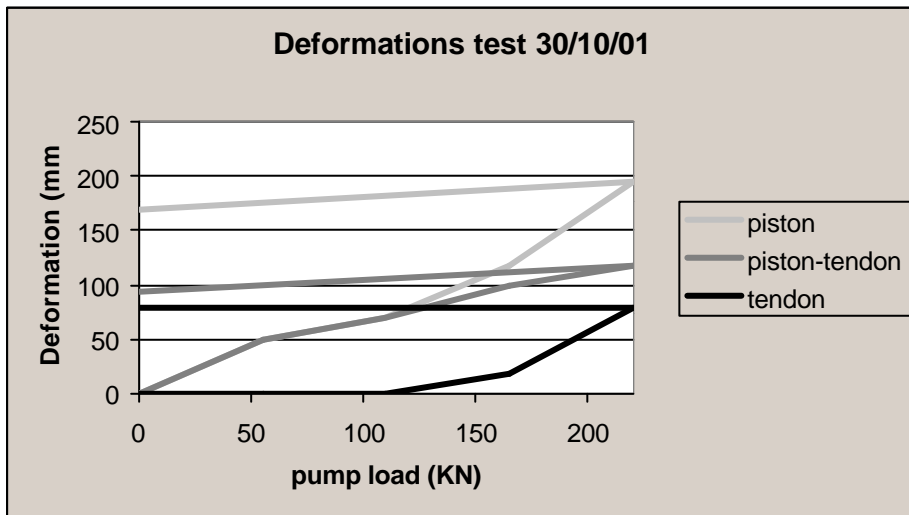


Figure A-3 Deformations monitored at test 30/10/01

Table A-1 Results of the test on 30/10/01

Pump force (kN)	Bottom sag (mm)	Piston extension (mm)	Tendon yield (mm)	Energy absorbed (kJ)	
				Tendons	Fabric + blocks
0	0	0	0	0	0
55	40	50	0	0	1.37
110	80	70	0	0	3.02
165	125	118	19	2.61	7.01
220	210	195	79	14.16	10.28
0		170	79		

The conebolts started yielding at a prop force between 110 kN and 165 kN pressures and due to excessive deformations a force of 220 kN, no further load increments were applied and the test was concluded. The monitored forces in the tendons did not appear to have reached a maximum at that stage, as can be seen from Figure A -4. The maximum bolt force recorded was approximately 50 kN, which is less than the yield force of a typical cone bolt. The conebolts used for this particular test were however specifically designed to offer a lower resistance in order to obtain a more balanced support system. This purpose was in fact achieved, as no support failure occurred. From Table A-1 and Figure A-3 it may be appreciated how the tendons gradually absorb the induced energy and associated deformations. The fact that this is a gradual process indicates an increase in yield resistance with increasing deformations. It is likely that the grout hasn't cured uniformly along the conebolts at the time of these tests other wise a more abrupt change would have been observed whereby all deformations would be associated with the yielding of the tendons and no further (differential) movement would be induced in the fabric and the assembly of bricks.

It is not immediately obvious from these observations to what extent the mesh and lacing contribute to the load distribution. There is no way to determine what percentage of the imposed load is transferred to the tendons via the mesh and lacing unless calibrated load-deformation characteristics are available. However, in subsequent tests, these characteristics have been calibrated and the results suggest that in this particular test, at maximum deformation, the mesh and lacing are carrying approximately 100 % of the prop load. (see the results of the test on 14/02/02).

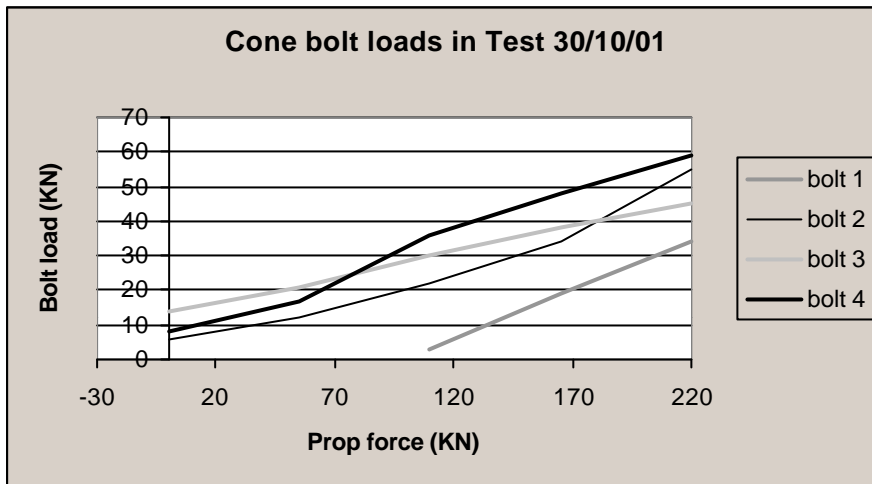


Figure A-4 *Monitored bolt loads for all channels*

Note that bolt 1 doesn't appear to absorb any load until a prop force in excess of 100 kN was imposed. The reason for this is maladjustment of the recording equipment and the actual load in bolt 1 is in fact about 20 kN larger as recorded in Figure A -4. The sum of the bolt forces should equal the prop force and this appears to be correctly recorded, taking into account the above-mentioned problem.

A2 Test on 09/11/01

Extra strong tendons were selected for this test in order to test the fabric capacity. This test also allows a comparison with the previous test with cone bolts. Bolts with a diameter of 30 mm were used in this test and the theoretical yield strength should be in excess of 150 kN.



Figure A-5 *Test on 09/11/01 with 30 mm bolts*

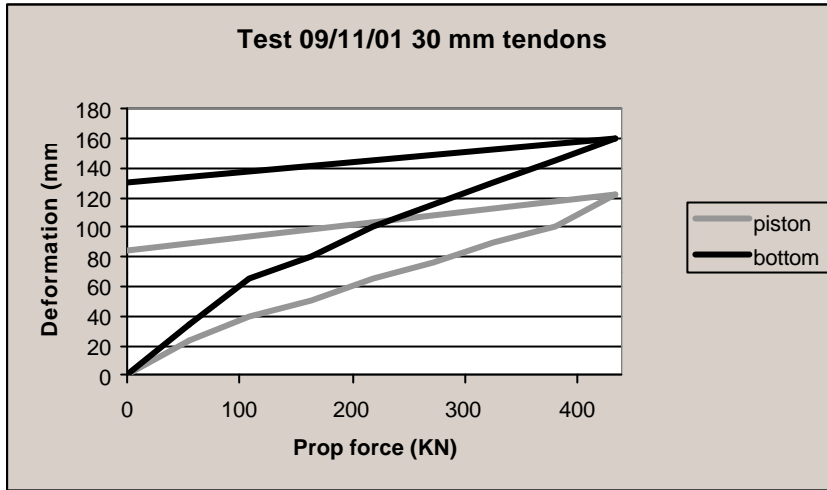


Figure A-6 Monitored load-deformation characteristics

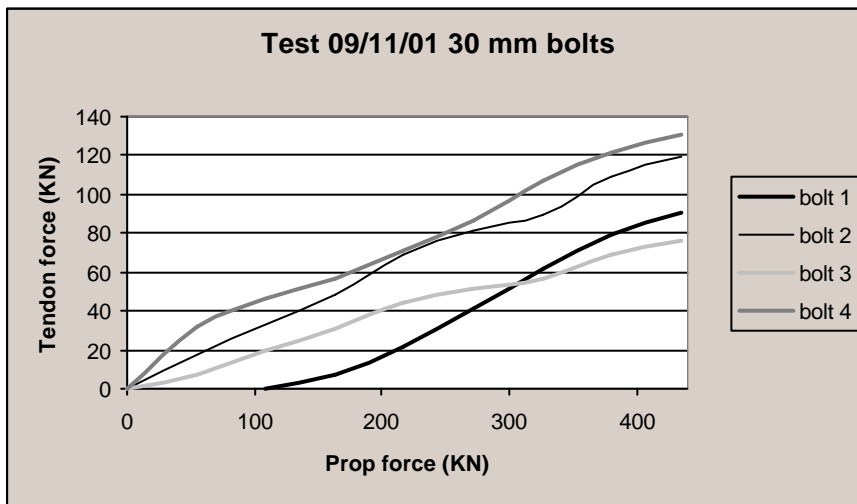


Figure A-7 Monitored tendon forces

At a maximum prop force of around 440 kN, the system still did not fail. Tendon forces in excess of 100 kN were measured and the only evidence of failure could be observed around the washers at some of the tendons (Figure A -7). The imposed load is accounted for by the sum of the tendon forces. It is therefore unlikely that much load is transmitted through the lacing away from the tendons.



Figure A-8 *Localised mesh failure near the tendon*

The mesh and lacing appear to carry approximately 50 % of the prop load at maximum load and deformation. This estimation is based on calibrations that have been done in direct tests on mesh and lacing. Compared with the previous tests, it is obvious that a larger percentage of the load is directly transferred through the brick assembly in this test. This is associated with a stiffer system response and it is not immediately clear why the change in tendons has such a profound effect on the system stiffness. One possible suggestion is that the thicker tendons offer more resistance against shearing across the bricklayers. Such a resistance may restrain bending and associated vertical deformations.

As the tendons do not contribute to the energy absorption in this particular test, the fabric is deformed until failure occurs. Unfortunately, the capacity of the prop was not sufficient to induce ultimate failure, but initiation of failure did take place. Further failure of the fabric could be prevented if the tendons would start yielding at the maximum load and thus the ideal yield load would be around 100 kN in this particular case.

From Figure A-6 and Table A-2 it is clear that deformations and associated energy absorption progressively increase close to the end of the test. Compared with the previous test, the system stiffness has increased dramatically and this can only be attributed to the difference in tendons.

Table A-2

Prop force (kN)	Bottom sag (mm)	Piston extension (mm)	Energy absorbed (kJ)	
			Tendons	Fabric + bricks
0	0	0	0	0
55	35	23	0	0.63
110	65	40	0	2.03
165	80	51	0	3.54
220	100	65	0	6.24
275	115	76	0	8.96
330	130	90	0	13.19
400	145	100	0	16.84
430	160	122	0	25.97
250		115		
0		85		
250		107		
0		90		
130		100		
0		87		

A3 Test on 19/11/01

This test was similar to the previous one except for the fact that no lacing was used in this case. The 30 mm bolts spaced at 1.0 m were applied again with the diamond mesh. The frame, in which the mesh was suspended, was however supported by brick columns in this case.



Figure A-9 **Test 19/11/01 with 30 mm bolts and without lacing**

The load deformation characteristics are shown in Figure A-10. At a prop force in excess of 22 kN the mesh ripped open and excessive deformations occurred. The 30 mm tendons were subjected to extreme bending due to the horizontal dilation of the concrete bricks (Figure A-9). Comparing Figure A-6 and A -10, it is clear that the absence of lacing results in a gradual decrease in system stiffness. The maximum difference is approximately 50 % at the end of the test. What is not immediately obvious is why the mesh fails at a maximum deformation of around 140 mm in the absence of lacing, while hardly any failure is observed at a deformation of 160 mm, with lacing (previous test). A possible explanation may be the restraining and reinforcing effect of the cable. In the absence of the cable, initiation of mesh failure, at locations of high stress concentrations, quickly escalates into system failure, while in the presence of lacing local mesh failure does not have to lead to system failure. The cable can accommodate the loss of mesh resistance as it has sufficient load carrying capacity.

Unlike the previous test, the fabric (mesh in this case) appears to carry less than 40 % of the load near the end of the test. This estimation is based on the results of the tests on 13/12/01 and 11/01/02. As the deformations are smaller, reduced fabric contribution is explained based on a relative competent "rock mass". With further deformations, the concrete bricks will loose coherence and in increasing percentage of load will have to be carried by the fabric.

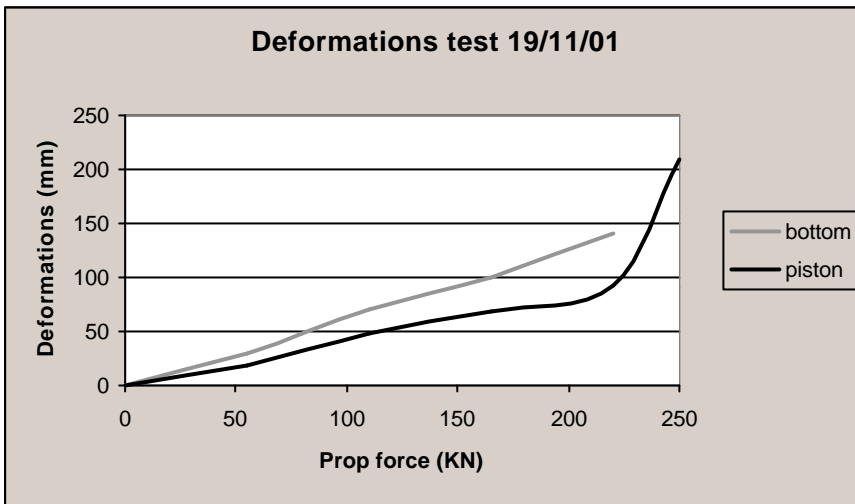


Figure A-10 *Monitored load-deformation characteristics*

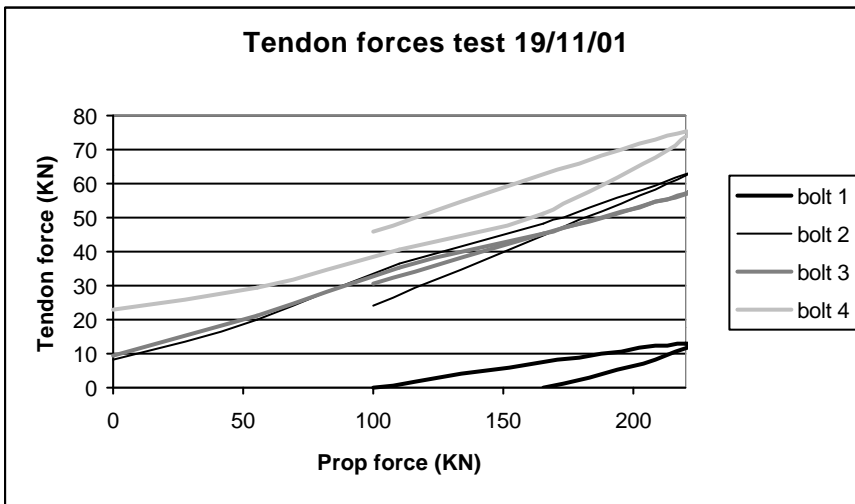


Figure A-11 *Monitored tendon forces*



Figure A-12 **Failure of mesh (and system) in test 19/11/01**



Figure A-13 **Bending of bolts in test 19/11/01**

The maximum tendon forces at failure were approximately 60 kN. The total tendon forces account again for the applied load (around 220 kN), if the readings for bolt 1 are adjusted. After

the mesh failure, the total load carried by the tendons appears to be around 100 kN. The remainder of the load is most likely directly transmitted to the ground (see Figure A -9).

Table A-3 Test 19/11/01

Prop force (kN)	Bottom sag (mm)	Piston extension (mm)	Energy absorbed (kJ)	
			Tendons	Mesh + bricks
0	0	0	0	0
55	30	19	0	0.52
110	70	48	0	2.91
165	100	68	0	5.66
220	140	93	0	10.47
<275		210	0	>35.0

Compared to the previous test, the absorbed energy is larger for the same forces. This is obviously associated with the reduced stiffness and the associated increase in deformations. In fact, most of the energy is absorbed at the end of the test, when failure takes place. It is clear that the mesh is “stretched” beyond capacity and while this stretching accounts for a relatively large energy absorption capacity, it results in system failure. The estimated maximum load which is carried by the mesh is approximately 40 % of 250 kN = 100 kN. Failure of the mesh could be prevented in this case if the tendons would have yielded at a yield force of around 60 kN.

A4 Test on 21/11/01

Unlike the previous tests, this test and all the following ones do not incorporate the artificial rock mass. The main purpose of the quasi-static tests is to quantify the fabric performance. This was not possible in the previous test, as the contribution of the artificial rock mass could not be quantified. In addition, it became clear that relevant properties of the artificial rock mass changed in response to loading and deformation. This complicated matters even further.

Diamond mesh with an aperture of 100 mm and a wire thickness of 4.2 mm was used again in this test. Suspended in the standard bar frame and supported on brick columns underneath the frame. The effective span was therefore 2.0 m. The load spreading system consisted of three layers of concrete blocks (5 x 5, 4 x 4 and 3 x 3), one layer of square steel blocks of 32 cm length, and one layer of square steel blocks of 28 cm length. The load deformation characteristics are displayed in Figure A-14. Unfortunately, no photographs are available.

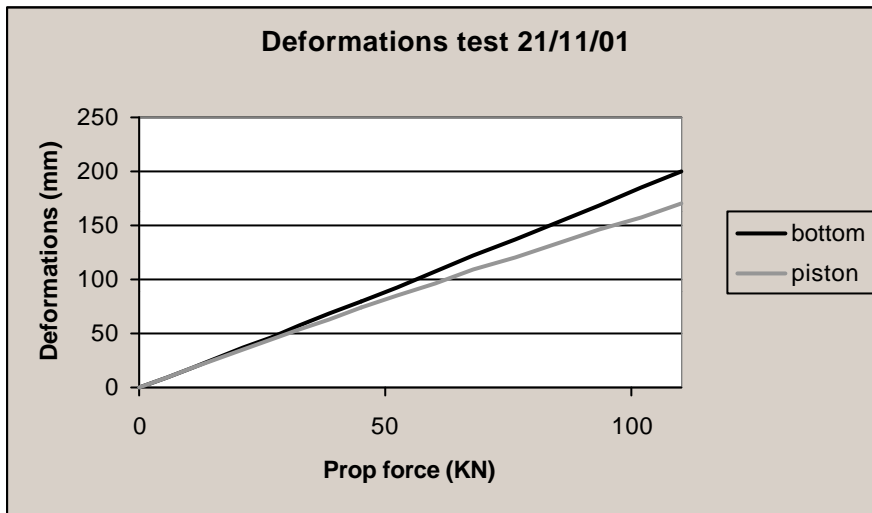


Figure A-14 Monitored load deformation characteristics.

At a prop force of 110 kN, excessive bending of the mesh frame was observed and the test was terminated (the frame had to be straightened subsequently). In this particular test, no additional reinforcement was applied to the frame. In most of the other tests, the mid span of each bar of the frame was reinforced by a pre-stressed cable tie, which is anchored into the concrete floor. This reinforcing system can be expected to lead to a substantial increase in strength as the effective bar spans are halved. Obviously, the stiffness of the system will also be increased because of such reinforcing.

TableA-4 Test 21/11/01

Prop force (kN)	Bottom sag (mm)	Piston extension (mm)	Energy absorbed (kJ)
0	0	0	0
45	80	75	1.8
110	200	170	11.1

A5 Test 06/12/01

The “Brunswick” support system that was subjected to previous impacts has been used in this quasi-static test. This system is the same one, which has been used on 4 December 2001 for impact testing. After having been subjected to two subsequent drops with an impact energy of $3000 \times 10 \times 1.2 = 36$ kJ and $3000 \times 10 \times 1.8 = 48$ kJ respectively, the system was loaded by the hydraulic prop. Table A 6.1 shows the results for the two centre bolts. The system was in a pre-deformed and pre-stressed state because of the previous loading history.

It is of interest to note that additional yielding in the cone bolts is initiated at a prop force of only 55 kN. While this may suggest an extremely low yield resistance in the cone bolts (<30 kN), it is possible that residual forces are acting on the tendons, even in the absence of loading. This seems to be rather unlikely however. Further increases in pressure are all associated with further yielding. No failure of the mesh was induced. Unfortunately, the piston extension was not

recorded in this test and no attempts have been made to estimate the energy absorption in this case.

Table A-5 Test 06/12/01

Prop force (kN)	Bottom sag (mm)	Bolt yield (mm)
0	0	0
55	0	5
110	5	10
165	5	15
220	10	20
275	10	30
330	20	35

A6 Test on 12/12/01

Diamond mesh with an aperture of 100 mm and a wire thickness of 4.2 mm was used again for this test. The mesh was suspended in the standard bar frame and supported on brick columns underneath the frame. The effective span was therefore 2.0 m. The load spreader consisting three layers of concrete bricks (5 x 5, 4 x 4 and 3 x 3), one large steel plate, one steel plate 40 x 40cm, two steel plates 30 x 24 cm, and three steel plates 25 x 25 cm. The results are depicted in Figure A -15 where it can be seen that the system response is much stiffer than in the case of test on 21/11/01. The reason for this difference is the absence of any frame reinforcement in the latter test. While the bar frame did not yield, the mesh was ripped of the bar frame at a load in excess of 110 kN.

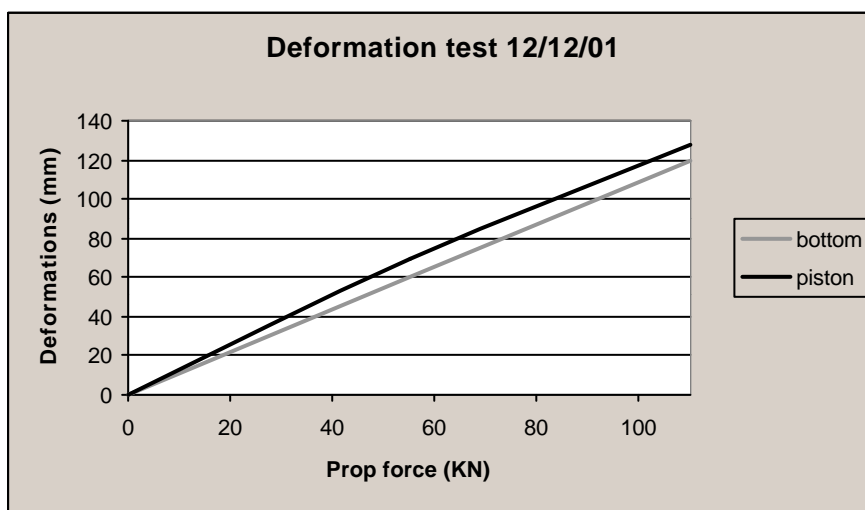


Figure A-15 Monitored load-deformation characteristics.

This particular test was thus also subject to premature failure, as the mesh unravelled along the edges of the frame. This specimen construction problem cannot be related to a realistic failure mode.

Table A-6 Test 12/12/01

Prop force (kN)	Bottom sag (mm)	Piston extension (mm)	Energy absorbed (kJ)
0	0	0	0
55	60	70	1.92
110	120	128	4.78
<165	Failure along the bar frame (unravelling)		

A7 Test on 13/12/01

Diamond mesh with an aperture of 100 mm and a wire thickness of 4.2 mm was also used in this test. The mesh was again suspended in the standard bar frame and directly supported on brick columns with a spacing of 1.0 m. The load spreader consisting of three layers of concrete bricks (5 x 5, 4 x 4 and 3 x 3), one large steel plate, two steel plates 33 x 25cm and two steel plates 32 x 28 cm. The deformations are depicted in Figure A-16, where it can be seen that the system stiffness has decreased with respect to the previous test on the 12/12/01 with the larger span. The explanation for this apparent inconsistency may be found in the fact that the brick columns act as stress concentrators. In the previous test, a uniform distribution of load and associated deformation can be expected from the bar frame towards the load spreader. However, in the case of the brick columns, most of the load will be distributed directly to the brick columns. Therefore, only a limited portion of the mesh will be effectively utilised and therefore subjected to relatively high stresses and associated deformations.

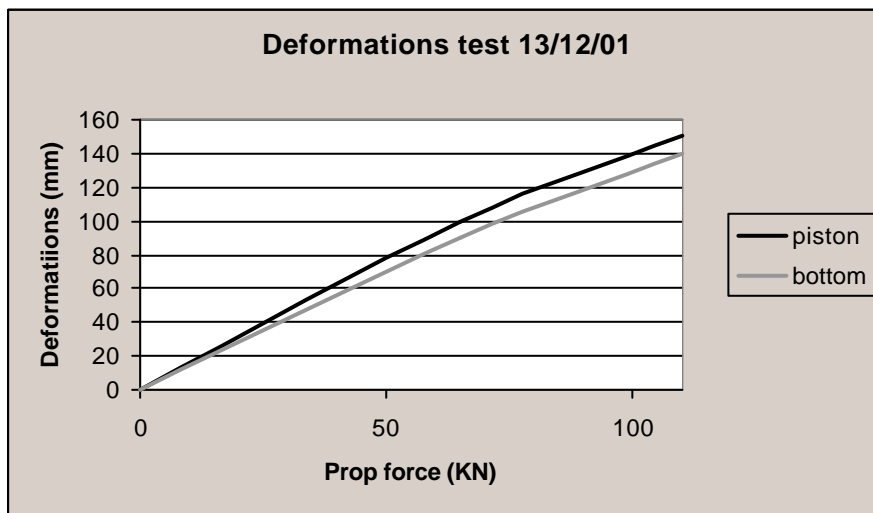


Figure A-16 Monitored load-deformation characteristics

When the prop force was increased beyond 110 kN, localised mesh failure occurred around the brick columns. This is consistent with the stress concentrations that can be expected around these stiff “intrusions”, and similar phenomena have been observed around the tendons in most of the impact tests.

Table A-7 Test 13/12/01

Prop force (kN)	Bottom sag (mm)	Piston extension (mm)	Energy absorption (kN)	In-plane stiffness (ton/m)
0	0	0	0	
65	90	100	3.25	1,650
110	140	150	7.62	900
<165	Failure around brick columns			

A8 Test on 09/01/02

Diamond mesh with an aperture of 100 mm and a wire thickness of 4.2 mm has been used again for this test. The mesh was suspended in the standard bar frame and directly supported on brick columns spaced at 0.7 m. The load spreader consists of three layers of concrete bricks (5 x 5, 4 x 4 and 3 x 3), one large steel plate, two steel plates of 33 x 25 x 6cm and two steel plates of 32 x 28 x 6 cm. The results are depicted in Figure A -17. It is clear that the system stiffness has increased dramatically in comparison with any of the previous tests. The increase of stiffness appears to be excessive and cannot be accounted for by a decrease in span only. A possible explanation is that a substantial part of the load is directly transmitted into the brick columns through the load spreader. These normal forces effectively clamp the mesh to the brick columns and this would create additional stiffness. At a prop force in excess of 110 kN, localised mesh failure occurred around the brick columns and system instability was initiated. Although only a part of the imposed load was transmitted through the mesh, the increased stiffness would have rendered the system less effective by inducing relatively larger stresses into the mesh. Failure could thus have taken place at a reduced loading on the mesh.

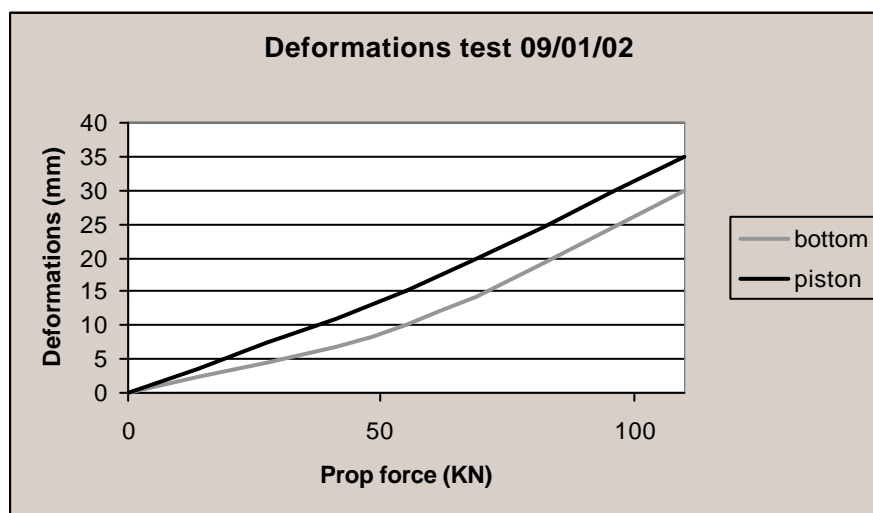


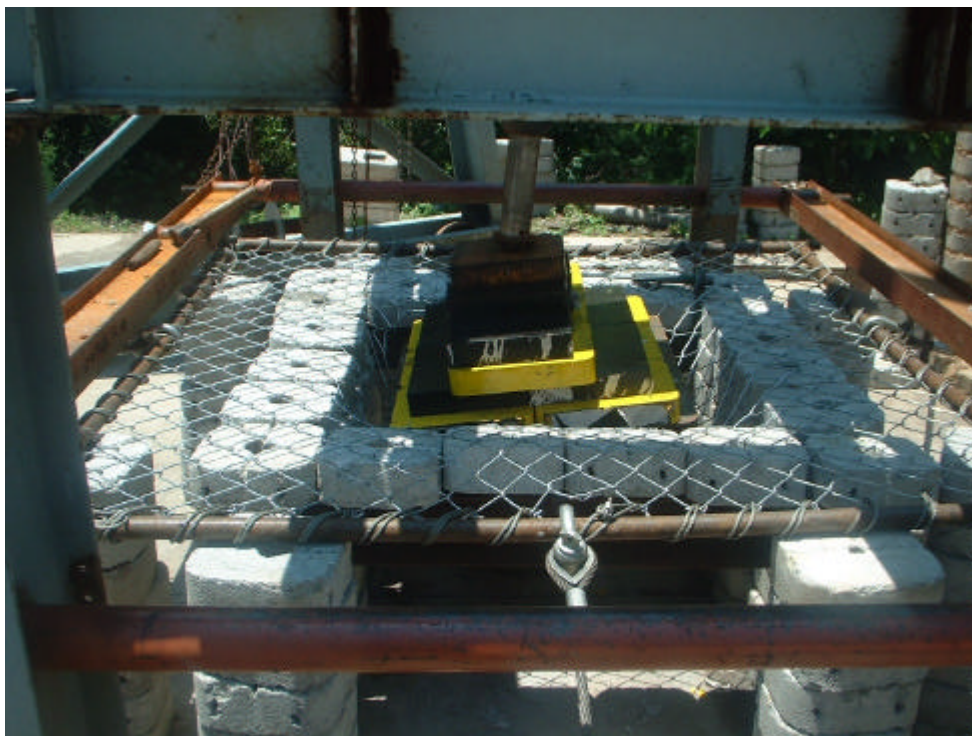
Figure A-17 Monitored load-deformation characteristics

Table A-8 Test 09/01/02

Prop force (kN)	Bottom sag (mm)	Piston extension (mm)	Energy absorbed (kJ)	In-plane Stiffness (ton/m)
0	0	0	0	
55	10	15	0.41	200,000
110	30	35	2.06	31,500
<165	Failure around brick columns			

A9 Test on 11/01/02

Diamond mesh with an aperture of 100 mm and a wire thickness of 4.2 mm and suspended in the standard bar frame. Directly loaded onto a 75 x 75 cm steel plate with additional steel blocks on top. Supported by brick walls spaced 1.0 m wall to wall (see Figure A 9.1). This set up was selected in order to avoid the stress concentrations associated with the brick columns.



In addition, the effect of those stress concentrations might be evaluated by comparison.

Figure A-18 Failure of mesh in test 11/01/02

The monitored deformations are shown in Figure A -19.

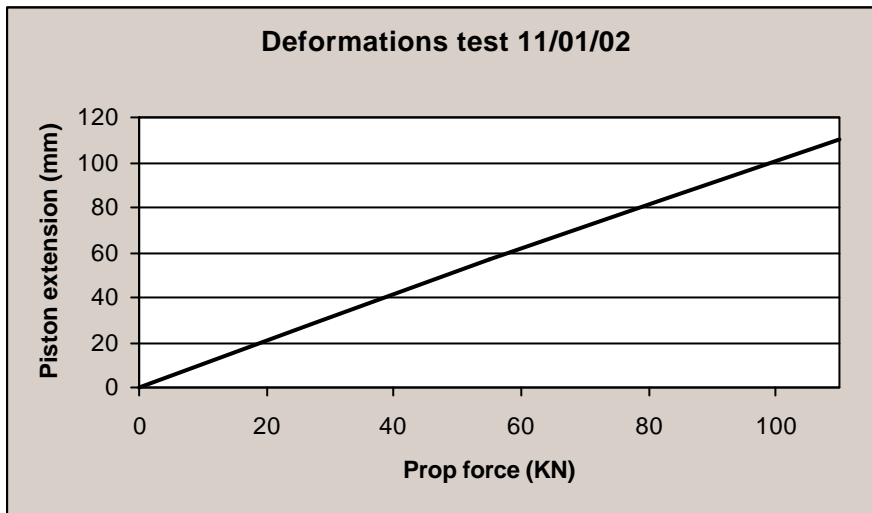


Figure A-19 *Monitored load-deformation characteristics*

If the graph in Figure A-19 is compared with the graphs in Figure A-16 it appears that a nominal increase in stiffness is obtained. This may be explained from a more uniform load distribution associated with the wall support.

The load spreading system in this test is also different from the previous ones. Instead of the three layers of concrete blocks, a single steel plate has been used. At a prop force in excess of 110 kN, the mesh failed around the edges of this steel plate.

Table A-9 *Test 11/01/02*

Prop force (kN)	Bottom sag (mm)	Piston extension (mm)	Energy absorbed (kJ)	In-plane Stiffness (ton/m)
0	0	0	0	
55	50	57	1.57	7,500
110	100	110	5.94	2,100
<165	Failure around the steel plate			

A10 Test on 14/01/02

In this test the effect of lacing was evaluated. The lacing was supported across brick walls with an internal spacing of 1 m. Load was applied through a large steel plate while various other



steel blocks were used as spacers. (Figure A -20)

Figure A-20 Test 14/01/02 on lacing only

The monitored deformations are shown in Figure A-21, where it can be seen that the system stiffness gradually increases with increasing load and deformation. This is to be expected as the lacing becomes more effective with increasing vertical deformation. Final failure occurred at a prop force in excess of 165 kN and manifested itself as cable breakage initiating from the edge of the steel plate. At a prop force of 110 kN it was observed that some of the concrete bricks, which were in direct contact with the lacing, showed signs of local crushing (Figure A -20).

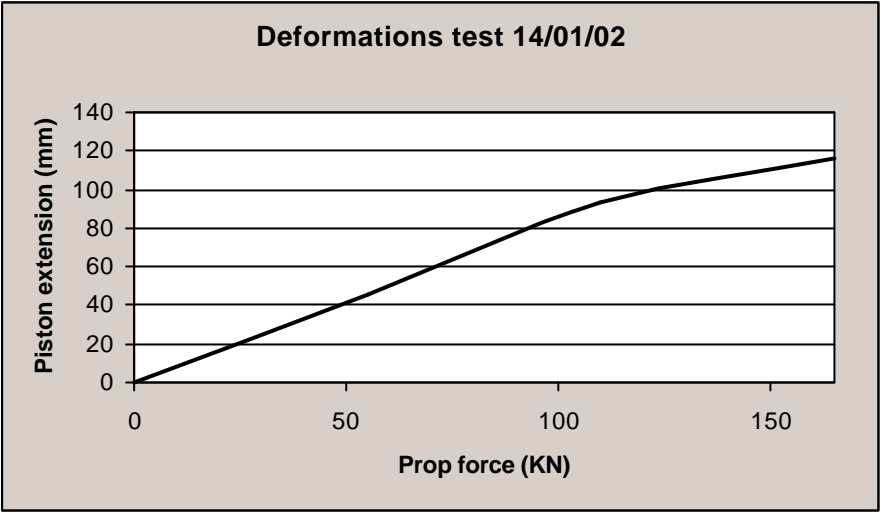


Figure A-21 *Monitored load-deformation characteristics*

Table A-10 Test 14/01/02

Prop force (kN)	Piston extension (mm)	Energy absorbed (kN)	<i>In-plane</i> stiffness (ton/m)
0	0	0	
55	46	1.26	14,200
110	93 (bricks start crushing)	5.14	3,500
165	116	7.30	2,750
<220	151 (cut at corner)		

A11 Test on 21/01/02

In this test, diamond mesh with an aperture of 100 mm and a wire thickness of 4.2 mm was used again. The mesh was suspended in the standard frame and was directly supported on brick walls with an internal spacing of 1.0 m. The difference with this test and the one conducted on 11/01/02 is in the load spreading. Load was applied via a relatively small steel plate of 20 x 20 cm in this particular test. The load-deformation characteristics of this test could not be established as failure occurred at a prop force of less than 110 kN. It was however observed that relatively large deformations occurred and the system appeared therefore less stiff. Reduced strength is explained from the high stress concentrations associated with the smaller load spreader. Larger deformations can also be expected from a smaller load spreader, as the applied load is more concentrated at the mid span of the mesh and the associated stresses and strains are therefore larger.

Figure A -22 shows how the small steel plate has punched through the mesh.



Figure A-22 **Failure in the test on 21/01/02**

Table A-11 **Test 21/01/02**

Prop force (kN)	Piston extension (mm)
0	0
<20	290 (failure around plates)

A12 Test on 24/01/02

In this test, a welded mesh with an aperture of 100 mm and a wire thickness of 3.15 mm was used. The mesh was suspended in the standard bar frame which in turn was supported on brick walls with an internal spacing of 1.0 m. The load was applied via a layer of concrete bricks underneath the 75 x 75 cm steel plate. Final failure took place at a prop force of approximately 70 kN and manifested itself as broken strands along the edges of the brick wall and the edges of the layer of concrete bricks. The monitored deformations are shown in Figure A -24 and these results are comparable with the results on diamond mesh in the test on 11/01/02, which are depicted in Figure A-19 Although a nominal increase in stiffness can be observed in the welded mesh, the difference appears to be marginal and not sufficient to explain the decrease in strength. The smaller wire thickness in the welded mesh will account for a theoretical reduction in strength, as well as stiffness, of around 60 %. This may account for the strength reduction. Welded mesh is typically found to be much stiffer than diamond mesh; a stiffness reduction of 60 % would normally not be sufficient to reduce the stiffness of welded mesh to that of a diamond mesh. It is possible that due to the geometry of these tests, whereby the loaded area is relatively large compared to the total mesh area, the effect of mesh stiffness is less pronounced than in tests with a (relatively) smaller loaded area.



Figure A-23 *Failure of welded mesh in test 24/01/02*

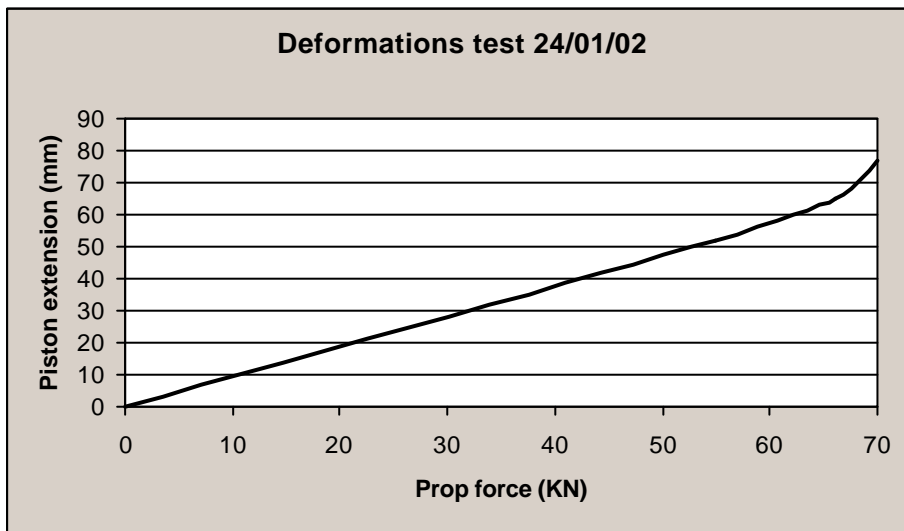


Figure A-24 *Monitored load-deformation characteristics*

Table A-12 *Test 24/01/02*

Prop force (kN)	Piston extension (mm)	Absorbed energy (kJ)	<i>In-plane</i> Stiffness (ton/m)
0	0	0	
55	52	2.47	9,900

66	65 (3 wires failed near the edge of the plate)	3.26	6,100
70	77 (further failure along plate and wall)	4.08	3,900

A13 Test on 12/02/02

Welded mesh with an aperture of 100 mm and a wire thickness of 3.15 mm suspended in the standard bar frame was used for this test. In addition to the mesh, the standard lacing was used. The system was supported on brick walls with an internal spacing of 1.0 m. Loading was via a 75 x 75 cm steel plate directly onto the mesh. The resulting deformations are shown in Figure A -26. Mesh failure, at a prop force of less than 110 kN, appears to be associated with an increase in the rate of deformation. Further loading of the system resulted in a decrease in the rate of deformation, similar to that observed in the test on lacing (see Figure A -21).



Figure A-25 Failure in the test on 12/02/02

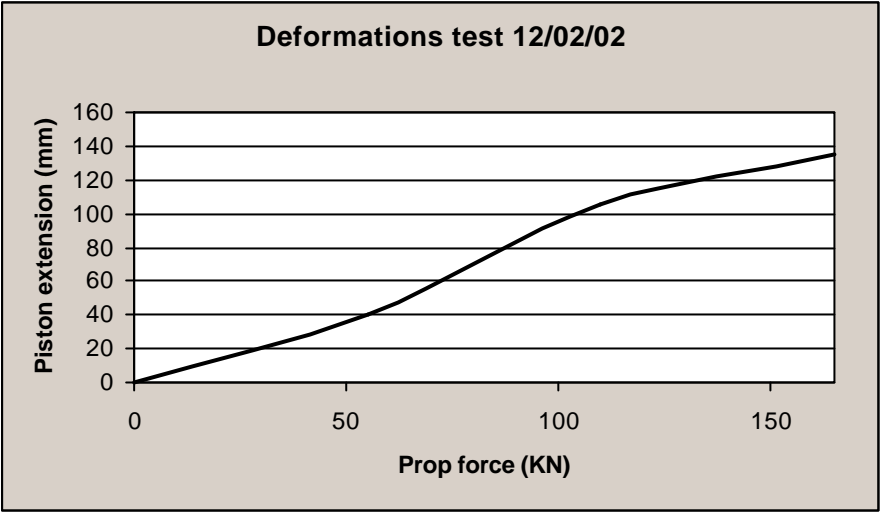


Figure A-26 *Monitored load-deformation characteristics*

Table A-13 Test 12/02/02

Prop force (kN)	Prop extension (mm)	Energy absorbed (kJ)	<i>In-plane</i> stiffness (ton/m)
0	0	0	
55	40	1.16	21,000
110	105 (mesh broke along 2 plate edges)	6.46	2,500
165	135	10.58	1,800
<220	150 (cable broken near plate edge)		

A14 Test on 14/02/02

Diamond mesh with an aperture of 100 mm and a wire thickness of 4.2 mm suspended in the standard bar frame was used for this test. In addition, standard lacing was used. The system was supported on brick walls with an internal spacing of 1.0 m. Load was applied through a 75 x 75cm steel plate directly onto the mesh. Failure only took place at a prop force in excess of 220 kN and manifested itself in the form of mesh rupture and cable unraveling at one corner of the steel plate (see photo in Figure A -27). The system strength benefited from the combined contribution of mesh and cable as can be appreciated from Figure A -28. An increase in strength as well as in stiffness can be observed if the graph in Figure A -28 is compared to the one in Figure A-26, which represent the deformations in welded mesh and lacing. However, comparing the graph in Figure A -28 with the one for lacing only, in Figure A -21, does not demonstrate any increase in system stiffness. It is not immediately obvious why this is the case, although local conditions (brick crushing, etc.) could have a strong effect on overall behaviour.



Figure A-27 Failure of mesh and lacing in the test on 14/02/02

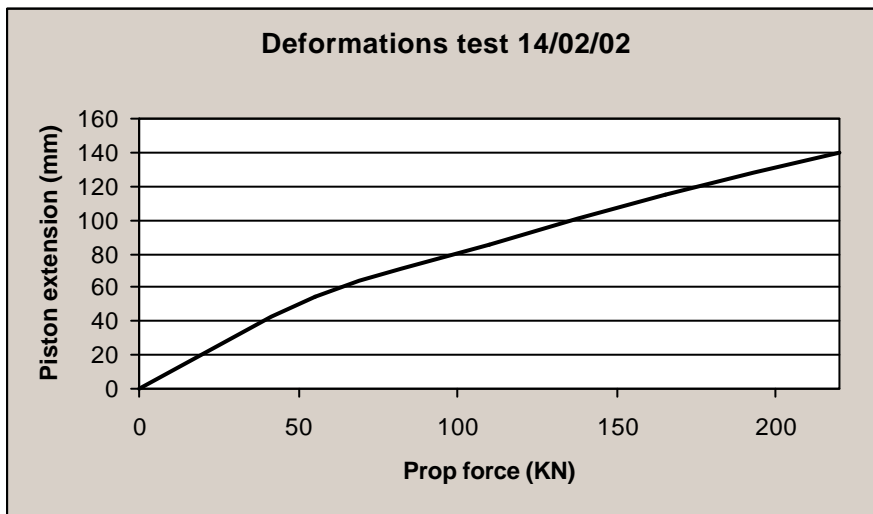


Figure A-28 Monitored load-deformation characteristics

Table A-14 Test 14/02/02

Prop force (kN)	Prop extension (mm)	Energy absorbed (kJ)	In-plane Stiffness (ton/m)
0	0	0	
55	55	1.51	8,300

110	85	3.98	4,600
165	115 (brick crushed under cable)	8.11	2,800
220	140	14.30	1,100
<275	160 (cable and mesh failure in SE corner)		

A 15 Test on 20/02/02

In this test diamond mesh with an aperture of 100 mm and a wire thickness of 4.2 mm, suspended in the standard bar frame, was used. The system was supported on brick walls with an internal spacing of 1.5 m. Load was applied via a 75 x 75 steel plate directly onto the mesh.

It is clear from the graph in Figure A -30 that the system stiffness has decreased substantially compared to the tests with 1.0 m spans. Failure occurred at a prop force in excess of 80 kN, but below 110 kN. As can be seen from the photograph in Figure A-33, the mesh ripped open at one of the corners of the steel plate. Theoretically, the increased deformations are directly and linearly related to the increased span, as deformation to span ratio can be expected to remain constant. The ratio between the size of the load spreader (75 x 75 cm) and the span has however not been maintained in this test and this may account for an additional decrease in stiffness and strength. The observed strength reduction, relative to the test on diamond mesh with a 1.0 m span (Figure A -19), is thus explained from the decreased ratio of the load spreader size to the span. In a similar way to the smaller loading plates causing a reduction in strength in the test on 21/01/02, the increase in stress concentration around the edges of a plate which is relatively small with respect to span, leads to failure at lower loads. Increasing the span while maintaining the size of the loading plate has therefore a similar effect as decreasing the size of the loading plate while maintaining the span.



FigureA-29 *Mesh failure in the test on 20/02/02*

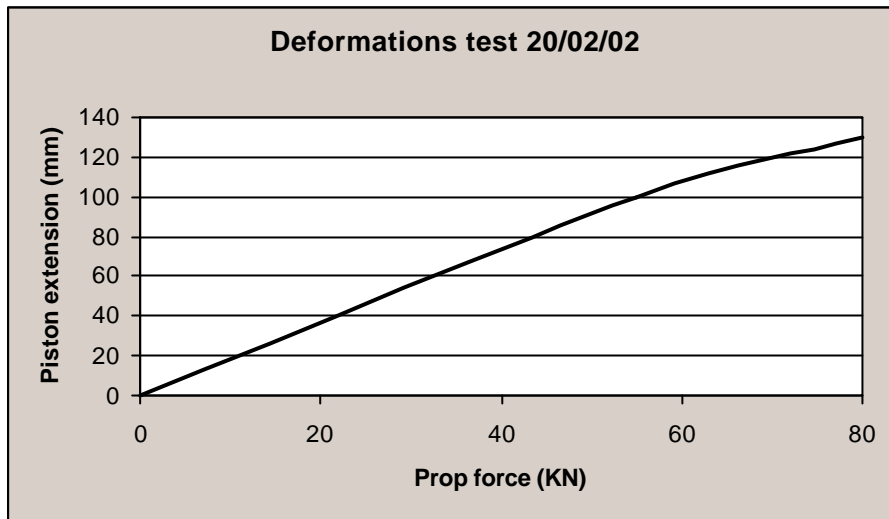


Figure A-30 *Monitored load-deformation characteristic*

Table A-15 Test 20/02/02

Prop force (kN)	Prop extension (mm)	Energy absorbed (kJ)	In-plane Stiffness (ton/m)
0	0	0	
55	100	2.75	3,100
80	130	4.78	1,050
<110	190		

A16 Tests on 27/02/02

In this test a diamond mesh with an aperture of 100 mm and a wire thickness of 4.2 mm suspended in the standard bar frame was used together with standard lacing. The load was applied via a 75 x 75 cm steel plate directly onto the mesh. The system was supported on brick walls with an internal spacing of 1.5 m. Two tests have been conducted on this particular system. The first test resulted in premature instability associated with the prop. In this case, the prop rotated away from the test rig due to slippage along the loading plate. It was established that this loading plate was initially not placed perpendicular to the prop, but was slightly tilted and thus allowed for sliding to occur. This instability took place at a prop force of less than 165 kN. It was also noted that some of the lacing clamps slipped as well during this test.

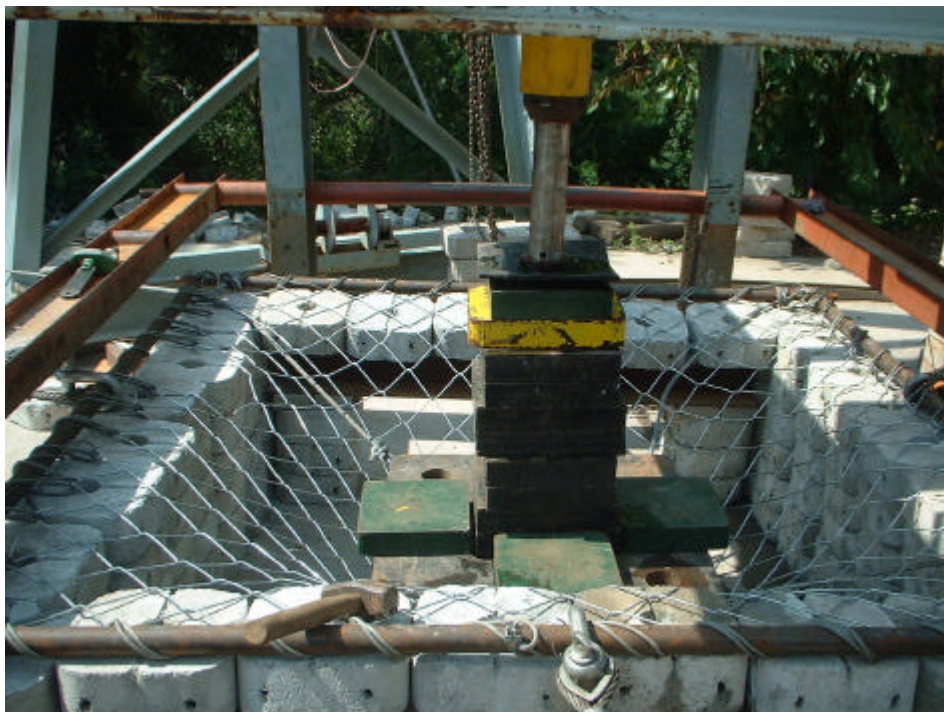


Figure A-31 Failure of mesh and lacing in the test on 27/02/02

In the following test on the same system, failure of the system occurred when the prop force exceeded 165 kN. The main cause of failure occurred near one of the anchor points where the

cables become detached. It was also observed that the mesh started to tear off the frame, but this may have been a secondary effect. No other failure was observed.

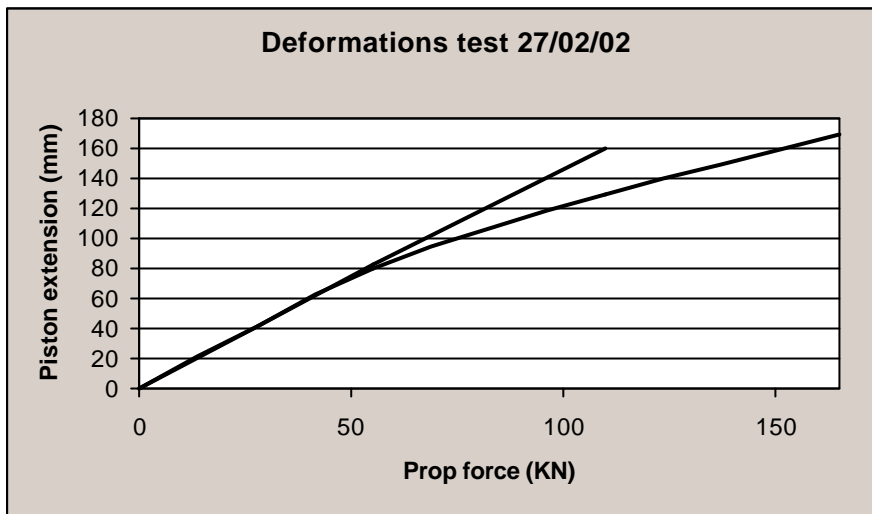


Figure A-32 Monitored load-deformation characteristics for both tests

Table A-16 First test on 27/02/02

Pump force (kN)	Prop extension (mm)	Absorbed Energy (kJ)	In-plane Stiffness (ton/m)
0	0	0	
50	83	2.08	4,900
110	160	7.12	1,550
<165	Prop slipped out		

Table A-17 Second test on 27/02/02

Prop force (kN)	Prop extension (mm)	Absorbed energy (kJ)	In-plane Stiffness (ton/m)
0	0	0	
55	80	2.20	6,400
110	130	6.33	2,900
165	170	11.83	1,950

<220	230 failure
------	-------------

A17 Test on 05/03/02

Test on welded mesh with an aperture of 100 mm and a wire thickness of 3.15 mm suspended in the standard bar frame. The mesh was supported on brick walls with an internal spacing of 1.5 m and loading was introduced through a 75 x 75cm steel plate directly onto the mesh. The mesh failed at a prop force of less than 55 kN and deformations could therefore not be recorded. The low failure load can be attributed to the relatively small ratio between the size of the load spreader and the relatively low strength of the wired mesh (60 % of the diamond mesh, in theory). The photograph in Figure A-33 shows the post failure situation.



Figure A-33 Mesh failure in the test on 05/03/02

Table A-18 Test 05/03/02

Prop force (kN)	Prop extension (mm)
0	0
<10	170 (failure along plate edge)

A 18 Test on 07/03/02

In this test a welded mesh with an aperture of 100 mm and a wire thickness of 3.15 mm suspended in the standard bar frame was used. In addition, standard lacing was applied and the load was introduced through a 75 x 75 cm steel plate. The system was supported on brick walls with an internal spacing of 1.5 m. At a prop force of 55 kN two strands of the mesh broke and at a force of 110 kN the mesh was broken along two edges of the steel loading plate. At a prop force of 165 kN further mesh damage could be observed and increasing the force beyond 165 kN led to cable failure and crushing of supporting concrete bricks (Figure A-34). The

system stiffness of the welded mesh and lacing is less than that of the diamond mesh and lacing (Figure A-32) and this may be attributed to the failure of the welded mesh at a relatively early stage.



Figure A-34 Mesh and cable failure in the test on 07/03/02

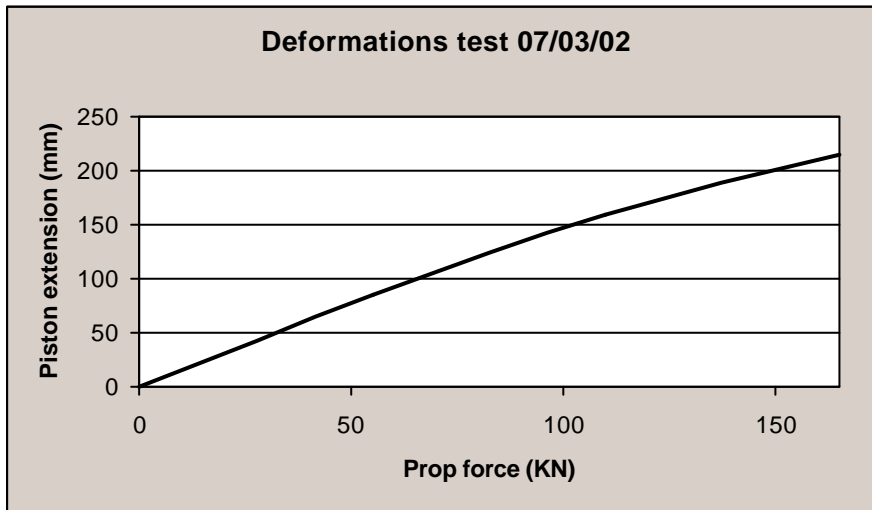


Figure A-35 Monitored load-deformation characteristics

Table A-19 Test 07/03/02

Prop force (kN)	Prop extension (mm)	Energy absorbed (kJ)	In-plane stiffness (ton/m)
0	0	0	
55	85 (two wires broken)	2.34	5,050
110	160 (mesh failure along two edges)	8.53	1,550
165	215 (more mesh damage)	16.1	1,000
<220	330 (cable broken and brick crushed)		

B Results of impact testing

B1 Test on 04/12/01

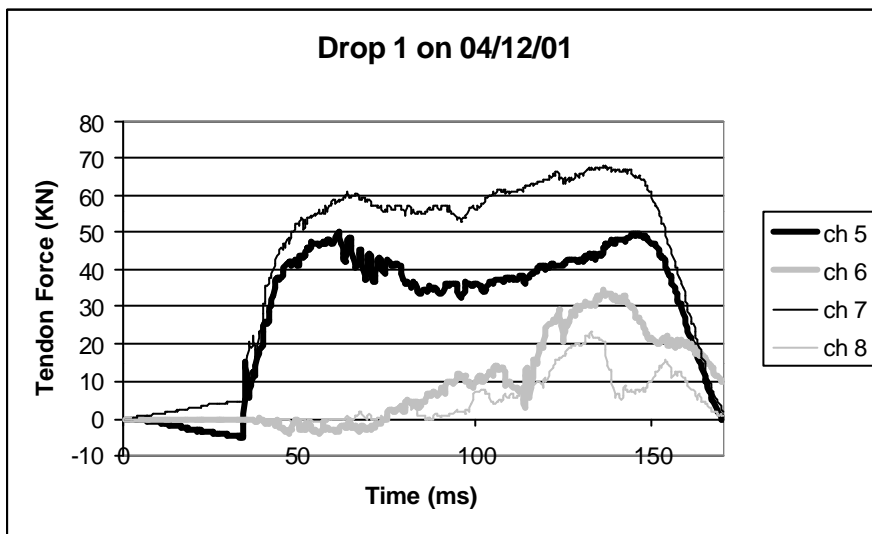
In this test, the assembly of blocks was suspended from six cone bolts arranged in two rows of three. A so-called “Brunswick” support system, consisting of heavy welded mesh plus additional straps of extra heavy welded mesh between the individual tendons, was used to complement the support system. A weight of 3 tons was impacted in the middle of the two center bolts, which were connected by a strap of extra heavy welded mesh. The spacing between neighbouring bolts was 1.0 m.

The first drop height was 1.2 m, which resulted in 150 mm yield in the two center bolts. The recorded forces in these bolts show a yield force ranging between 4 and 6.5 tons for a duration of approximately 0.12 seconds. The absorbed energy in the two yielding bolts is thus around 15 kJ, which is approximately 40 % of the impact energy. During the same impact the external bolts experienced a maximum impact force of around 3 tons. In addition to these impact forces, the change in force because of the impact was monitored as well. Although the drop weight was resting on the assembly after the drop, the center bolts showed a decrease in force of around 0.4 ton whereas the external bolts showed a similar increase. Removal of the weight resulted in a reduction in tendon forces varying between 0.1 and 0.4 ton. No accelerations were recorded during this test.

The second drop height was 1.8 m, which resulted in an additional 70 mm yield in the center cone bolts. The recorded forces in these bolts show a yield force averaging 5.5 tons for a duration of 0.08 seconds. However, both bolts experienced a peak force of more than 9 tons at the beginning of this impact. This excessive initial force could be attributed to the presence of a retaining ring welded around the steel tube containing the cone bolts. This phenomenon is therefore an anomaly not representative of cone bolt behaviour. The absorbed energy is difficult to calculate, as it is not obvious what the average yield force was. Assuming a yield force of 7.5 tons, the energy absorbed by the yielding bolts is still only about 10 kJ or 20 % of the impact

energy. It is not obvious where the remainder of the energy is dissipated, but (elastic) energy absorption in the mesh and lacing is a major contributor. Crushing of concrete blocks and a less effective load transmission in the load-distribution pyramid are additional possibilities. The external bolts recorded peak forces of around 4 tons during the same impact. The permanent change in force constituted a decrease between 0.1 and 0.3 tons for the center bolts and an increase between 0.4 and 0.6 tons for the external bolts.

It is clear that most of the impact is absorbed in the center bolts, especially in the first drop where a force of 10 tons over a duration of 0.12 seconds is sufficient to arrest a mass of 3 tons traveling at 5 m/s. In the second drop a smaller percentage of the impact energy is absorbed in the center bolts and a relatively larger percentage is transferred to the external bolts. If all bolt forces are combined, a total force of around 22 tons is acting for duration of 0.08 seconds. This is sufficient to arrest the same weight traveling at 6m/s. The energy absorbed in the yielding bolts accounts for about 40 % of the impact energy in the first impact, while it only accounts for about 20 % in the second one. This is indicative of the change in load distribution associated with the induced deformations. After the first drop permanent vertical deformations, as well as bending of the brick layers and stretching of the mesh, are introduced into the system. As the resistance and the stiffness of the mesh increases with its curvature, the mesh is able to transfer a larger portion of the load to the external bolts during the second drop. This explains the decreased contribution of the center bolts and the increased action in the external bolts. The monitored accelerations seem to suggest relatively large vibrations subsequent to the impact in the second drop. It is not clear if these observations have been corrupted, but no plausible alternative appears to be possible.



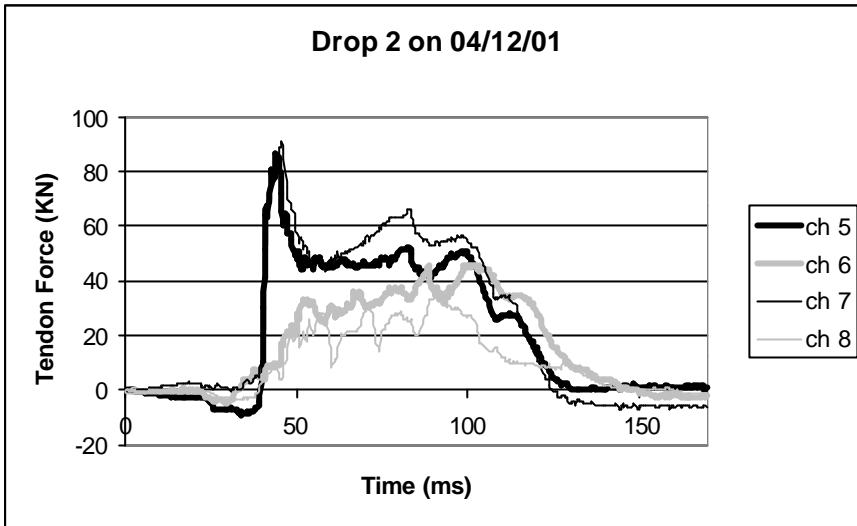


Figure A-36 Impact forces monitored during the impacts on 04/12/01

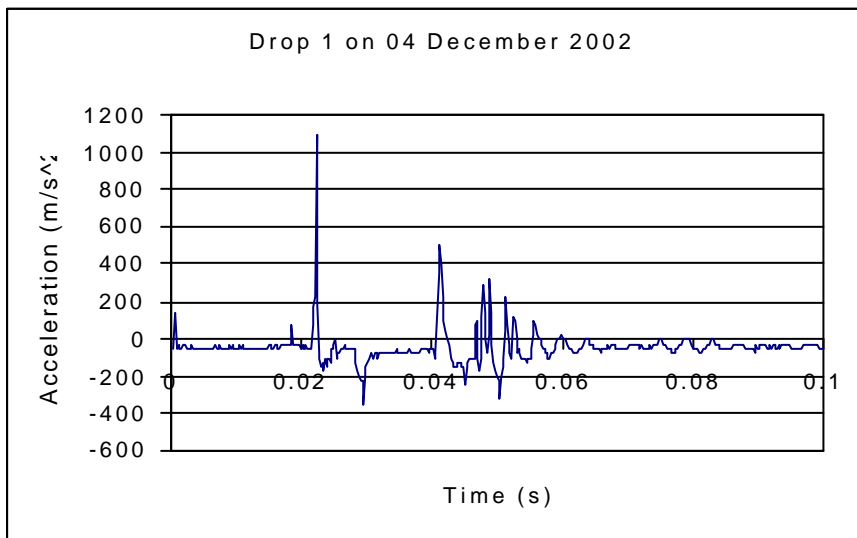
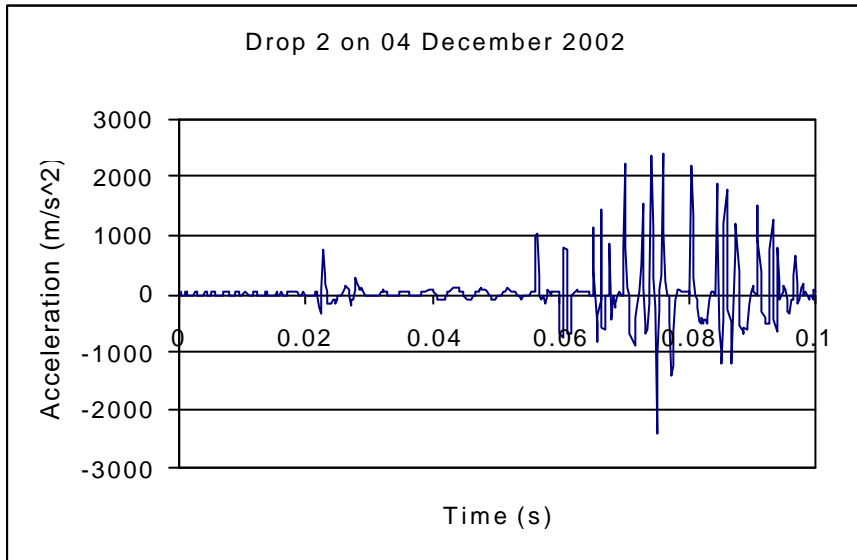


Figure A-37 *Accelerations monitored during the impacts on 04/12/01*

B2 **Test on 17/01/02**

For this test, welded mesh with an aperture of 100 mm and a wire thickness of 3.15 mm was selected. This mesh was suspended in a steel bar frame. Lacing, which runs diagonally across the bottom of the assembly, was attached via a yielding device to the anchor points. The assembly was suspended from four Durabars with a spacing of 1.0 m. The 3 ton mass was dropped from a height of 1.25 m onto the load spreader in the center of the four bolts.



Figure A-38 *Mesh failure in the test on 17/01/02*

While the bolts did not yield during the impact, the yielding devices attached to the lacing did yield. The welded mesh failed and it appeared that most of the impact was absorbed via the lacing (see Figure A-38). The photograph in Figure A-39 demonstrates how the mesh failure is initiated from the tendons cutting through the mesh. The stress concentration around the tendon and the horizontal deformation of the tendon cause the mesh to be cut locally. Notice the absence of a bearing plate and the fact that the mesh is supported via the lacing and not directly by the tendons. The restraint against horizontal tendon deformations is therefore limited in this case. No impact forces were monitored during this test.



Figure A-39 *Initiation of mesh failure in the test on 17/01/02*

B3 Test on 23/01/02

In this test, a diamond mesh with an aperture of 50 mm and a wire thickness of 3.15 mm has been used. The mesh was suspended in the standard bar frame and four Durabars were used to suspend the total assembly. Two diagonally crossing cables were used as lacing and a 3 ton mass was dropped from a height of 1.25 m onto the load spreader in the center of the assembly.

Limited damage was observed in the mesh around some of the tendons (Figure A-40). In this case the stress concentrations around the tendons are more effectively absorbed without causing excessive damage. Note the absence of a bearing plate around the tendon, which results in the mesh being supported by the lacing and not directly by the tendons. This has a limiting effect on the restraint against horizontal tendon deformation.

No yielding occurred in the Durabar tendons, although forces in excess of 11 tons were monitored during the impact. Such large forces may have contributed to the (localised) mesh failure. Slip of the lacing was observed in special yielding devices. This yielding renders the lacing more compliant and less stiff than a lacing in which such deformations are inhibited.



Figure A-40 Localised mesh damage around tendons in the test on 23/01/02

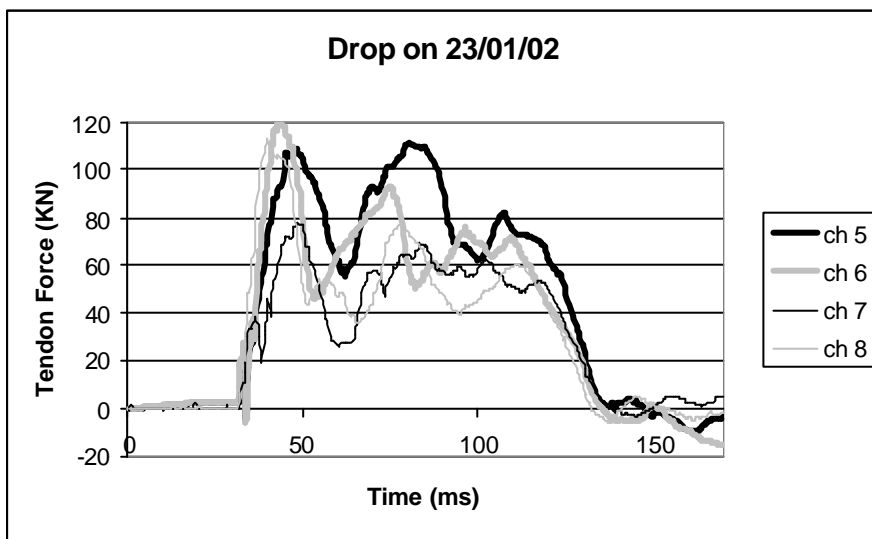


Figure A-41 Impact forces recorded during the test on 23/01/02

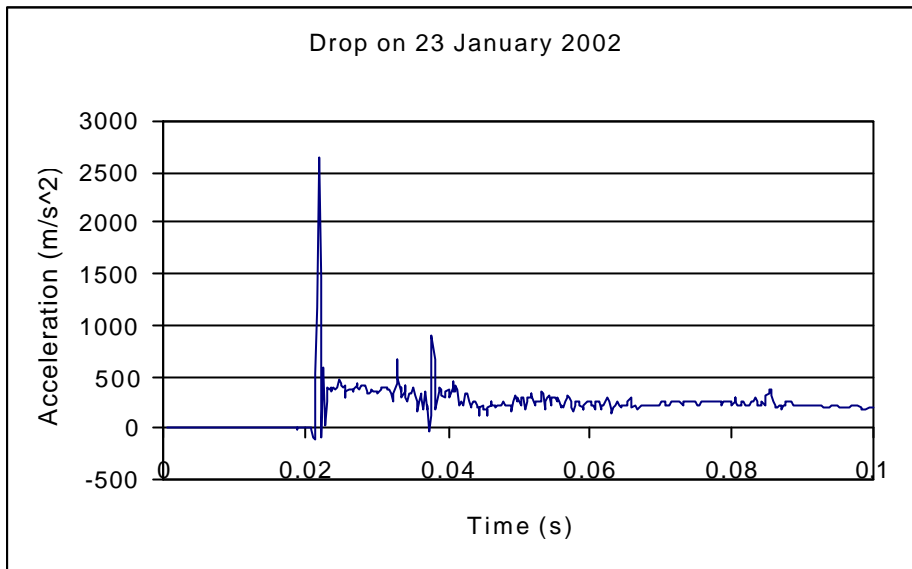


Figure A-42 Accelerations monitored during the impact on 23/01/02

B4 Test on 29/01/02

Diamond mesh with an aperture of 75 mm and a wire thickness of 3.15 mm was used for this test. The mesh was suspended in the standard bar frame and diagonally crossing lacing was used as well. Four Durabars with a spacing of 1.0m were used to suspend the assembly from the test rig and a weight of 3 tons was dropped from a height of 1.25m onto the center of the assembly.

A nut was stripped of one of the tendons during the impact. No yielding took place in any of the tendons, but different degrees of localised mesh damage could be observed around the tendons. Unlike the previous tests, the mesh is clamped between a bearing plate and the bottom layer. As a result the restraint against outward horizontal deformations will be larger in this case and the stress concentrations are probably also increased due to the reduced freedom of movement. Premature mesh failure may be explained from this. The monitored forces during the impact show maximum tendon forces of around 9 tons, which was less than in the previous test on 23/01/02. The (premature) nut failure will have contributed to a reduced performance in this case. Slip of the lacing was also observed in the special yielding devices in this test.



Figure A-43 Localised mesh damage around a bearing plate in the test on 29/01/02

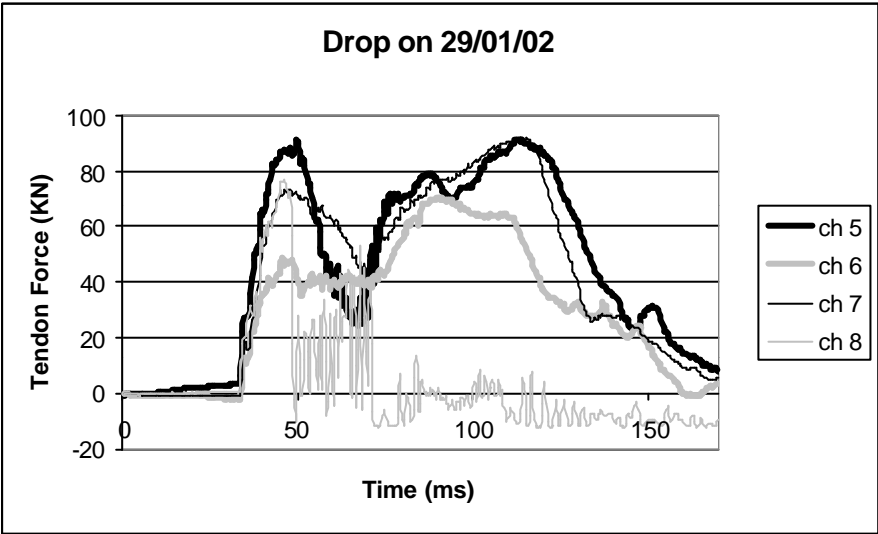


Figure A-44 Forces monitored during the impact on 29/01/02



Figure A-45 Limited mesh damage around a bearing plate in the test on 02/02/02

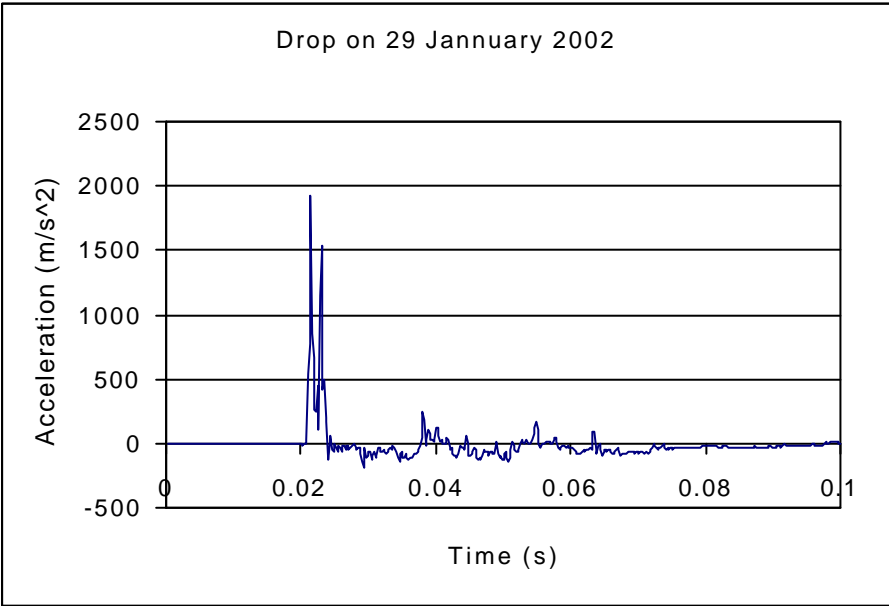


Figure A-46 Accelerations monitored during the impact on 29/01/02

B5 Test on 02/02/02

Test on “Brunswick” mesh with diagonally crossing lacing. The mesh is suspended in the standard bar frame and four Durabars are used to suspend the total assembly from the test rig. The mesh is clamped between a bearing plate and the lower brick layer so that a more direct contact between mesh and tendon is obtained. (Figure A-46). This test is *not* directly comparable with the other tests on “Brunswick” mesh in the six-tendon arrangement. As the

impact location is different, the effective span between the tendons has changed, affecting stiffness and associated impact forces.

An initial impact test, using a mass of 3 tons and a drop height of 1.25 m did not induce any yielding in the tendons and only limited damage in the mesh. Monitored tendon forces reached maximum values of around 8 tons. A second impact test, using the same mass and drop height, did induce around 75 mm yield in the Durabar tendons, without causing additional damage in the mesh. Maximum tendon forces of around 10 tons were monitored during this impact. The fact that no yielding was induced in the first impact can be explained from the limited support resistance offered by the mesh in that case. The impact could be absorbed with a limited resistance, as the associated mesh deformations were relatively large. In the second drop test, the deformed mesh offered more resistance and an increased stiffness. As a result, the impact forces increased sufficiently to induce yielding in the Durabar tendons. The forces in the mesh were not sufficient to cause excessive damage. This is not just attributed to the strength of the mesh, but also to the fact that the brick assembly has not unraveled and is thus capable of transmitting a relatively large percentage of the impact load directly to the tendons. This test demonstrates compatibility of the various support components.

During the first impact, a relatively large amount of slip took place in the yielding devices of the lacing. This can directly be associated with the induced vertical deformations (221 mm) resulting from that impact. The second impact only induced an additional 77 mm of permanent vertical deformation and a limited amount of slip in the lacing. No accelerations could be recorded during the second impact.

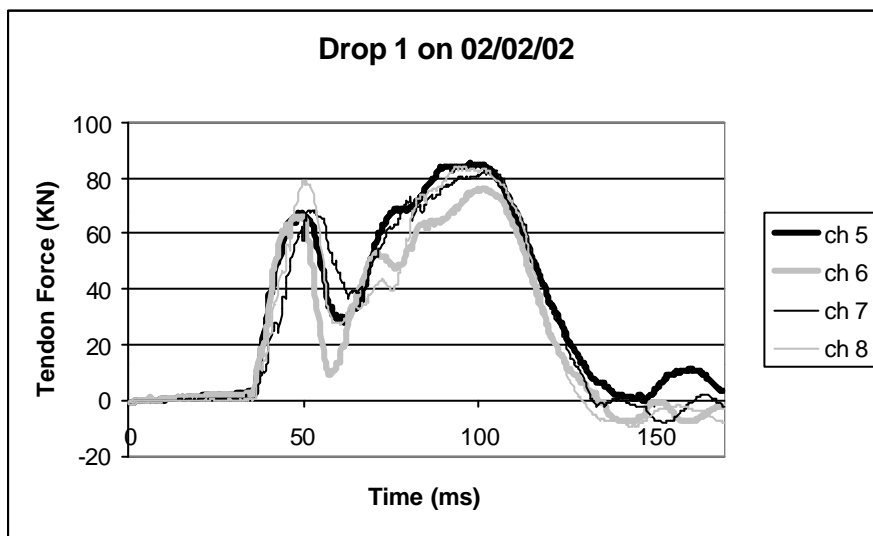


Figure A-47 Forces monitored during the first impact on 02/02/02

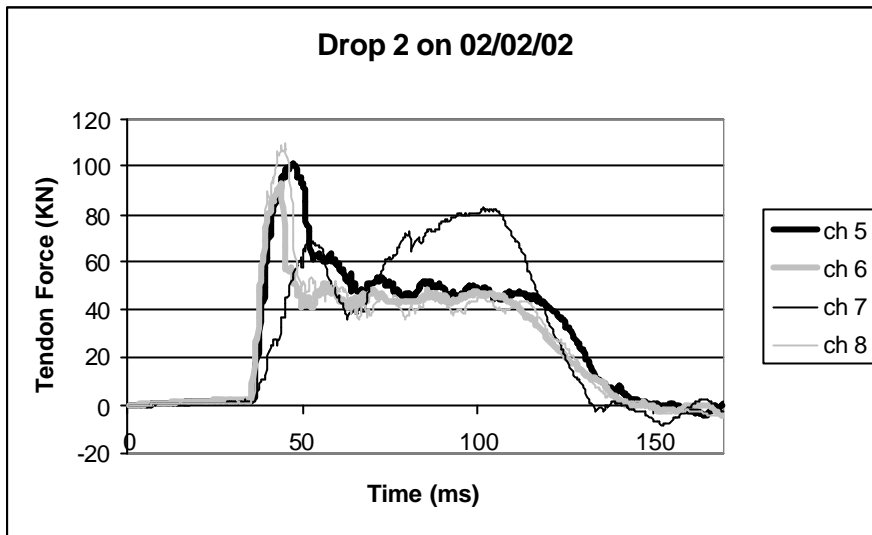


Figure A-48 Forces monitored during the second impact on 02/02/02

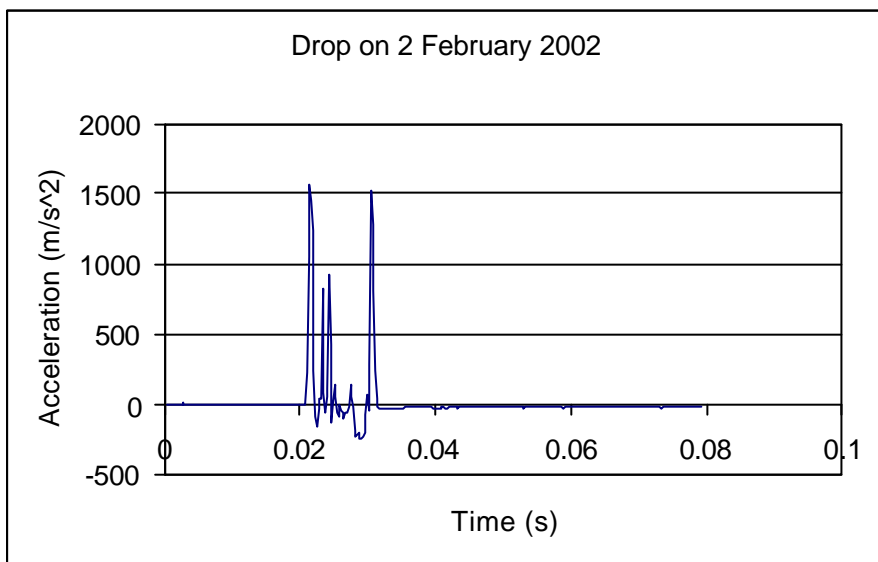


Figure A-49 Accelerations monitored during the first impact on 02/02/02

B6 Test on 07/02/02

In this test the “Brunswick” mesh was used again, but in this case without lacing. The mesh was suspended in the standard bar frame and clamped via bearing plates to the tendons. Four Durabars, spaced at 1.0 m, were used as tendons.

The 3 ton mass was dropped in the center of the brick assembly, on to of the load spreader. An initial drop height of 0.6m was used and localized damage around three of the four tendons could be observed. (Figure A-50) No yielding of the Durabar tendons took place. The forces and accelerations could only be recorded during this first impact and maximum tendon forces approaching 10 ton were monitored in one of the tendons.

A second impact with the same mass and the same drop height of 0.6 m did not result in additional damage to the mesh, but did cause a further separation between the mesh and the tendons at the areas of previously induced localized damage.

A third and final impact with the same mass, but from a height of 1.25 m resulted in the stripping of the nuts from two tendons. As a result, the brick assembly disintegrated and failed. No yielding of the tendons was observed in this case as well.



Figure A-50 Localised mesh damage around a bearing plate in the test on 07/02/02

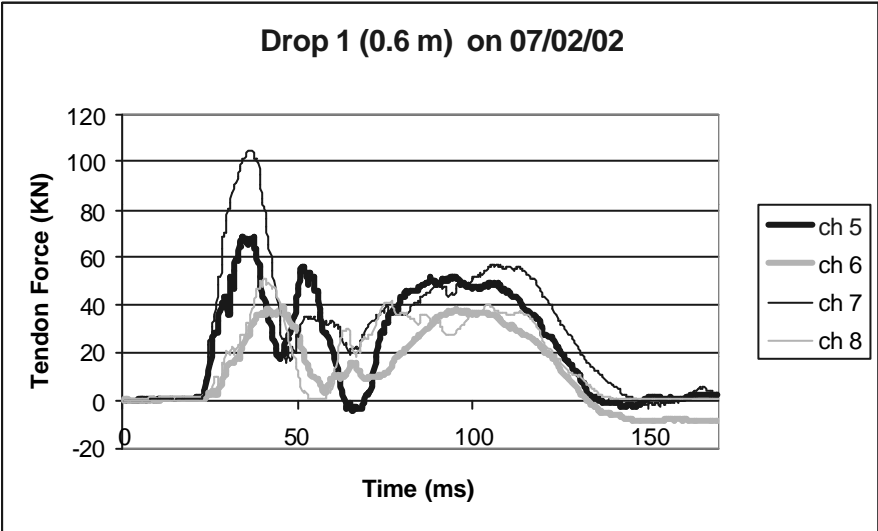


Figure A-51 Forces monitored during the first impact on 07/02/02

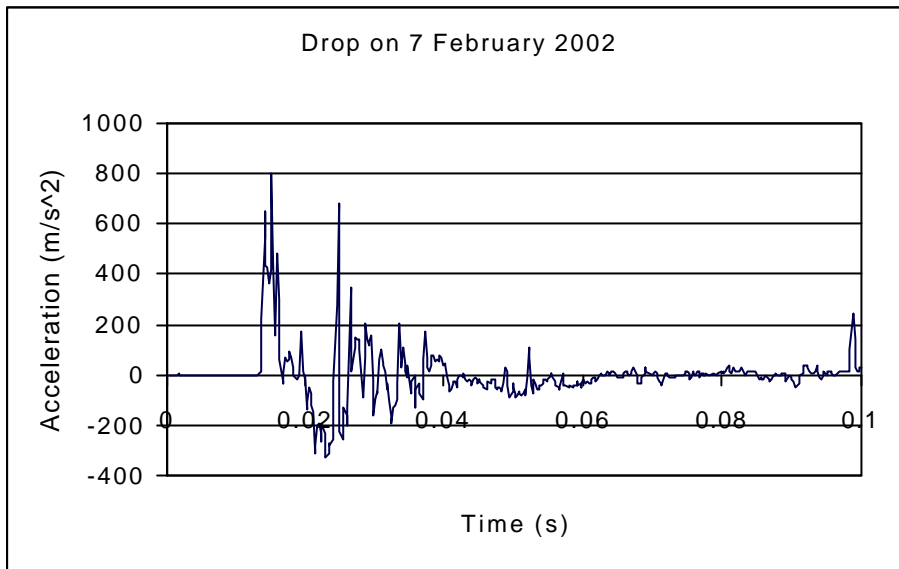


Figure A-52 Accelerations monitored during the first impact on 07/02/02

B7 Test on 19/02/02

In this test a diamond mesh with an aperture of 100 mm and a wire thickness of 4.2 mm has been used. The mesh was suspended in the standard bar frame and diagonally crossing lacing was used as well. The assembly of bricks and support was suspended from the test rig by four Durabar tendons, spaced at 1.0 m.

A mass of 3 tons was impacted into the center of this assembly after it was released from a drop height of 1.25 m. Marginal yielding of around 1 to 2 mm could be observed on the tendons after the impact and localized mesh damage could be observed around the tendons as well. (Figure A-53)

The mesh was clamped against the bottom layer of bricks by bearing plates and two nuts were used on each tendon in this case. No yielding occurred on the Durabar tendons, while tendon forces approaching 10 tons was recorded during the impact. Slip did take place in the yielding devices connecting the lacing to the anchor points.



Figure A-53 Mesh damage around the bearing plate in the test on 19/02/02

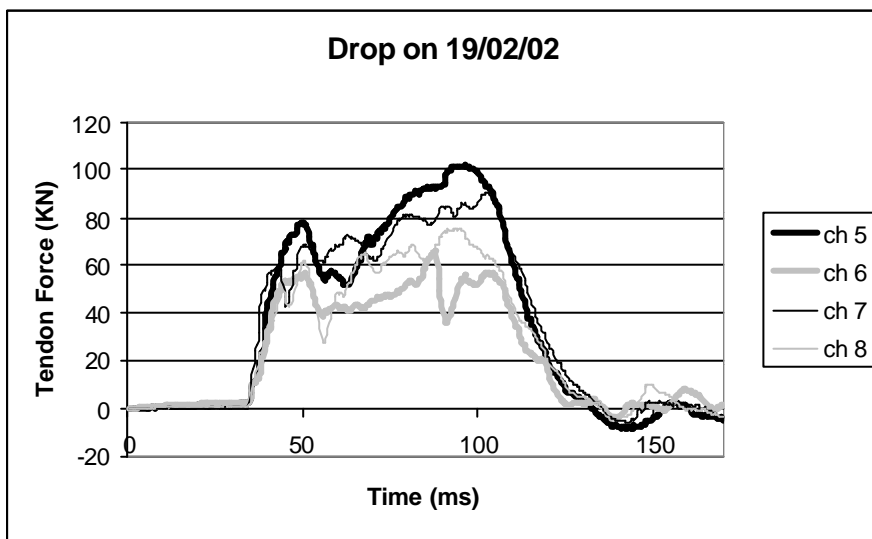


Figure A-54 Forces monitored during the impact on 19/02/02

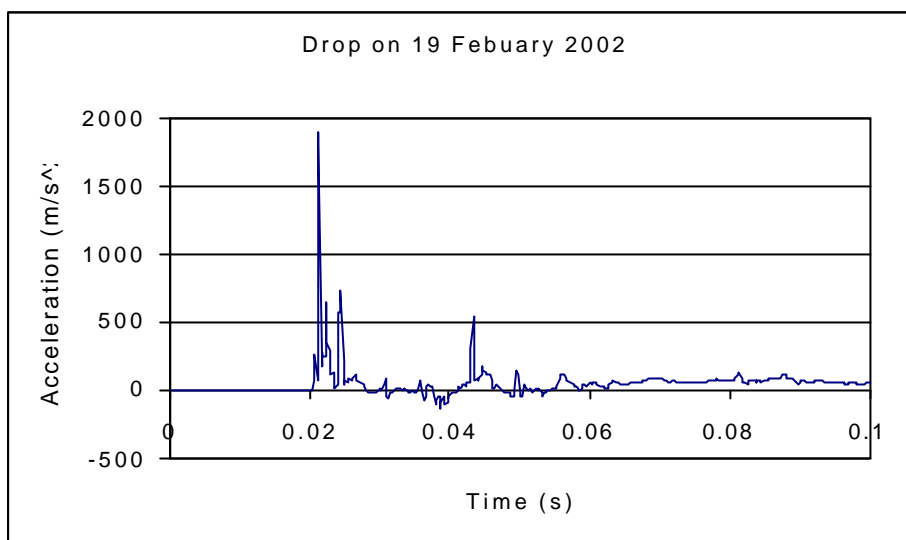


Figure A-55 Accelerations monitored during the impact on 19/02/02

B8 Test on 25/02/02

In this test, a diamond mesh with an aperture of 100 mm and a wire thickness of 4.2 mm was used. The mesh was suspended in the standard bar frame and diagonally crossing lacing has been used in addition. The assembly of bricks and support was suspended from four Durabar tendons, which were spaced at 1.25 m.

A 3 ton mass was dropped from a height of 1.25 m onto the load spreader in the center of the four bolts. As a result, localised mesh damage and occasional brick ejection could be observed. No yielding took place in any of the tendons, but slip was observed in the yielding device connected to the lacing.

The mesh was clamped to the bottom layer of bricks by bearing plates attached to the tendons. Compared to the smaller span of 1.0 m in the previous test, the damaged areas appear to be slightly larger. It is likely that with a larger span, a larger percentage of impact force is transmitted via the mesh and lacing while a relatively smaller portion is directly transmitted to the tendons. On the other hand, the associated reduction in stiffness would lead to smaller impact forces. The forces, monitored during the impact, do indeed indicate a substantial reduction in tendon forces combined with a longer rise time.



Figure A-56 Localised mesh damage around the bearing plates in the test on 25/02/02

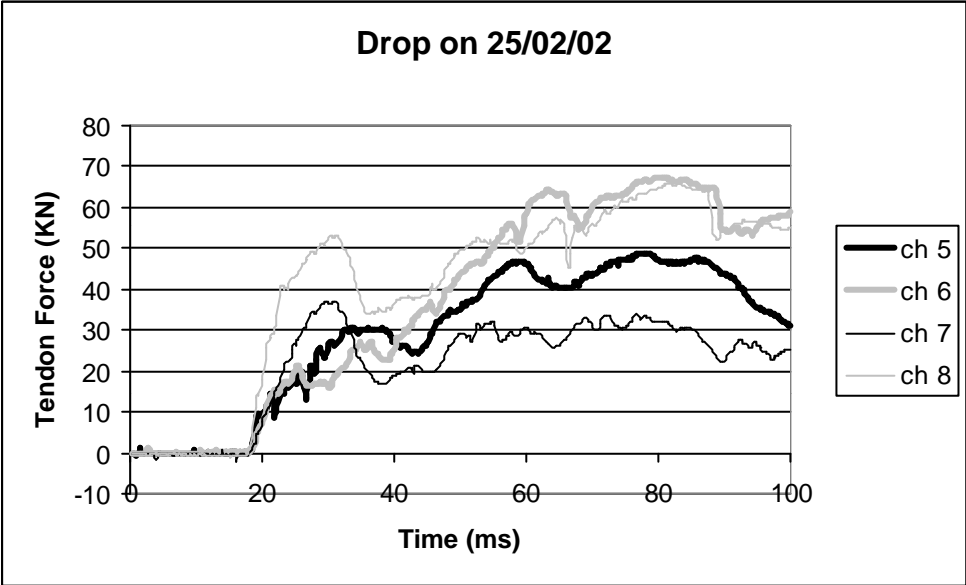


Figure A-57 Forces monitored during the impact on 25/02/02

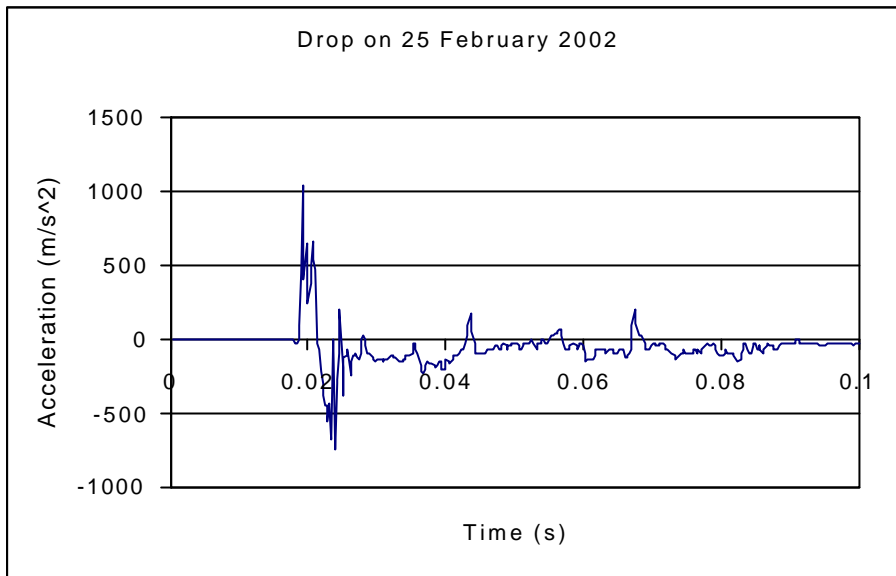


Figure A-58 Accelerations monitored during the impact on 25/02/02

B9 Test on 04/03/02

This test is a repetition of the previous one and a diamond mesh with an aperture of 100 mm and a wire thickness of 4.2 mm has therefore been used in combination with a diagonally crossing lacing. Four Durabar tendons spaced at 1.25 m supported the total assembly from the test rig.

The impact, induced by a mass of 3 tons, which was dropped from a height of 1.25 m, caused similar damage as in the previous test. While no yielding of the tendons could be observed, localised mesh damage occurred around the same three tendons as in the test on 25/02/02. (Figure A-56) The lacing was observed to slip in the special yielding device. Although no bricks happened to be ejected from this assembly, it is believed that the extent of mesh damage is equivalent to the previous test.

The mesh was clamped to the bottom layer of bricks by a bearing plate and two nuts were used on each tendon. Due to a malfunctioning of the equipment, no forces and accelerations were recorded during the impact, but a similar response as in the previous test can be expected.



Figure A-59 *Mesh failure around bearing plates in the test on 04/03/02*

B10 **Test on 11/03/02**

In this test a diamond mesh with an aperture of 100 mm and a wire thickness of 4.2 mm has been used in combination with diagonally crossing lacing. The mesh was suspended in the standard bar frame and the total assembly of bricks and support was suspended from four Durabar tendons spaced at 0.75 m. A mass of 3 tons was impacted onto the load spreader positioned in the center of the four tendons. The drop height was 1.25 m.

Two tendons yielded upon impact, but this was associated with the rupture of a weld in the metal sleeve in which the tendon was embedded (Figure A-60). The associated rupture forces were recorded to be around 4 and 9 tons respectively, while forces of around 9 and 12 tons were recorded in the non-yielding tendons.

Of practical interest is the fact that no mesh failure occurred around the two yielding bolts, while localised mesh failure could be observed around the two stiffer, non-yielding tendons.



Figure A-60 Rupture of two tendons in the test on 11/03/01

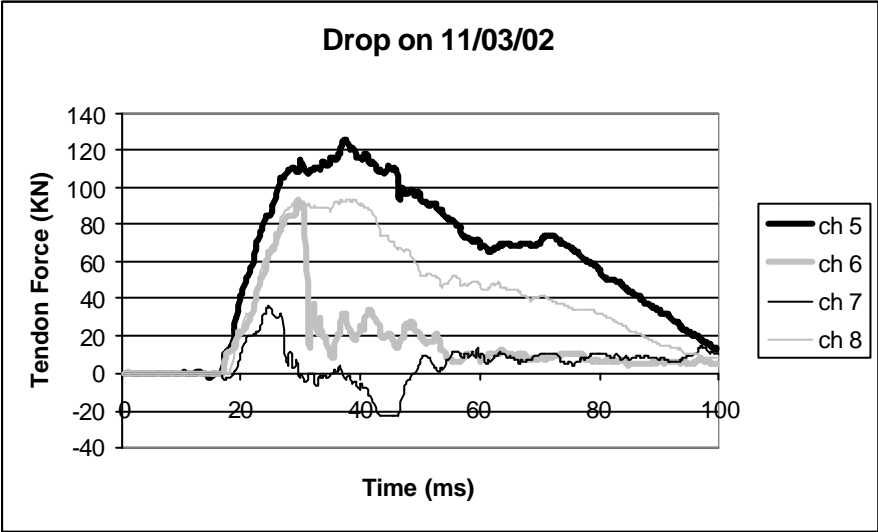


Figure A-61 Forces monitored during the impact on 11/03/02

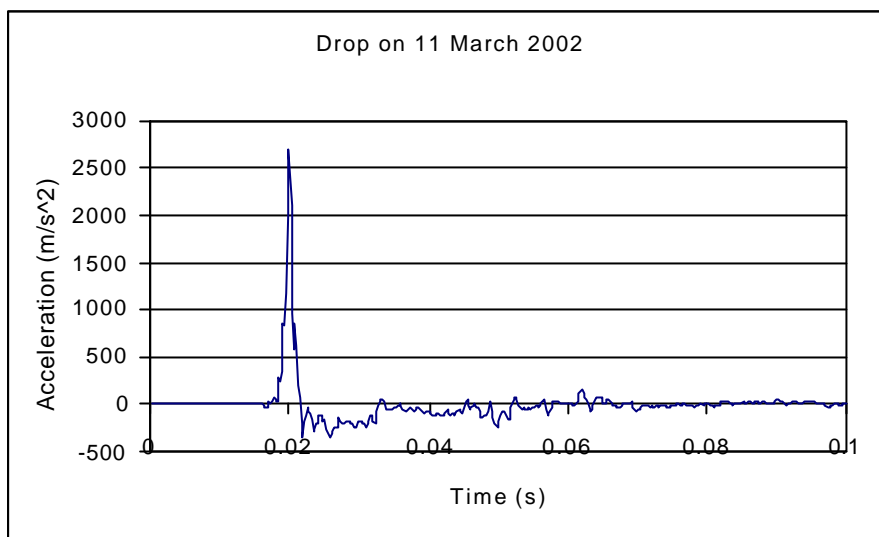


Figure A-62 Accelerations monitored during the impact on 11/03/02

B11 Test on 19/03/02

This test is effectively a repetition of the previous one. The tendon was repositioned in such a way that the weld could not be exposed to the impact force. A diamond mesh with an aperture of 100mm and a wire thickness of 4.2 mm in combination with diagonally crossing lacing was used again. The mesh was suspended in the standard bar frame and the total assembly was suspended from four Durabar tendons spaced at 0.75m. The mesh was clamped to the bottom layer of bricks by a bearing plate, which in turn was secured to the tendons by two nuts.

A mass of 3 ton was dropped from a height of 1.25m onto the load spreader in the center of the suspended assembly of bricks and support. No yielding could be observed on any of the tendons, while localised damage was induced in the mesh around some of the tendons. (Figure A-63) A few bricks were ejected through the damaged mesh. A limited amount of slip could be observed in the yielding devices connected to the lacing. The relatively small vertical deformations that were induced during the impact are directly related to the reduced yield in the lacing.

The shorter span between the tendons should lead to a stiffer system in which less of the load is transmitted via the mesh and lacing. However, the increased stiffness of the mesh and lacing should also lead to larger forces being generated during the impact. The loads monitored in the load cells nevertheless only show maximum values between 8 and 10 tons and it seems that the failure of the mesh is associated with the limited forces being induced. The impact energy is therefore not completely absorbed by the support system, but is partly lost in the damage processes.

Even with the shorter span and the associated reduction of loads which may be transmitted through the mesh and lacing, there seems to be a mismatch between the strength of the mesh and the yielding capacity of the tendons. This is indicative of the incompatibility of the support components in this case.



Figure A-63 Mesh damage around bearing plate in the test on 19/03/02

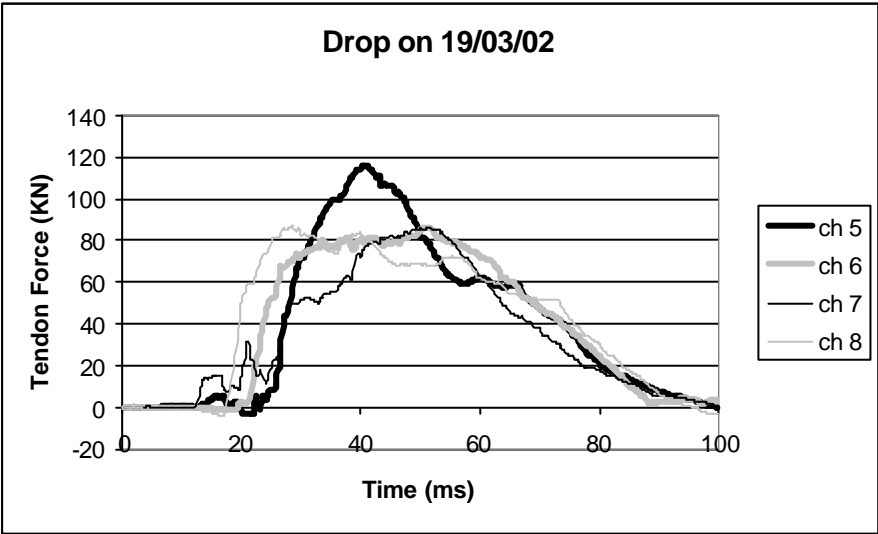


Figure A-64 Forces monitored during the impact on 19/03/02

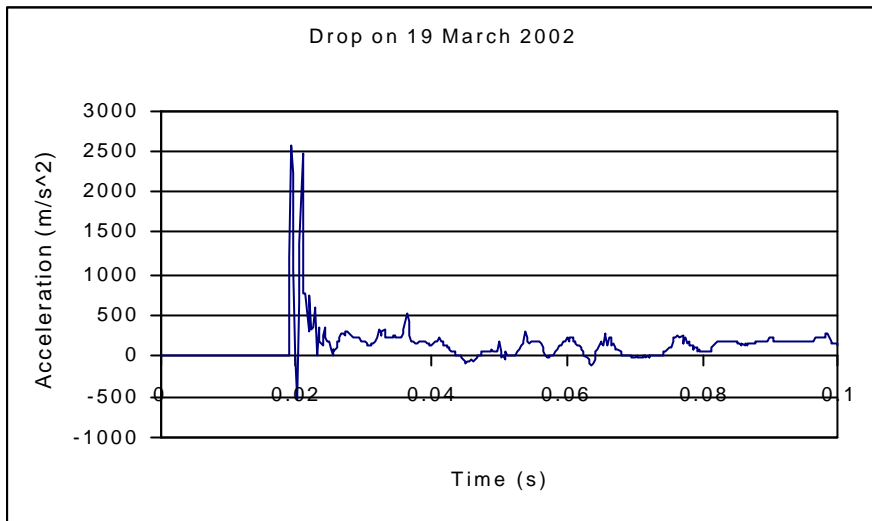


Figure A-65 Accelerations monitored during the impact on 19/03/02

B12 Test on 22/03/02

During impact one of the tendons broke at a force in excess of 10 tons. No yielding of tendons could be observed because of the impact, which induced maximum tendon forces varying between 10 and 12 tons. Limited damage of mesh around the tendons and lacing could be observed as well.



Figure A-66 Local mesh damage around lacing and tendon in the test on 22/03/02

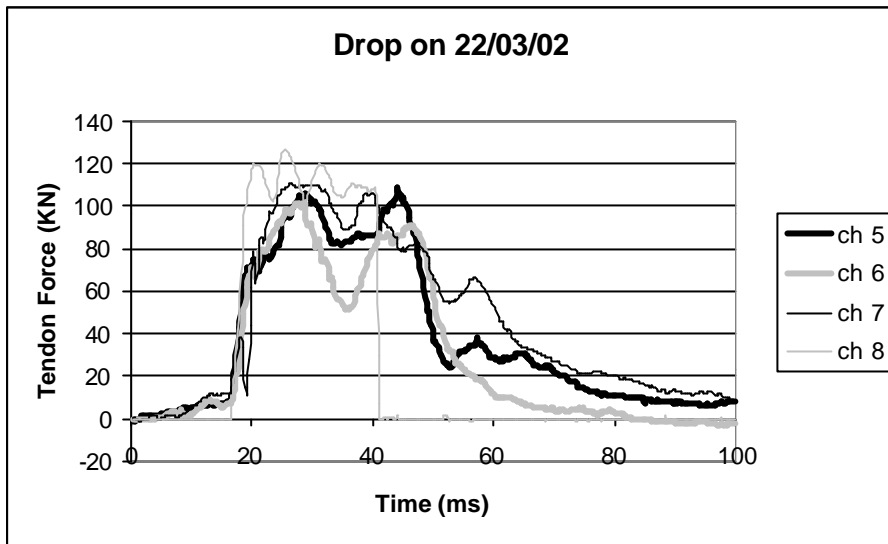


Figure A-67 Forces monitored during the impact on 22/03/02

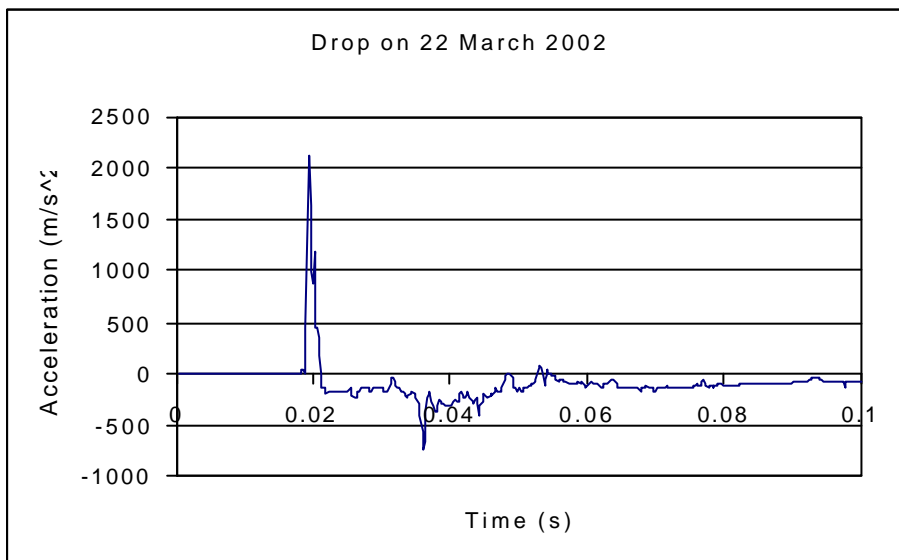


Figure A-68 Accelerations monitored during the impact on 22/03/02

B13 Tests on 12/04/02 and 15/04/02

In the tests the “Brunswick” type welded mesh was used, in combination with specially designed strips of welded mesh consisting of wires bend into a wavy shape. The mesh was suspended in an enlarged bar frame and the assembly of bricks and support was suspended from six Durabar tendons arranged in two rows of three and spaced at 1.0m. The specially designed strips of “wavy” mesh were used between two individual tendons and offered additional support to the main mesh. Large bearing plates were used to clamp both the regular mesh as well as the strips of special mesh to the bottom layer of bricks.

A load spreader was located between the center bolts of the two rows of tendons and a mass of 3 tons was dropped various heights onto this load spreader. An initial accidental drop from a height of 0.3 m did not induce any damage or yielding, whereas a second drop from a height of 1.2 m caused the two center bolts to yield by approximately 50 mm. One strand was broken in the mesh. (Figure -69) A third drop from a height of 1.8 m induced an additional 140 mm yield in

the two centre bolts without causing any further damage in the mesh. A final drop from a height of 2.0 m induced a further 65 mm yield in one of the center bolts and 95 mm in the other one without causing any additional damage in the mesh. Some stretching could be observed in the center strip of wavy mesh. The yielding of bolts, in the absence of any damage in the mesh, is representative of a balanced support system in which the components are compatible. Both the preservation of the “rock mass” integrity and the capacity of the mesh are important issues in this respect. By restraining the tendons from horizontal movements, the first issue is addressed largely. The capacity of the mesh should be such that the forces, which are generated in the mesh, should never exceed the strength of the mesh. The fact that the bolts yield indicates that the mesh is sufficiently strong, as it is implausible that higher forces will be generated in that case. The increase in yield between the second and third drop is explained from the stiffer response of the stretched mesh. The decrease in yield between the third and fourth drop is explained from an increase in the contribution of the four external tendons. With increasing deformations and tendon yield, a larger percentage of the impact force will be transmitted to the external tendons, thereby relieving the center ones.



Figure A-69 Broken strand in the test on 15/04/02

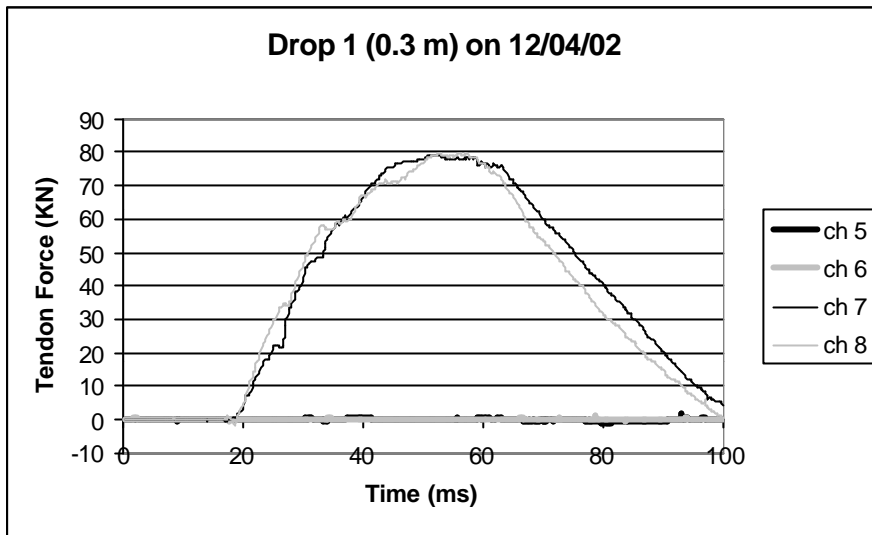


Figure A-70 Forces monitored during the first drop on 12/04/02

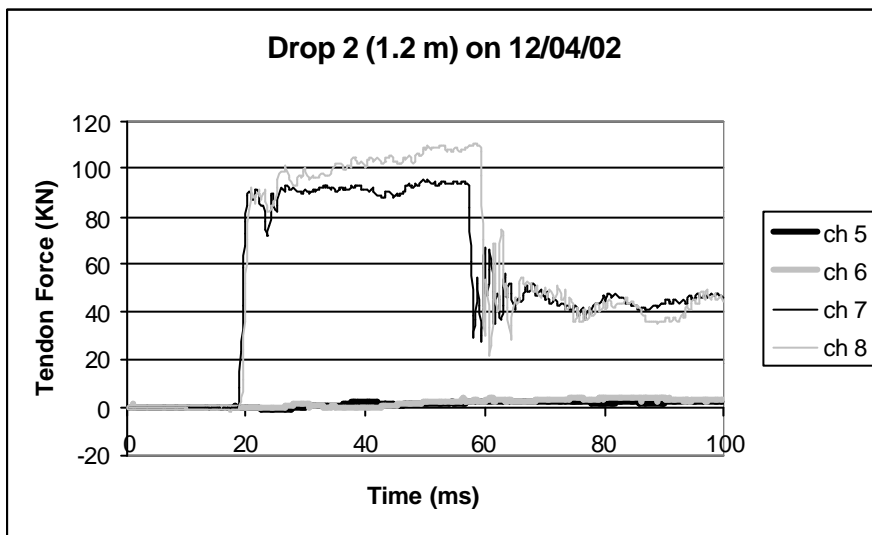


Figure A-71 Forces monitored during the second impact on 12/04/02

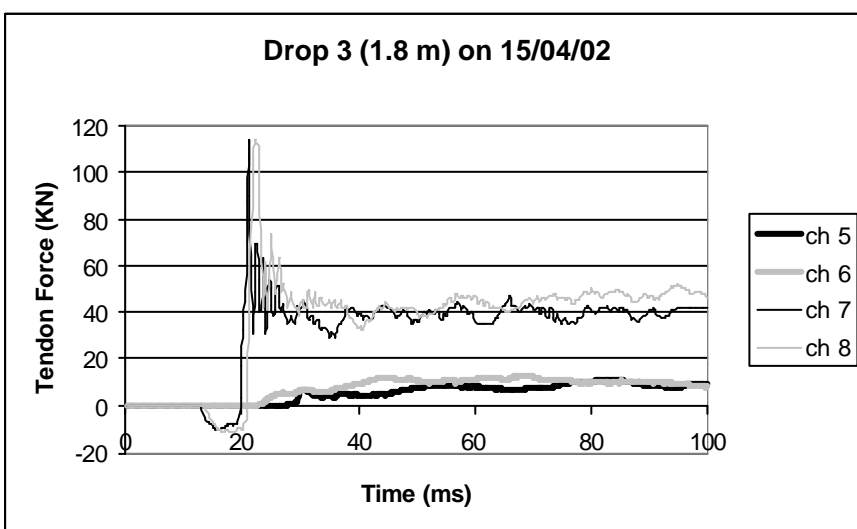


Figure A-72 Forces monitored during the third impact on 15/04/02

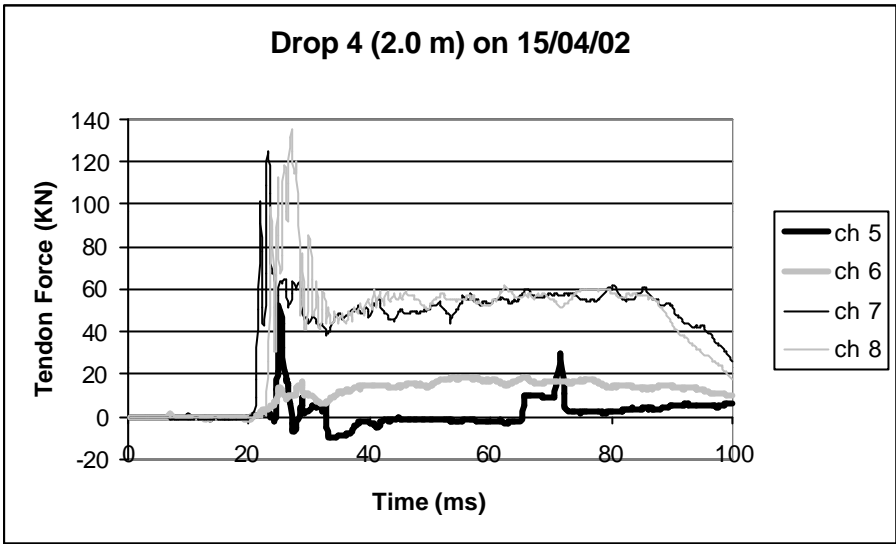


Figure A-73 Forces monitored during the fourth impact on 15/04/02

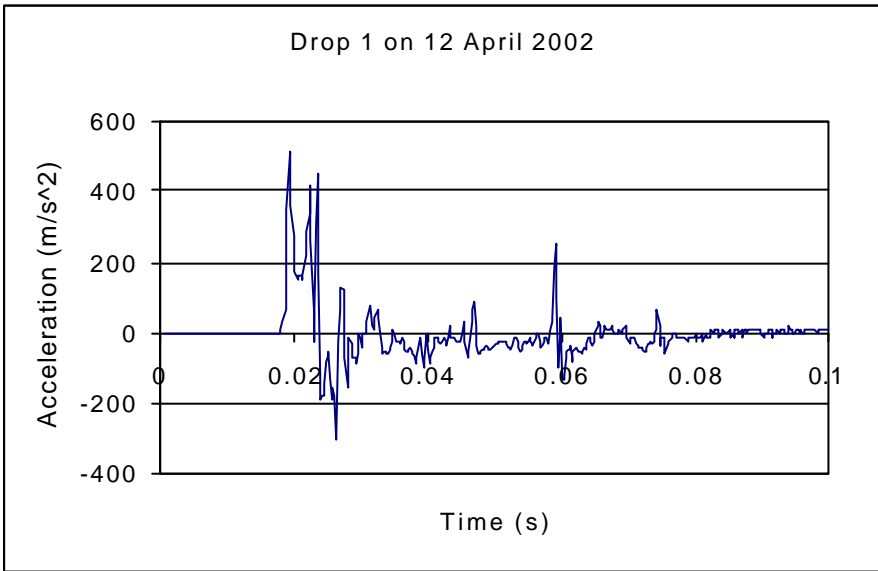


Figure A-74 Accelerations monitored during the first impact on 12/04/02

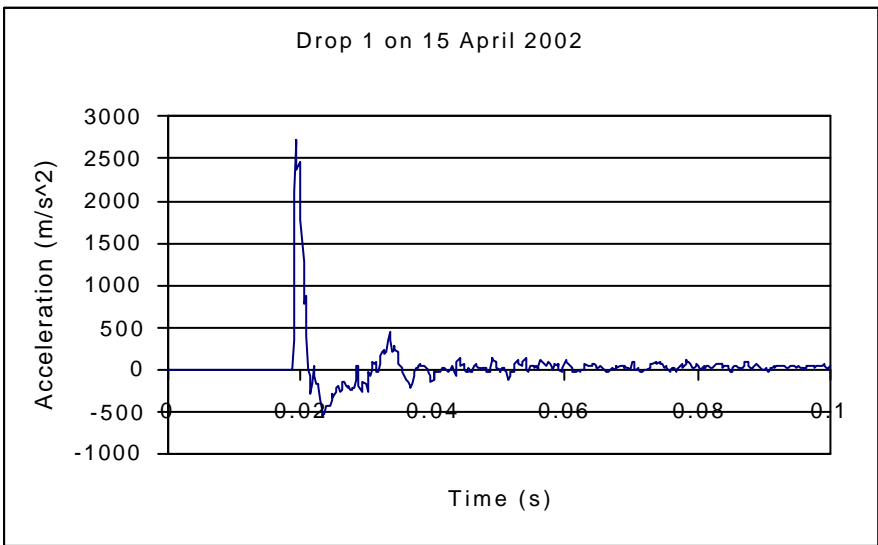


Figure A-75 Accelerations monitored during the third impact on 15/04/02

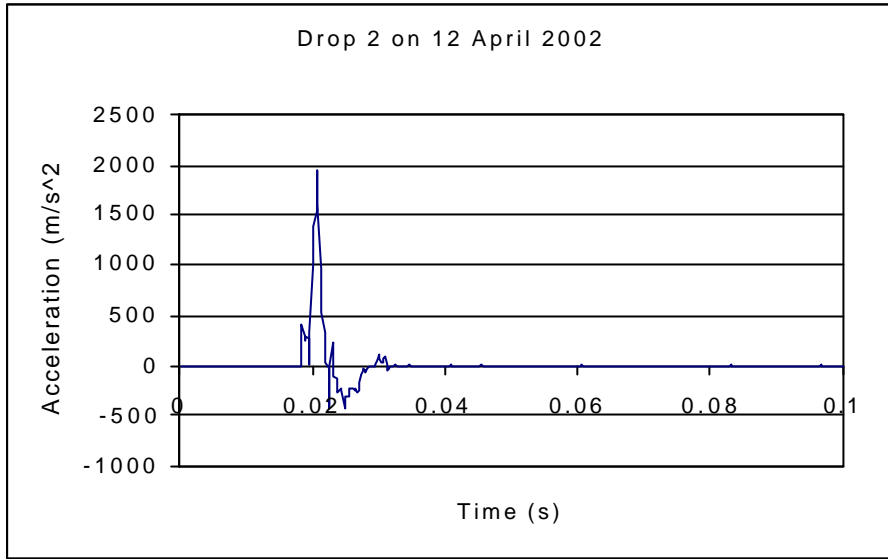


Figure A-76 Accelerations monitored during the second impact on 12/04/02

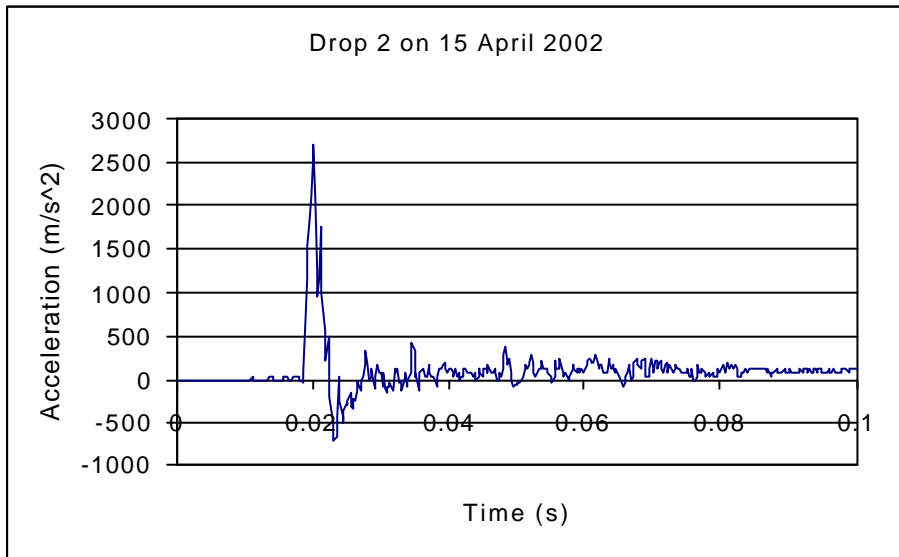


Figure A-77 Accelerations monitored during the fourth impact on 15/04/02